Roles of IFT-A paralogs, *Thm1* and *Thm2*, in the pathogenesis of ciliopathies

By

Wei Wang
MBBS, Bachelor of Medicine and Bachelor of Surgery, Xi'an Jiaotong University, 2012

Submitted to the graduate degree program in Anatomy and Cell Biology and the Graduate Faculty of the University of Kansas in partial fulfillment of the requirements for the degree of Doctor of Philosophy.

_____
Committee Chair: Dr. Pamela Tran

_____
Dr. Prachee Avasthi

_____
Dr. James Calvet

_____
Dr. Brenda Rongish

_____
Dr. Madhulika Sharma

Date Defended: 29 April 2020

The dissertation committee for Wei Wang certifies that this is the approved version of the following dissertation:

Roles of IFT-A paralogs, *Thm1* and *Thm2*, in the pathogenesis of ciliopathies

_____

Chair: Dr. Pamela Tran

_____

Graduate Director: Dr. Julie Christianson

Date Approved: 11 May 2020

Abstract

Primary cilia are antenna-like sensory organelles that extend from the apical surface of most vertebrate cells. Mutation of ciliary genes results in ciliopathies, which commonly manifest renal and hepatic cystic diseases, via mechanisms that remain unclear. To address this knowledge gap, I investigated the role of the intraflagellar transport-A (IFT-A) gene, *Thm1*, in the polycystic kidney disease (PKD) and polycystic liver disease (PLD) of juvenile and adult Autosomal Dominant PKD (ADPKD) mouse models, caused by conditional deletion of *Pkd2*. *Thm1* deletion in juvenile *Pkd2* conditional knock-out (cko) mice both ameliorated and exacerbated different aspects of PKD in a renal tubular-specific manner, while *Thm1* deletion in an adult *Pkd2* cko mouse, markedly attenuated virtually all facets of PKD renal cystogenesis. Further, while perinatal deletion of *Thm1* alone caused a non-cystic liver phenotype – a ductular reaction, characterized by abnormal proliferation of cholangiocytes and biliary fibrosis, *Thm1* deletion in juvenile *Pkd2* cko mice exacerbated liver enlargement and necrosis of the PLD. In contrast, *Thm1* deletion in adult *Pkd2* cko mice attenuated liver enlargement of the PLD in male mice. These data suggest that differential factors between cell types and between developing versus mature renal and hepatic microenvironments influence cilia dysfunction and ADPKD pathobiology.

Additionally, using mouse embryonic fibroblasts (MEF), I explored the roles of *Thm1* and its paralog, *Thm2*, in cilia homeostatic processes and signaling. Analyses of *Thm1*, *Thm2*, and *Thm1;Thm2*-mutant MEF and embryos reveal that *Thm1* and *Thm2* interact to regulate serum-induced cilia loss, ciliary import of membrane-associated proteins, Hedgehog signaling, and embryogenesis. Taken together, this dissertation reveals novel physiological and mechanistic roles for IFT-A in healthy and diseased states, laying groundwork for the design of future therapeutic strategies against ciliopathies, such as ADPKD.

Acknowledgement

It is a long and not easy journey to pursue a Ph.D. in an unfamiliar country with a different culture. There was frustration, self-doubt, and I even thought about giving up. However, when I decided to continue my education and research in Dr. Tran's lab, I could not have imagined how fascinating life would be with the enormous support, trust and friendship from the people I would meet. For this, I have many individuals to thank.

To my mentor, Dr. Pamela Tran - you are the best mentor I could ever have in my life and no words can describe how lucky I was when I chose to join your lab 4 years ago. Not only did you teach me basic techniques required for research, you taught me how to think critically about results and generate new ideas for our projects. You also encouraged me to attend conferences and helped me to improve my scientific writing and presentation skills, which are needed for my future career in an academic setting. More importantly, you are not only my mentor, but also my friend. Thank you for all the things you have done for me and thank you for all your trust and support.

To my committee members - Dr. Prachee Avasthi, Dr. James Calvet, Dr. Brenda Rongish, Dr. Madhulika Sharma and Dr. Pamela Tran - thank you for your invaluable comments and suggestions, not only for my project, but also for my career as an independent research scientist. I appreciate all the time, guidance, support and good will you have given me throughout the years. I hope to gain your wisdom and experience as I pursue my career.

To our collaborators - Dr. Udayan Apte and Dr. Michele Pritchard – thank you for your guidance on the liver project. When we first looked at the H&E slides of the *Thm1* cko livers, we had no idea what to do until we met with Dr. Apte and Dr. Pritchard. Thank you for generously offering your time to help us set up experiments and for providing valuable comments to move the project forward.

To the Anatomy and Cell Biology Department- thank you for your support of graduate students. Thank you to Dr. Dale Abrahamson, the Chair of our Department, for always being present and offering help to students, and for leading such an excellent team in both research and education. I also thank Dr. Julie Christianson for listening to students, keeping students on track and helping students to move forward. It is a wonderful experience to be a graduate student in the Anatomy Department.

To the Jared Grantham Kidney Institute- thank you to everyone for being so supportive. Thank you for all the seminars and festivities. I really enjoy working here.

To my lab mates – thank you very much for the fun and support in the lab. You all are not only my lab members, but also my friends. Bailey - you helped train me when I joined the lab. I learned a lot from you, not only the experimental techniques, but also how you organize things and your fabulous presentation skills, thank you. Damon – you were always there to offer help with troubleshooting, thank you for your support. Luci- it was a great joy to work by your side, and thank you for all the chats we had, for the suggestions you gave me, and for the support during hard times. Tana- you are such a positive and well-organized person. You have helped me a lot with experiments, thank you. Henry- as the newest person in lab, I am glad that you learn things quickly and can do most experiments independently now. Thanks for your help with dissections and other experiments. Thank you to all again and I greatly look forward to having all of you as colleagues and friends in the future.

To my friends in China- thank you for having you all in my life for over ten years. I can always feel your support no matter how far we are and how long we have not seen each other. Thank you for listening and the warm welcome every time I come back.

To my Mom (Xiaorong) and Dad (Li) – I am so lucky to have you as my parents. You are always there to listen, encourage and help me overcome all the difficulties. Thank you Mom for helping me to take care of my daughter, and thank you Dad for your kindness and hard work, which has greatly impacted me since I was a child. Thank you for all your love.

To my husband Ruochen and my daughter Chloe- Ruochen- thank you for your company, endless support and continued patience. Chloe- thank you for coming into my life. Having you is the best thing in my life, and you make me want to be a better person.

Table of Contents

List of Figures

List of Tables

Chapter One: Introduction

1.1 Primary cilia structure

Cilia are microtubule (MT)-based structures that project from the cell surface. They are evolutionarily conserved organelles and exist in a large variety of eukaryotic cells, ranging from single cell *Chlamydomonas reinhardtii* to almost every vertebrate cell. Cilia are classified into two categories by function and structure: motile and non-motile. Non-motile cilia, also termed primary cilia, sense extracellular mechanical and chemical cues and mediate signaling cascades[1]. Motile cilia typically generate motion[2], although sensory function in motile cilia has also been observed[3].

The cilium consists of a MT-based axoneme that extends from a basal body, and is surrounded by a ciliary membrane, an extension of the cell plasma membrane. The axoneme of a motile cilium is comprised of nine doublet peripheral MTs and two single central MTs. In contrast, the axoneme of a primary cilium contains only nine doublet peripheral MTs and lacks a central MT pair[4]. At the base of primary cilia is a region known as the ciliary transition zone (TZ), which functions as a gate with structures like Y-links to regulate the entrance and exit of ciliary proteins, thereby forming a unique environment that allows for compartmentalization[5, 6] (Figure 1.1).

Primary cilia are dynamic organelles that are cell cycle-coordinated. Cilia assembly occurs when cells become quiescent, while disassembly occurs in cells that re-enter the cell cycle[7-9]. The cilium is built and maintained by intraflagellar transport (IFT), which was first described in the green alga, *Chlamydomonas reinhardtii* and mediates the bidirectional transport of proteins along the ciliary axoneme. IFT can be divided into two multiprotein subcomplexes: IFT complex B (IFT-B) and IFT complex A (IFT-A), which contain 16 and 6 different IFT particles, respectively[10]. IFT-B and the kinesin motor are required for anterograde IFT, which transports protein cargo from the base to the tip of the cilium, whereas IFT-A and the dynein motor are

essential for retrograde IFT, which transports cargo from the tip to the base of the cilium. IFT-A is also required for ciliary entry of signaling and membrane-associated proteins[11-13]. In addition, another protein complex, the BBSome, is comprised of eight Bardet-Biedl Syndrome (BBS) proteins, and is identified as a planar coat that resembles the IFT complex and travels together with IFT complexes like an adaptor along the ciliary axoneme[14]. The BBSome proteins were initially thought to promote ciliary entry of signaling receptors; however, more recent studies now propose that the BBSome is primarily involved in ferrying activated signaling receptors out of primary cilia[15].

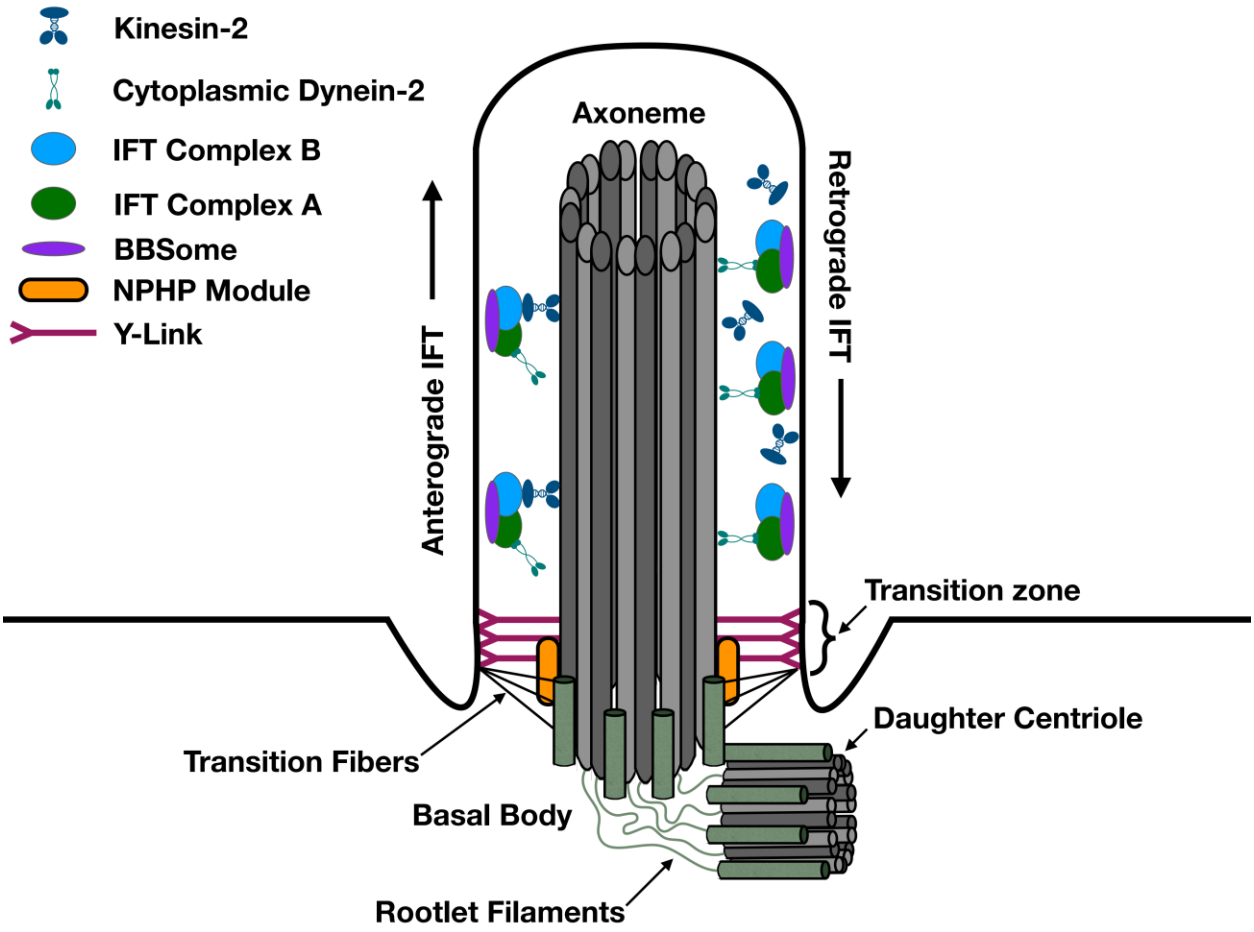

Figure 1.1 Primary cilia structure
Primary cilia consist of an axoneme that extends from a basal body, surrounded by a ciliary membrane. The transition zone and IFT are also represented in the image. Reprinted with permission from Silva, L.M., et al., *Analysis of primary cilia in renal tissue and cells*. Methods Cell Biol, 2019. **153**: p. 205-229.

1.2 Primary cilia function

The unique compartmentalized environment of the cilium is enriched in numerous ion channels such as PC1, PC2 and TRPV4[16, 17], receptors that mediate transduction of signals such as Hedgehog (Hh), Wnt, and pathway intermediates such as mTOR[10]. This compartmentalization allows primary cilia to function as sensory organelles to interpret mechano/chemo- extracellular signals that are essential for embryonic development and homeostasis of adult tissue.

1.2.1 Primary cilia function as a sensory organelle

Primary cilia have been proposed as mechanosensors in many types of cells and tissues. The basal levels of Ca^{2+} are higher in primary cilia[18, 19], and membrane potential is ~30 mV depolarized relative to the cell body[17, 18]. In renal tubule epithelial cells, flow-induced deflection of primary cilia results in an increased level of intracellular calcium in a primary cilia-dependent manner[20, 21]. Similarly, in bile duct cholangiocytes, primary cilia respond to fluid flow with increased Ca^{2+} influx, as well as a decreased intracellular cAMP level[22]. Disruption of cilia significantly inhibited the fluid flow-induced changes in Ca^{2+} and cAMP levels[22].

Much of the early work led to the prevailing hypothesis that several proteins such as the polycystins, TRPM4, TRPV4, and TRPC1[23-27], comprise mechanosensitive Ca^{2+} channels in the ciliary microenvironment, which are activated by fluid flow. This hypothesis, however, was challenged by studies from the Clapham lab, which showed a lack of acute changes in ciliary Ca^{2+} in response to physiological or even highly supraphysiological levels of fluid flow affecting primary cilia of various tissues[28]. These contradictions could be due to the possibility that mechanosensation of primary cilia is not via ciliary Ca^{2+} signaling, or be due to different imaging

techniques used by different investigators. Therefore, how cilia regulate mechanotransduction remains incompletely understood.

1.2.2 Hedgehog signaling

The mammalian Hh pathway, first identified by genetic screens in *Drosophila melanogaster* 40 years ago[29], is the best characterized cilia-dependent pathway, playing essential roles in embryonic development and adult tissue homeostasis. It is a highly conserved evolutionary pathway that is involved in signal transduction from the cell surface to the nucleus. The core components of the Hh pathway include Hh ligands, the Patched receptor (PTCH), the Smoothened signal transducer (SMO), and the Glioma-associated oncogene (GLI) transcription factors[30].

In mammals, canonical Hh signaling occurs only in the presence of primary cilia. There are three Hh ligands: Sonic Hedgehog (*Shh*), Indian Hedgehog (*Ihh*) and Desert Hedgehog (*Dhh*), which act in a tissue-specific manner. *Shh* is the most studied Hh ligand and plays essential roles in the development of multiple organs, including the central nervous system, lungs, teeth, intestines and hair follicles, during embryogenesis[31-37]. *Ihh* is mostly involved in bone development[38], while *Dhh* plays a key role in the differentiation of germ cells[39]. In the absence of Hh ligands, PTCH, a large multipass transmembrane transporter-like protein, is enriched in and around primary cilia to prevent SMO, a 7-transmembrane receptor belonging to the class F (Frizzled) family of GPCRs, from entering into primary cilia, and in this way, represses the activity of SMO[1]. This promotes proteolytic cleavage of GLI transcription factor to the repressor form of GLI (GLIR), which migrates to the nucleus and binds to Hh target gene promoters to switch off transcription[10]. When Hh ligands bind to PTCH, the Hh-PTCH complex exits the cilium and is

degraded in lysosomes[40], which allows SMO to become enriched and activated inside primary cilia. Activated SMO leads to the formation of activator forms of GLI (GLIA), which then migrate to the nucleus and switch on transcription of target genes (Figure 1.2)[41]. There are three members of the GLI family of transcription factors: GLI1, GLI2 and GLI3. GLI1 is an obligate transcriptional activator and its expression, induced by Hh ligand, provides a positive feedback for Hh signaling. GLI2 mainly functions as a transcriptional activator, while GLI3 acts predominantly as a repressor (GLI3R)[42-45]. This canonical Hh signaling cascade is dependent on Hh ligands regulating SMO and the GLI family of transcription factors[30]. Non-canonical Hh signaling pathways, which regulate GLI activity, via cilia-independent, as well as GLI- or SMO-independent mechanisms also occur[10]. However, these pathways are less understood than canonical Hh signaling.

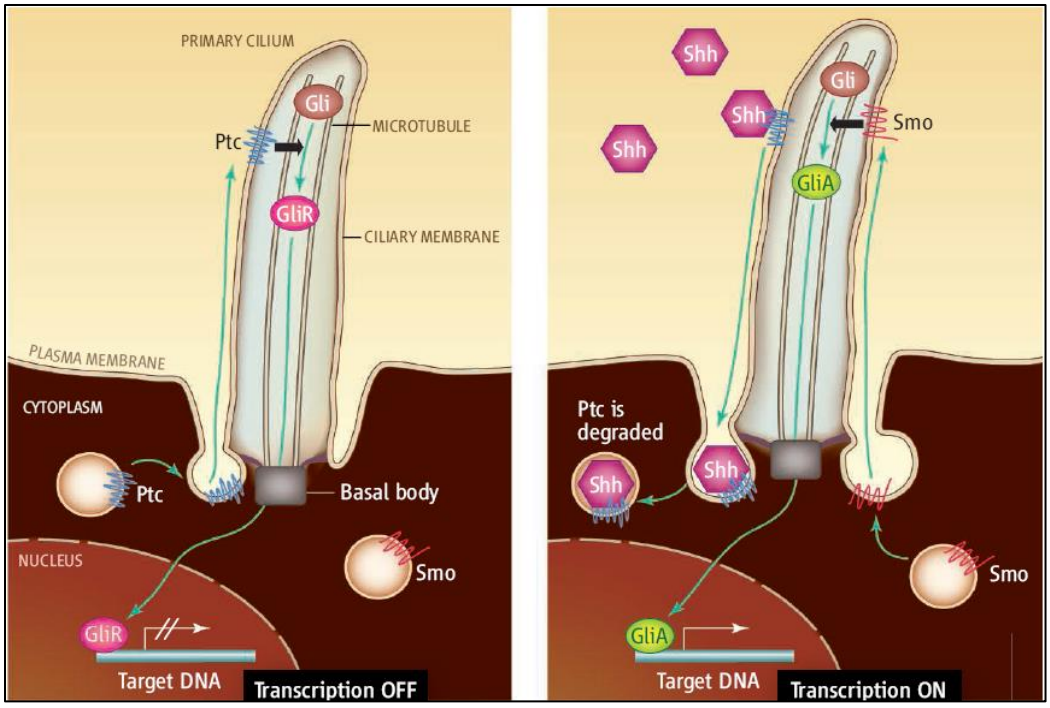

Figure 1.2 Schematic diagram of mammalian hedgehog signaling
Left: in the absence of Hh ligands, PTCH receptor is localized in primary cilia, preventing SMO entering the primary cilia. Right: in the presence of Hh ligand, the Hh-PTCH complex exits the cilium, which allows SMO to be enriched in the cilium and leads to the formation of the active form of GLI (GLIA) transcription factors. GLIA transcription factors translocate to the nucleus to switch on Hh target gene transcription. From Christensen ST, Ott CM., *Cell signaling. A ciliary signaling switch.* Science 2007. **317**(5836): p. 330-1. Reprinted with permission from AAAS Image.

Most components of the canonical Hh pathway localize to primary cilia in a dynamic manner, indicating that primary cilia play a critical role in coordinating Hh signaling. Genetic screens and targeted mutations have identified numerous cilia-associated proteins in vertebrate Hh signaling[46]. In mice, IFT is required for Hh transduction during embryonic development. Mutations in *Ift-B* genes, such as *Ift72*[47], *Ift88*[47], *Ift52*[48], and *Ift57*[49], cause absent or shortened primary cilia and reduced Hh signaling with a loss of ventral markers in the caudal neural tube[45]. Mutations in *Ift-A* genes show a more complex effect on Hh signaling. Deletion of *Thm1*[50] and *Ift122*[51] results in shortened cilia with proteins accumulated at the distal tip and has been shown to increase Hh signaling during embryogenesis, with expansion of ventral markers in the caudal neural tube[45]. This activation of the Hh pathway in *Ift-A* mutants is independent of Hh ligand, indicating that IFT-A plays a specific role in keeping the pathway turned off in the absence of ligand[52]. A hypomorphic mutation in *Ift144* shows similar ciliary and neural tube phenotypes as those seen in *Thm1* and *Ift122* mutants. However, a null mutation in *Ift144* that results in very short cilia causes reduced Hh signaling in the neural tube. Additional loss of *Ift122* in the hypomophic *Ift144* mutants produces short bulged cilia and a loss of Hh signaling similar to the null *Ift144* mutants, suggesting that some IFT-A proteins have overlapping functions[53]. In addition to IFT proteins, disruption of ciliary membrane proteins can also affect Hh signaling. In the absence of ARL13B, an ARF-family GTPase, cilia are shortened, and the neural tube fails to specify both the most ventral and the most dorsal cell types[54]. Deletion of *Inpp5e*, which encodes a phosphoinositide 5-phosphatase to regulate ciliary phosphoinositide content, leads to inappropriately increased levels of TULP3 and IFT-A proteins in cilia with disrupted Hh signaling[55, 56]. Collectively, these data suggest that Hh signaling is finely tuned by primary cilia.

1.2.3 Other cilia-associated signaling pathways

Several other receptors, including Wnt[57], Notch[58], and transforming growth factor β (TGFβ)[59] were identified in the membrane of primary cilia, suggesting that primary cilia regulate other signaling pathways.

The role of primary cilia in coordinating Wnt signaling is controversial. Wnt signaling is evolutionarily conserved and includes two prominent branches: canonical Wnt-β-catenin and non-canonical Wnt-planar cell polarity (PCP) pathways. In the canonical pathway, Wnt ligands bind to Frizzled receptors to promote stabilization of the transcription factor β-catenin, which enters the nucleus to activate Wnt signaling[60]. When *Kif3a*, which encodes a ciliary motor protein that facilitates anterograde IFT, is mutated in mouse embryos, there are increased levels of canonical Wnt singling; and mouse embryonic fibroblasts (MEFs) with disrupted ciliogenesis respond more robustly to a Wnt ligand[61]. This work reveals that primary cilia restrain Wnt signaling. However, extensive analysis of *Kif3a, IFT88, Dync2h1,* and *Thm1* mutant embryos *in vivo* and MEFs *in vitro* shows normal Wnt activity[62]; and mutations in *Ift* genes in mouse embryos do not cause phenotypes that are associated with Wnt signaling dysregulation, such as gastrulation and axis duplications[1]. Thus, the role of primary cilia in regulating Wnt signaling still remains unclear; these results suggest that Wnt signaling is probably partially associated with cilia in a tissue-specific manner and within a constrained window of time. Further effort to explore the links between Wnt signaling and primary cilia are necessary.

1.3 Ciliopathies

Dysfunction of motile and/or primary cilia results in numerous diseases and developmental disorders, collectively termed ciliopathies. Since cilia exist on almost every cell throughout the

body, ciliopathies affect nearly all organ systems, with overlapping clinical manifestations, including polycystic kidney disease, polycystic liver disease, retinal degeneration, obesity, skeletal malformations, brain anomalies and infertility[1] (Figure 1.3). There are no curative therapies available for patients, instead, symptomatic therapies are the main treatments for ciliopathies. The number of currently reported ciliopathies is 35 and is likely increasing, as well as the number of ciliopathy-associated genes[63]. Understanding the etiology and molecular mechanisms of ciliopathies can increase our knowledge of how cilia are built and maintained and how cilia function physiologically in a healthy population. Importantly, even though ciliopathies are rare genetic disorders with an incidence of 1:1000 to 1:150,000[64], some of the same clinical manifestations, such as obesity and male infertility, are also present in the general population. For instance, obesity affects more than 1 in 3 adults in the United States[64]. Infertility affects around 7 percent of adult males[65]. Thus, investigating the molecular mechanisms in ciliopathy patients may help us to understand potentially shared etiologies of similar diseases in the general population.

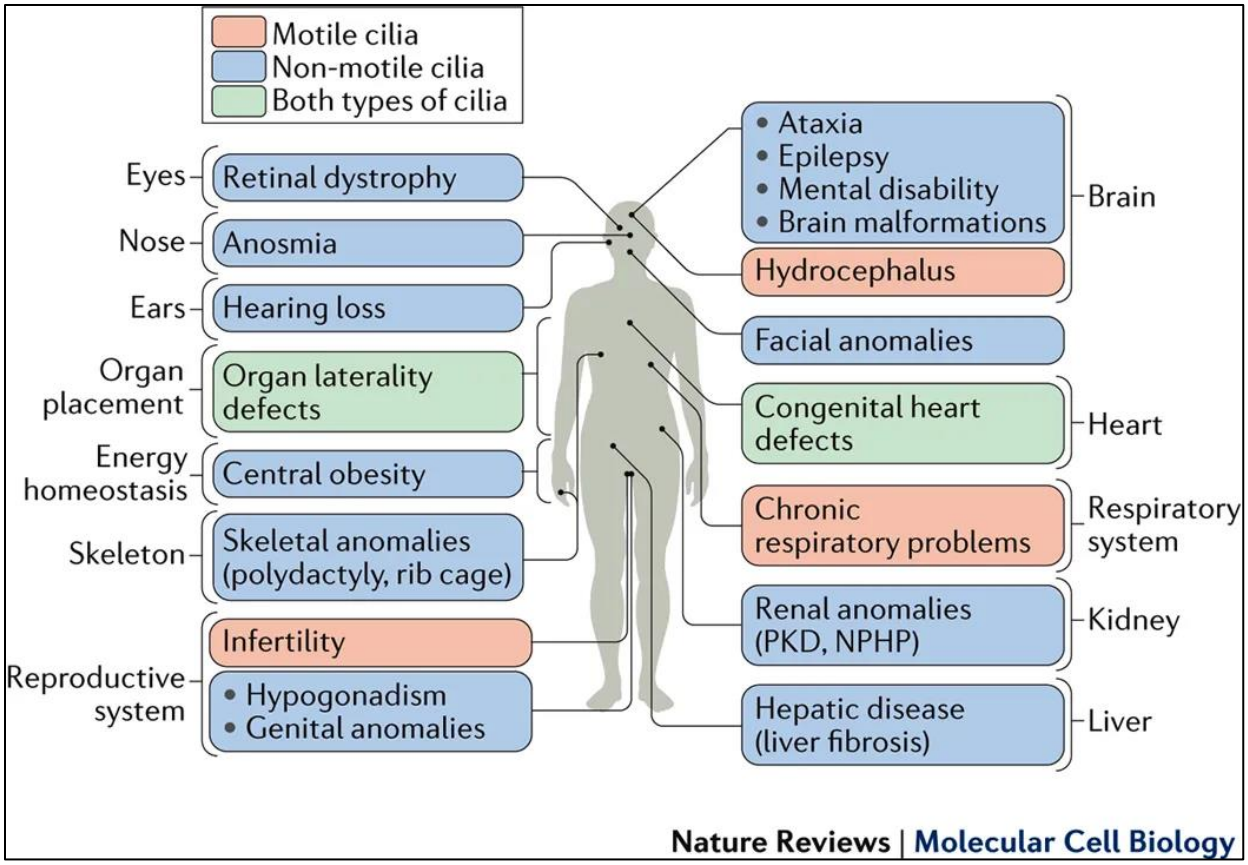

Figure 1.3 Clinical manifestations of ciliopathies
Diagram shows the different organ systems or tissues that are affected in diverse ciliopathies. Renal manifestations of ciliopathies are the most common abnormalities and are the focus of my study. Reprinted with permission from Reiter, J.F. and M.R. Leroux, *Genes and molecular pathways underpinning ciliopathies.* Nature Reviews Molecular Cell Biology, 2017. **18**(9): p. 533-547.

1.4 Renal cystic disease

Within the kidney, primary cilia are present on the apical surface of renal tubular cells and project into the lumen of the renal tubule, possibly affecting urine flow and indirectly its composition and osmolarity[66]. Ciliary dysfunction, at any age of life, can cause development of cystic kidneys, which represent the most common defects associated with ciliopathies. There are numerous ciliopathy-associated genes that can cause various cystic kidney diseases. The most common cystic kidney disease is Autosomal Dominant Polycystic Kidney Disease (ADPKD) [67], which occurs in approximately one in 1000-2500 adults worldwide[68, 69]. Other cystic kidney diseases include autosomal recessive polycystic kidney disease (ARPKD), nephronophthisis (NPHP), Bardet–Biedl syndrome (BBS), Meckel–Gruber syndrome (MKS), Joubert syndrome and related disorders (JSRD) as well as X-linked oral-facial-digital syndrome[66]. These inherited disorders are rare individually, however, the cumulative incidence rate adds up to about one in 2000 people[66, 70].

1.4.1 ADPKD

Although disease progression and prognosis are highly variable, ADPKD is characterized by the slow development and growth of fluid-filled renal cysts throughout an individual's lifetime (Figure1.4)[71]. Renal cysts can form as early as in utero, while kidney dysfunction is usually not apparent until the age of 30 to 40 years[72]. Approximately half of ADPKD patients will progress to end-stage renal disease (ERSD) between the fifth and sixth decade of life, which is the fourth leading cause of renal replacement therapy (RRT) including dialysis or kidney transplantation[73]. The majority of patients with ADPKD experience symptoms such as acute or chronic kidney pain, gross hematuria and cyst infection due to cyst expansion and kidney enlargement. Hypertension is

also very common in ADPKD patients with early stage disease who have a decreased glomerular filtration rate (GFR)[74]. As ciliopathies are multi-organ diseases, affected individuals can have extrarenal manifestations including hepatic and pancreatic cysts, intracranial aneurysms, abdominal hernias, and cardiac valvular lesions. Among them, liver cysts occur most frequently with a prevalence of 95% of ADPKD patients having these by the age of 35 years[75].

Figure 1.4 ADPKD in human
Kidneys of a 48-year old man with ADPKD. Reproduced with permission from Ekser, B. and P. Rigotti, *Images in clinical medicine. Autosomal dominant polycystic kidney disease.* N Engl J Med, 2010. **363**(1): p. 71, Copyright Massachusetts Medical Society.

1.4.2 ADPKD genetics and proteins

ADPKD is a genetically heterogeneous disorder that is caused mainly by mutations in *PKD1* (approximately 78%) and *PKD2* (approximately 15%), which encode the polycystin-1 (PC1) and polycystin-2 (PC2) proteins, respectively[76]. In 2016, genetic analysis in nine families with ADPKD uncovered a third gene, *GANAB*, in which mutations accounted for approximately 0.3% of ADPKD cases[77]. *GANAB* encodes the α subunit of glucosidase II, an enzyme of the endoplasmic reticulum involved in N-linked glycosylation. Dysfunction of the glucosidase II α subunit is associated with disrupted folding, maturation, and trafficking of membrane and secreted proteins, including PC1[77]. Recently, a new gene, *DNAJB11,* was identified by whole-exome sequencing in families with atypical presentation of ADPKD[78]. *DNAJB11* encodes a glycoprotein that functions as a co-chaperone of binding immunoglobulin protein (BiP), which is involved in proper folding and assembly of PC1 in the endoplasmic reticulum lumen[78]. The severity of ADPKD is strongly influenced by the particular mutation and the gene that is mutated. More than 1750 different mutations in *PKD1* and *PKD2* are described in the ADPKD mutation database[76]. In general, patients with a *PKD1* mutation have more severe clinical manifestations with a larger height-adjusted total kidney volume (HtTKV) and lower GFR than those of patients with a *PKD2* mutation[79]. Patients with a *GANAB* mutation have a relatively mild disease which is unlikely to progress to ESRD[77] . ADPKD with *DNAJB11* mutation is characterized by normal-si zed cystic kidneys yet progressive interstitial fibrosis resulting in late-onset ESRD[78].

PC1 is a large transmembrane protein of 4,303 amino acids, and has uncertain functions[80]. PC1 is comprised of an extensive N-terminal extracellular domain, 11 transmembrane domains, and a short cytoplasmic C-terminal domain (Figure 1.5)[81]. The extracellular domain contains a G protein-coupled receptor proteolytic site (GPS), where PC1 is

cleaved to generate a large N-terminal fragment that is subsequently tethered non-covalently to the C-terminal fragment [82]. This GPS cleavage provides a regulatory mechanism of PC1 biogenesis and trafficking[83]. The extracellular domain also contains other domains that are thought to bind to various proteins and carbohydrates, and are involved in cell-cell or cell-matrix interactions[84]. The cytoplasmic tail of PC1 interacts with the coiled-coil domain of PC2 [85]. The C-terminal tail also contains several proteolytic cleavage sites and a nuclear localization sequence (NLS). Thus cleaved C-terminal fragments can translocate to the nucleus and interact with transcription factors to regulate multiple signaling cascades[86]. In addition, PC1 has been proposed to function as a non-typical G protein coupled receptor with the C-terminal tail binding to heterotrimeric G proteins to activate G protein-associated pathways[84]. PC1 is present mainly on the membrane of primary cilia as well as in cell junctions such as focal adhesions, desmosomes, tight junctions and adherens junctions [87], indicating that PC1 plays critical roles in ciliary function and cell-cell/matrix interactions. Recent studies also reported that PC1 exists in urinary exosomes secreted by the renal epithelial cells[88].

PC2, a 968 amino acid transmembrane protein with six transmembrane domains and cytoplasmic N- and C- terminal domains (Figure 1.5), is a member of the transient receptor potential (TRP) cation channel family that localizes to the plasma membrane, endoplasmic reticulum and primary cilia[87]. As a TRP family member, PC2 forms a homotetrameric nonselective cation channel that is permeable to Ca^{2+}, Na^{+} and K^{+} ions and regulated by membrane depolarization and intracellular Ca^{2+} levels[89-91]. Furthermore, PC2 can form heteromeric channels via association with PC1 or other TRP channel subunits, including TRPC1 and TRPV4[92, 93]. Mutations in *PKD1* or *PKD2* produce similar phenotypes, indicating that PC1 and PC2 form protein complexes that work together. Structural analysis with cryo-electron

microscopy indicates that one PC1 interacts with three PC2 to form a non-canonical TRP channel architecture[94]. The function of the PC1-PC2 complex remains controversial. A prevailing hypothesis was that PC1 acts as a mechanosensing protein via its large extracellular domain, activating PC2 Ca^{2+} channels in the ciliary membrane in response to fluid flow. However, this theory was challenged by a study that reported the absence of a ciliary Ca^{2+} current in response to flow stimulus[28]. Further studies are required to better understand the role of the PC1-PC2 complex in regulating cellular Ca^{2+} influx. Nonetheless, it is widely agreed upon that the polycystins are important in maintaining cell function in multiple tissue types.

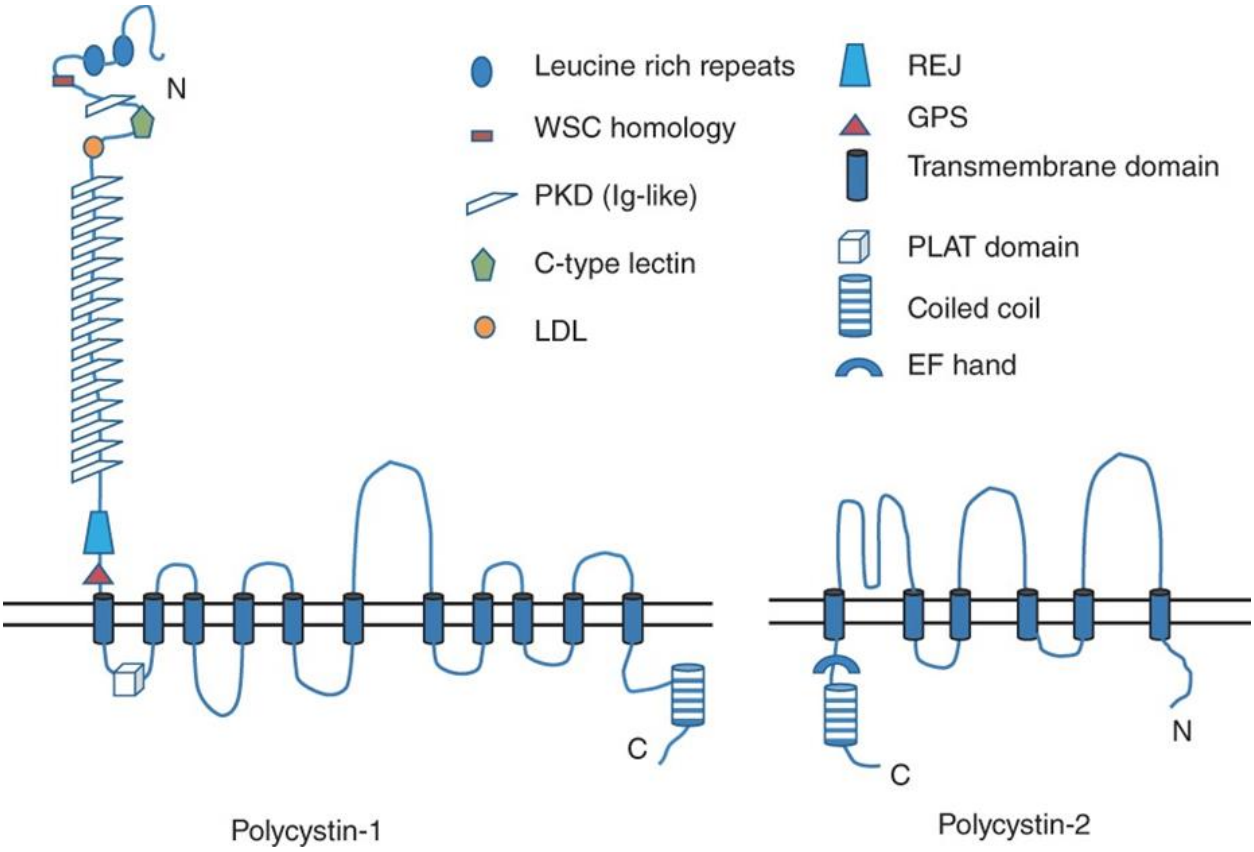

Figure 1.5 Structure of PC1 and PC2
PC1 and PC2 are multispan membrane proteins. PC1 has a large extracellular N-terminal domain and a short C-terminal tail, while PC2 has cytoplasmic N- and C- termini. Reprinted with permission from Paul, B.M. and G.B. Vanden Heuvel, *Kidney: polycystic kidney disease*. Wiley Interdiscip Rev Dev Biol, 2014. **3**(6): p. 465-87.

1.4.3 Mechanisms of renal cystogenesis

ADPKD patients inherit the disease in an autosomal dominant manner. Yet most cells with a germ-line mutation in one allele of *PKD1* or *PKD2* function normally, and cyst formation occurs in only a minority (less than 1%) of nephrons throughout the kidney[84], indicating that there is likely a second initiating event causing cystogenesis. One explanation is that a second somatic mutation in the remaining normal allele occurs to cause complete loss of *PKD* gene function[95, 96]. Another explanation is that reduced levels of functional PC1 or PC2 below a critical threshold, due to genetic, environmental or stochastic factors, may initiate renal cystogenesis[97, 98]. Once this happens, abnormal cell proliferation leads to dilation of renal tubules. As aberrant proliferation continues, the dilated region can become isolated and separate from the parental tubule to form a cyst. The cyst then enlarges over decades through continuous cell proliferation and fluid secretion, which are two hallmark features of ADPKD (Figure 1.6).

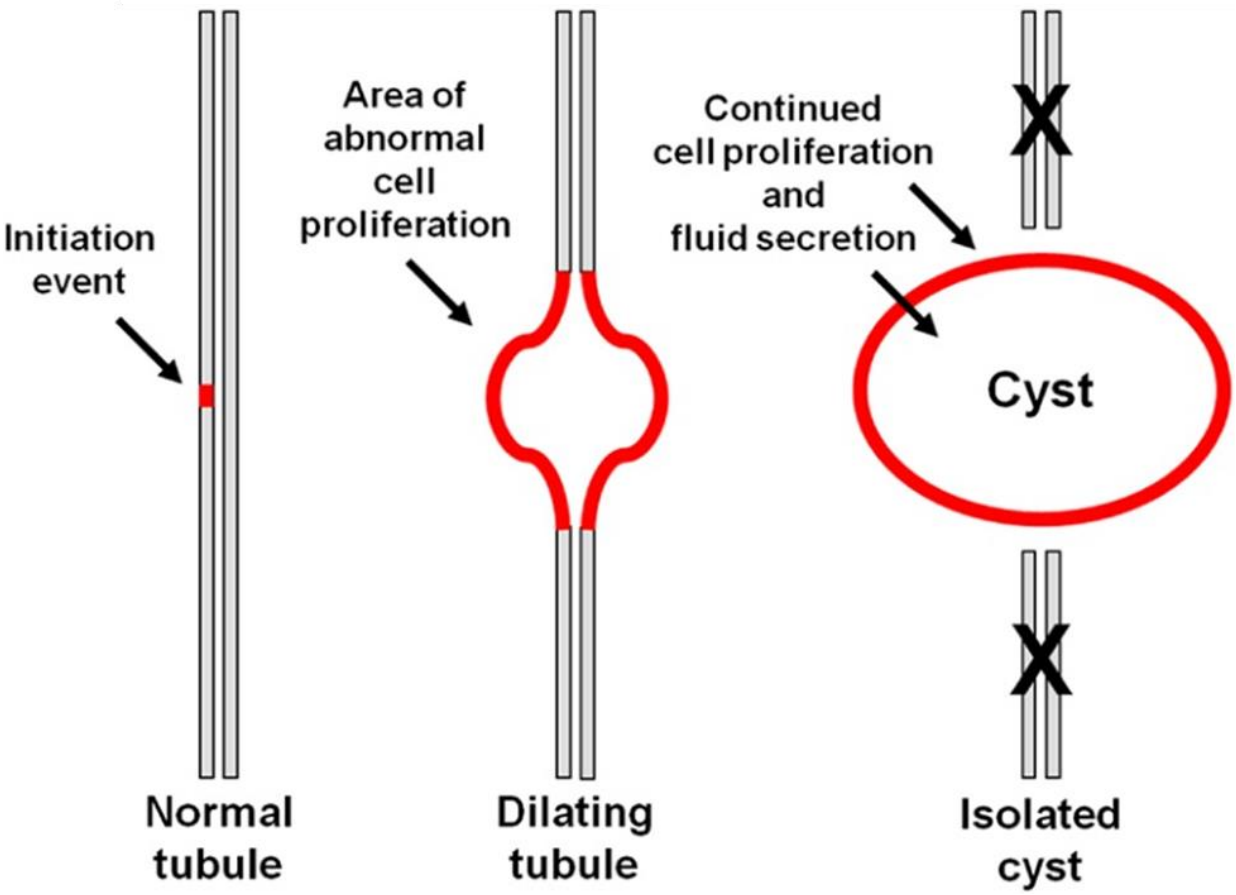

Figure 1.6 The process of cyst formation in ADPKD
An initiation event—either a second somatic mutation or threshold event, triggers abnormal cell proliferation that causes dilation in a small region of the tubule. Continued dilation separates from the nephron that leads to the formation of cysts, which keeps growing due to continued cell proliferation and fluid secretion. Reprinted with permission from Calvet, J.P., *The Role of Calcium and Cyclic AMP in PKD*, Polycystic Kidney Disease, X. Li, Editor. 2015, Codon Publications. Copyright: The Author.: Brisbane (AU). https://doi.org/10.15586/codon.pkd.2015.ch8

The second messenger adenosine 3', 5' cyclic monophosphate (cAMP) is influential in driving both cell proliferation and fluid secretion. High levels of cAMP are observed in primary renal cells derived from ADPKD patients, as well as in kidneys of PKD animal models [99, 100]. Many different pathways impact cAMP production and the cellular effect of cAMP. Abnormal Ca^{2+} homeostasis leading to reduced intracellular Ca^{2+} levels, due to dysfunction of PC1 and PC2 in kidney epithelial cells, promotes the proliferative effect of cAMP[101-103]. Additionally, decreased cytoplasmic Ca^{2+} leads to increased activity of adenylate cyclases (AC) and decreased activity of phosphodiesterases (PDEs), which results in increased levels of cAMP. Increased intracellular cAMP further drives activation of PKA-dependent signaling pathways, including cystic fibrosis transmembrane conductance regulator (CFTR)-mediated fluid secretion and several proliferative pathways, such as MAPK, mTOR, Wnt and STAT3 pathways[74] (Figure 1.7). Additionally, vasopressin 2 (V_2) receptor are present in the collecting ducts and distal convoluted ducts of mammalian kidney, and arginine vasopressin (AVP), can activate AC activity and stimulate cAMP production. The V2 receptor inhibitor, tolvaptan, which can reduce the increase in kidney size, slows the decline of renal function, and delays the onset of ESRD, is the only FDA-approved treatment for patients with ADPKD[104].

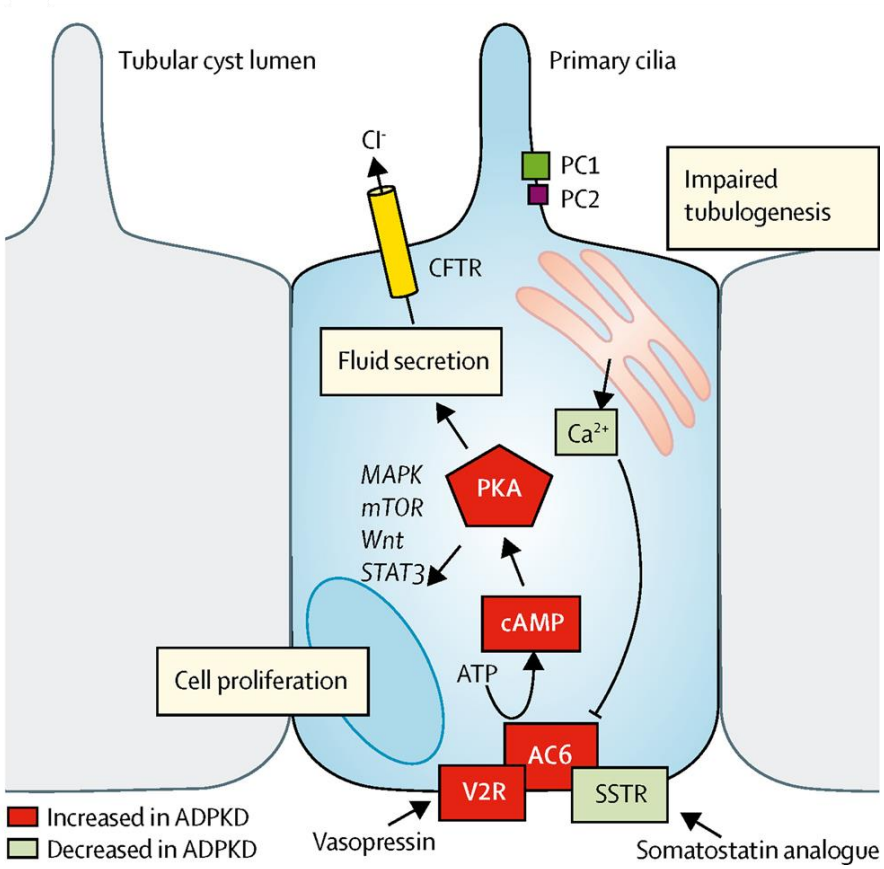

Figure 1.7 Mechanisms of cyst formation
A reduction of cytosolic Ca^{2+} levels result in increased intracellular cAMP concentrations, leading to activation of PKA regulated signaling pathways associated with fluid secretion and cell proliferation. Reprinted with permission from Cornec-Le Gall, E., A. Alam, and R.D. Perrone, *Autosomal dominant polycystic kidney disease*. The Lancet, 2019. **393**(10174): p. 919-935.

1.4.4 ARPKD

Autosomal recessive polycystic kidney disease (ARPKD) is a much rarer disease than ADPKD, with an incidence rate of 1 in 20,000 live births[105]. ARPKD primarily affects neonates and children can present with severe polycystic kidneys, biliary tract defects, pulmonary hypoplasia, a characteristic facies, and contracted limbs with club feet[106]. Approximately 30-40% of ARPKD neonates die shortly after birth, because of respiratory insufficiency caused by pulmonary hypoplasia[80]. For patients who survive the perinatal period, clinical manifestations are highly variable including systemic hypertension, renal dysfunction and portal hypertension[84]. Most ARPKD patients have mutations in *PKHD1*, which encodes fibrocystin, a large single transmembrane protein with an extensive extracellular N-terminal domain and a short C-terminal domain[105]. In addition, mutations in the gene, *DZIP1L*, which encodes a soluble zinc finger protein that localizes to the ciliary transition zone have also been described in some clinically moderate ARPKD patients[107].

1.4.5 PKD murine models

A number of animal models have been generated to investigate the pathogenesis of PKD as well as to test potential therapeutic treatments for PKD preclinically. There are two major types of murine PKD models: 1) genetically engineered models that harbor mutations in the human ADPKD orthologous genes, *Pkd1* and *Pkd2*, and 2) spontaneous hereditary models identified by the typical manifestations of PKD, yet with mutations in genes that are non-orthologous to the human ADPKD genes[108]. Homozygous loss of *Pkd1* or *Pkd2* in the germline is embryonic lethal and causes defects in formation of the kidney, pancreas, heart and lung[84]. Thus, to generate PKD models that survive postnatally and more closely mimic the human disease, additional alleles, such

as conditional, hypomorphic and overexpressing, have been designed. For example, conditional deletion of *Pkd1* in kidney tubule epithelial cells using *Pkhd1*-Cre and *Ksp*-Cre recombinases generates rapidly-progressing PKD models that develop kidney failure around the time of weaning[109]. Furthermore, the use of an inducible Cre system to delete *Pkd1* or *Pkd2* at different time points has revealed "a critical window" for renal cystogenesis. When *Pkd1* is deleted on or before postnatal day 12 (P12), severe PKD develops within 3 weeks, whereas deletion of *Pkd1* after P12 results in slowly-progressing PKD with a late renal cystic phenotype around 5 to 6 months of age[84]. One example of a spontaneous hereditary model is the *jck* (*juvenile cystic kidney*) mouse mutant. The *jck* allele has a missense mutation in the gene *Nek8*, which encodes NIMA (never in mitosis A)-related kinase 8[110]. The mutated gene product localizes to the proximal end of primary cilia. *jck* mice have been reported to develop a relatively slowly progressing cystic kidney disease, with obvious cystic disease around 8 weeks of age which resembles human ADPKD.

1.4.6 Primary cilia in PKD

Primary cilia play an essential role in the pathobiology of PKD. The first association between primary cilia and PKD was found in a PKD mouse model with mutations in *Tg737*, the orthologue of *Chlamydomonas ift88*. Primary cilia in the mutant kidneys are shorter than normal, indicating that ciliary defects can lead to PKD [111]. Additionally, in *jck* mutant mice, primary cilia in kidneys are significantly lengthened relative to those of control mice[112]. Subsequent studies showed that polycystins, as well as other protein products of PKD-associated genes, localize to primary cilia, suggesting that primary cilia may be central organelles in cystic kidney disease. Further, although PC1 and PC2 also localize to other subcellular compartments, such as

the plasma membrane and ER, analyses of human ADPKD primary renal epithelial cells, of genetic mouse models harboring human ADPKD mutations, and more recently, of an ENU-induced mouse mutant of *Pkd2* that causes exclusion of PC2 from the cilium, have demonstrated that absence or deficiency of PC1 and/or PC2 from the cilium is sufficient to cause ADPKD[113-115]. Interestingly, disruption of primary cilia in PKD adult mouse models either by mutation of ciliary genes or pharmacologically attenuates ADPKD severity, indicating that there is a component of cilia dysfunction that may have potential therapeutic value in ADPKD [42, 112, 116, 117].

1.5 Liver cystic disease

1.5.1 Overview of liver cystic disease

Liver cysts are relatively common and are increasingly found using routine abdominal imaging techniques in approximately 2.5-18% of the general population[118]. Polycystic liver disease (PLD) is characterized by the formation of numerous (>20) fluid-filled cysts in the liver that are derived from the biliary epithelial cells, termed cholangiocytes (Figure 1.8) [119, 120]. The severity of PLD can vary from the presence of a few small cysts to enlarged cysts causing hepatomegaly[80]. Unlike PKD that ultimately leads to renal dysfunction, PLD rarely causes hepatic insufficiency and most PLD is asymptomatic[121]. 20% of PLD patients have clinical manifestations including pain, digestive disorders and respiratory discomfort, that may be due to hepatomegaly or cyst complications, such as hemorrhage or infection[122]. Being female and increasing age are risk factors for more severe PLD[74]. Surgical interventions such as cyst aspiration and sclerosis, open or laparoscopic fenestration, liver resection with fenestration, and liver transplantation are used to alleviate symptoms and are tailored to individual patients[123].

PLD can be divided into two distinct hereditary disorders: 1) PLD in association with ADPKD and 2) PLD in isolation. In most cases, PLD occurs as an extrarenal manifestation of ADPKD patients. Hepatic cysts can be found in up to 94% of ADPKD patients older than 35 years of age[124]. PLD in the absence of renal impairment, is termed autosomal dominant PLD (ADPLD), a much rarer disease, affecting approximately 1 in 100,000 individuals[125]. ADPLD patients often have more and larger liver cysts, but their kidney function is typically not impaired[126].

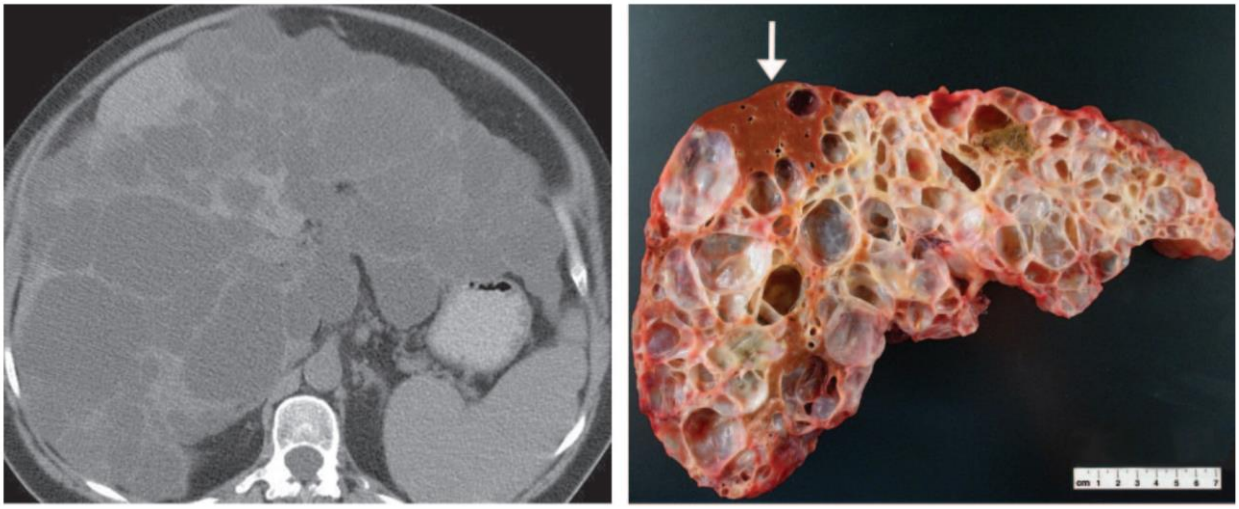

Figure 1.8 PLD in human
CT scan (left) and photograph of the sectioned cystic liver of a 58-year old woman with ADPKD. Reprinted with permission from Morgan D E, Lockhart M E, Canon C L, et al. *Polycystic liver disease: Multimodality imaging for complications and transplant evaluation*. RadioGraphics 2006; **26**: 1655-1668.

1.5.2 Genetics and proteins

ADPLD is caused by mutations in several genes. Mutations in *PRKCSH* (~15% of patients), *SEC63* (~7% of patients), *LRP5, GANAB, SEC61B, ALG8* and *PKHD1* have been identified in nearly 30% of ADPLD cases[119]. However, more than 70% of patients do not have an identifiable mutation. Mutations in *PKHD1*, which encodes fibrocystin, causes hepatic cystic dilations and liver fibrosis in ARPKD patients[127]. *LRP5* encodes LDL Receptor Related Protein 5 (LRP5), which is a transmembrane co-receptor that interacts with Frizzled receptors. The Frizzled/LRP complex can bind to Wnt to activate the canonical (β-catenin-dependent) Wnt pathway[128]. Except for *LRP5*, all other ADPLD-associated genes, encode proteins that localize to the ER to regulate protein maturation, folding and translocation (Figure 1.9)[129]. *ALG8* encodes Alpha-1,3-Glucosyltransferase (ALG8), which catalyzes the addition of the second glucose residue during ER protein glycosylation. *SEC63* and *SEC61B* encode proteins that form a complex that facilitates translocation of nascent polypeptides within the ER. Glucosidase II, which is composed of subunits α (GIIα) and β (GIIβ), encoded by *PRKCSH* and *GANAB* respectively, removes the second glucose, a process that is important for protein folding and quality control[130]. Since ADPLD is inherited in a dominant fashion, second-hit mutations that cause loss of heterozygosity in other genes associated with PLD, have been suggested in the pathogenesis of PLD.

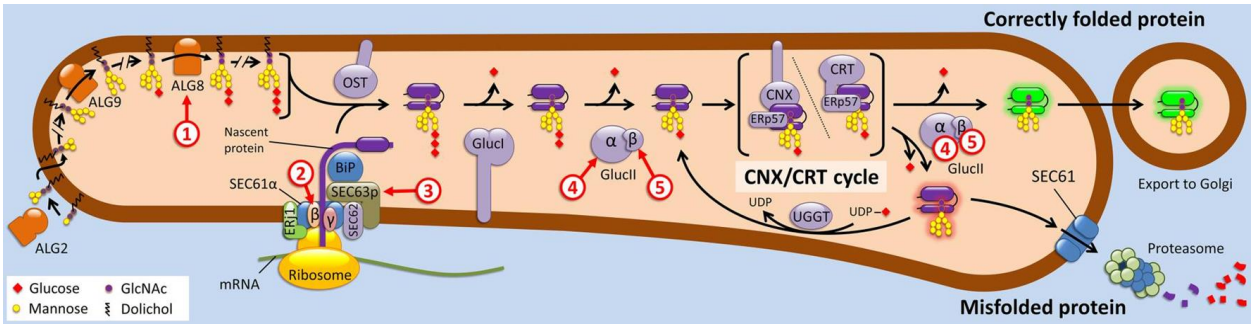

Figure 1.9 PLD-associated gene products in the ER biogenesis pathway
The gene products of *ALG8* (1), *SEC61B* (2), *SEC63* (3), *PRKCSH* (4) and *GANAB* (5) are all involved in the translocation and maturation of glycoproteins in the endoplasmic reticulum. Reprinted with permission from Besse, W., et al., *Isolated polycystic liver disease genes define effectors of polycystin-1 function*. The Journal of Clinical Investigation, 2017. **127**(5): p. 1772-1785. doi:10.1172/JCI90129

1.5.3 Mechanisms of hepatic cystogenesis

1.5.3.1 Ductal plate malformation

Key processes that lead to hepatic cystogenesis initiate during fetal development[131]. Accumulating evidence suggests that hepatic cystogenesis results from embryonic ductal plate malformation (DPM), which causes arrest of ductal plate development[132]. The ductal plate is established by a layer of hepatoblasts immediately adjacent to the portal tract mesenchyme, and is progressively remodeled to generate biliary tract cholangiocytes and periportal hepatocytes during biliary tract development[133]. Mechanisms driving DPM remain unclear, but studies implicate aberrant Notch, transforming growth factor β (TGFβ) and Wnt signaling pathways.

1.5.3.2 Primary cilia dysfunction

Primary cilia play an essential role in the pathogenesis of hepatic cystogenesis. Intrahepatic bile ducts are lined with ciliated cholangiocytes. Primary cilia on these cholangiocytes detect and transduce extracellular mechanical, chemical and osmotic signals into intracellular signaling cascades to regulate cholangiocyte proliferation and homeostasis[127]. Indeed, abnormalities of primary cilia in cholangiocytes are features of PLD animal models and ADPKD patients [134-136]. In addition, cystic livers, together with hepatic fibrosis, are frequently observed in ciliopathies such as Meckel-Gruber syndrome (MKS), nephronophthisis and Bardet-Biedl syndrome (BBS)[131]. Although most PLD-associated genes encode proteins that do not localize to primary cilia, disruption of these genes leads to aberrant expression and ciliary localization of PC1, which has been defined as the rate-limiting component in determining the severity of hepatic cystogenesis[132]. PC1 needs to translocate to primary cilia to fulfil its function, linking this

organelle to cyst formation in the liver. Disruption of PC1/PC2 results in decreased cytoplasmic Ca^{2+} concentrations and increased cAMP levels in cholangiocytes to drive cyst formation[128].

1.5.3.3 Enhanced proliferation and altered secretion.

PLD is characterized by enhanced proliferation of cholangiocytes[127]. Overproduction of cAMP, which activates the Ras/Raf/MEK/ERK1/2 signaling pathway in a PKA-dependent manner, is the major proliferative stimulus[137]. In addition, cholangiocytes are also sensitive to other growth factors such as epidermal growth factor (EGF), vascular endothelial growth factor (VEGF) and insulin-like growth factor 1 (IGF1) to induce cellular proliferation[132]. Altered fluid secretion into the lumen of the biliary ducts also plays a key role in hepatic cystogenesis. Increased levels of cAMP facilitate fluid secretion via activation of the chloride channel cystic fibrosis transmembrane conductance regulator (CFTR), anion exchange protein 2 (AE2), and aquaporin 1 (AQP1) in the apical membrane of cholangiocytes[127]. PLD animal models show overexpression and mislocalization of these apical plasma membrane proteins at the basolateral membrane[138].

1.6 THM1 and THM2

1.6.1 THM1

Tetratricopeptide repeat–containing hedgehog modulator-1 (*Thm1;* also known as *Ttc21b,* an orthologue of *Chlamydomonas reinhardtii Fla17/Ift139*) encodes an IFT-A protein of 1,317-amino acids, with a molecular weight of ~ 150 kDa and 11 predicted tetratricopeptide repeat (TPR) domains[50]. Loss of *Thm1* results in ciliopathies that affect multiple tissues. The role of *Thm1* was first revealed in a *N*-ethyl-*N*-nitrosourea–induced mutant mouse, *alien* (*aln*), which is homozygous for a missense mutation that causes absence of protein [50]. Early embryonic loss of

Thm1 causes perinatal lethality, preaxial polydactyly, split and fused ribs, cortical layering abnormalities, delayed eye and forebrain development, and neural tube defects[50, 139, 140]. Conditional deletion of *Thm1* in neural crest cells and surface ectoderm results in an enlarged forebrain and a failure of fusion between the frontonasal, lateral nasal and maxillary prominences in a time-dependent manner during forebrain and oral craniofacial development[141, 142]. This revealed a spatiotemporal requirement for *Thm1* in early development. In addition, global deletion of *Thm1* perinatally causes cystic kidney disease (Figure 1.10)[143], and its global deletion in adulthood causes obesity (Figure 1.10)[144, 145].

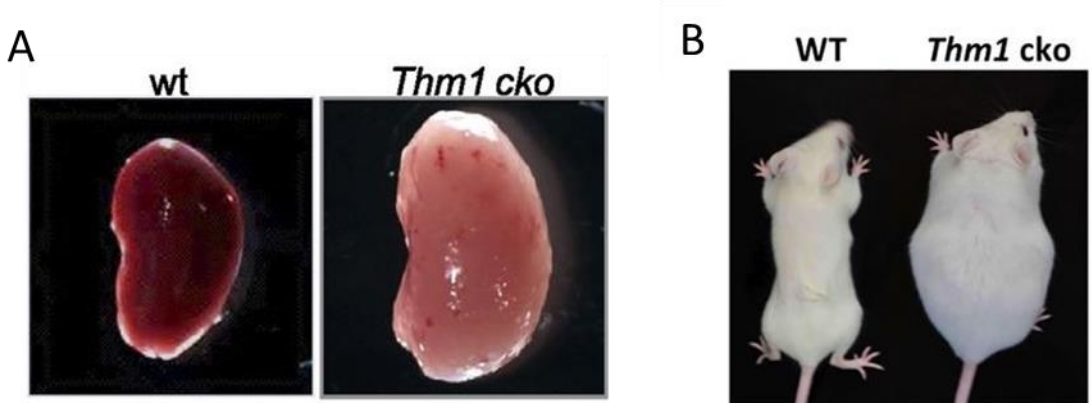

Figure 1.10 Loss of *Thm1* causes cystic kidney disease and obesity
(A) Whole-mount images of 6-week-old wt and *Thm1* cko kidneys with tamoxifen injection at E17.5; (B)Ad libitum-fed WT and *Thm1*-cko mice 13 weeks post-tamoxifen injection at 5 weeks of age. (A) Reprinted with permission taken from Tran, P.V., et al., *Downregulating hedgehog signaling reduces renal cystogenic potential of mouse models*. J Am Soc Nephrol, 2014. **25**(10): p. 2201-12. (B) Reprinted with permission from Jacobs, D.T., et al., *Dysfunction of intraflagellar transport-A causes hyperphagia-induced obesity and metabolic syndrome*. Dis Model Mech. 2016. **9**(7): p. 789-98.

THM1 localizes as puncta throughout the ciliary axoneme [50]. Analysis of the IFT-A complex with a visible immunoprecipitation assay revealed that the complex is divided into a core subcomplex (IFT122, IFT140 and IFT144) and a peripheral subcomplex (IFT143, IFT121 and THM1/IFT139), and THM1 localizes most distally in the peripheral subcomplex (Figure 1.11)[146]. Disruption of THM1 results in a shortened primary cilium with ciliary proteins (such as IFT-A, IFT-B and GPCRs) accumulating at the distal tip forming a bulb-like structure (Figure 1.11), consistent with retrograde IFT defects[50, 146, 147]. Data suggest that THM1 regulates Hh signaling in a positive or negative manner, depending on cell-type. In *Thm1*-null mouse embryos, the neural tube is ventralized and *Ptch1* expression is increased in the region of the maxilla and first branchial arches and in the somites, indicating overactivation of the Hh signaling pathway[50]. Inappropriate activation of Hh signaling has also been demonstrated in the embryonic forebrain of *Thm1*-null mutants[140]. These data suggest that THM1 functions as a negative regulator of Hh signaling. In contrast to these findings, ablating *Thm1* in Bergmann glia and Purkinje cells caused reduced Hh signaling in these cells, indicating a role for *Thm1* as a positive regulator of Hh signaling[148]. Other *Ift* genes have been shown to regulate Hh signaling negatively or positively in a cell-type dependent manner[141]. The factors that determine whether *Thm1* or other *Ift* genes will act as a positive or negative regulator of Hh signaling are unknown.

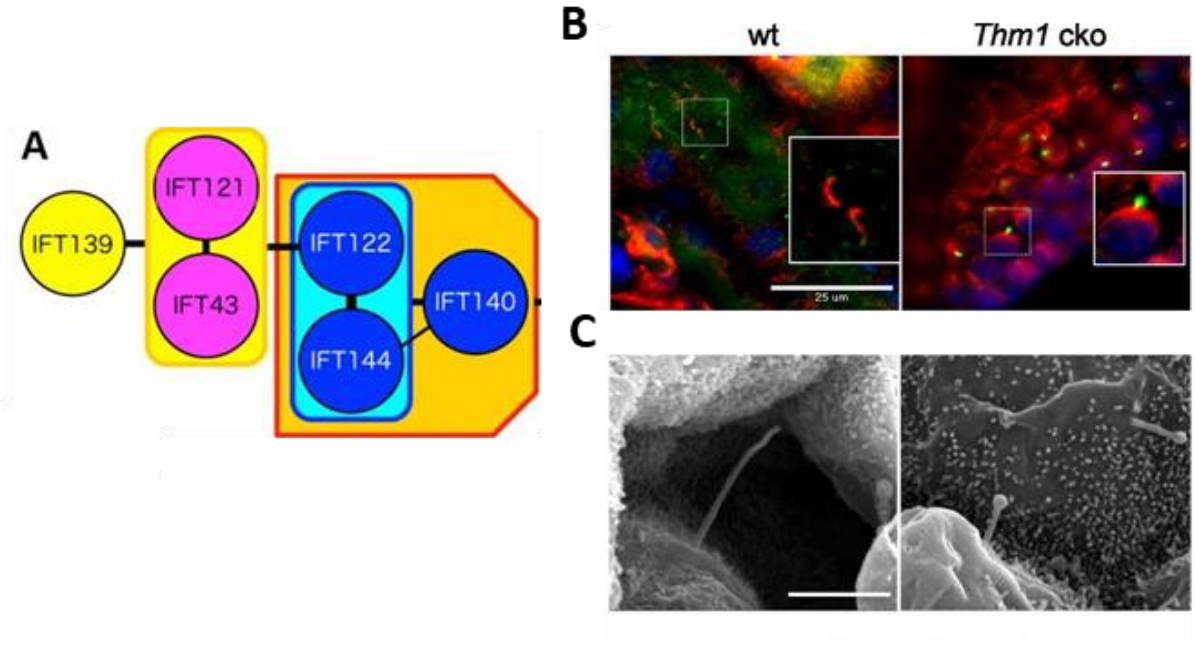

Figure 1.11 THM1 in peripheral IFT-A subcomplex and loss of *Thm1* results in shorterned primary cilia with a bulb like structure

(A) Schematic diagram of core and peripheral IFT-A complex proteins (B) Immunostaining of primary cilia with acetylated α-tubulin (red) and IFT88 (green) in wt and *Thm1* cko renal epithelial cells. (C) Scanning electron micrographs (SEM) of wt and *Thm1* cko collecting ducts. (A) Reprinted with permission from Hirano, T., Y. Katoh, and K. Nakayama, *Intraflagellar transport-A complex mediates ciliary entry and retrograde trafficking of ciliary G protein-coupled receptors.* Mol Biol Cell, 2017. **28**(3): p. 429-439. (B) and (C) Reprinted with permission taken from Tran, P.V., et al., *Downregulating hedgehog signaling reduces renal cystogenic potential of mouse models.* J Am Soc Nephrol, 2014. **25**(10): p. 2201-12.

THM1 is one of the most commonly mutated *Ift* genes, contributing pathogenic and modifying alleles to ~5% of ciliopathy patients[149]. Mutations in *THM1* have been found in patients with NPHP, BBS, and JATD[149-152]. Additionally, mutations in *THM1* were identified in patients with familial focal segmental glomerulosclerosis (FSGS), which affects podocytes and is characterized with structural alterations of the glomerular filtration barrier[152-154]. Among them, a homozygous missense mutation of *Thm1* causes late-onset FSGS without any other manifestations associated with ciliopathies. Since mature podocytes lack cilia, these data suggest a nonciliary role of THM1 in glomerular defects[153]. Lastly, mutations in *THM1* were reported in patients with pathologic myopia, indicating a role for THM1 in the structure and function of photoreceptors[155].

1.6.2 THM2

A BLAST homology search revealed *Thm1* has a paralog, *Thm2*, which encodes a protein that is 49% identical to THM1 and has a similar predicted protein structure with multiple TPR domains[50] (Figure 1.12). At embryonic day (E) 10.5, both *Thm1* and *Thm2* are widely expressed in whole mouse embryos[50] (Figure 1.12). The role of THM2 in primary cilia and ciliopathies is less known than THM1. Recently, mutations of *THM2* were reported in adult males with subfertility[156]. Additionally, increased *THM2* expression correlates with a favorable prognosis and a different proportion of immune cells in lung adenocarcinoma, indicating potential roles of THM2 in immune infiltration and tumor progression[157].

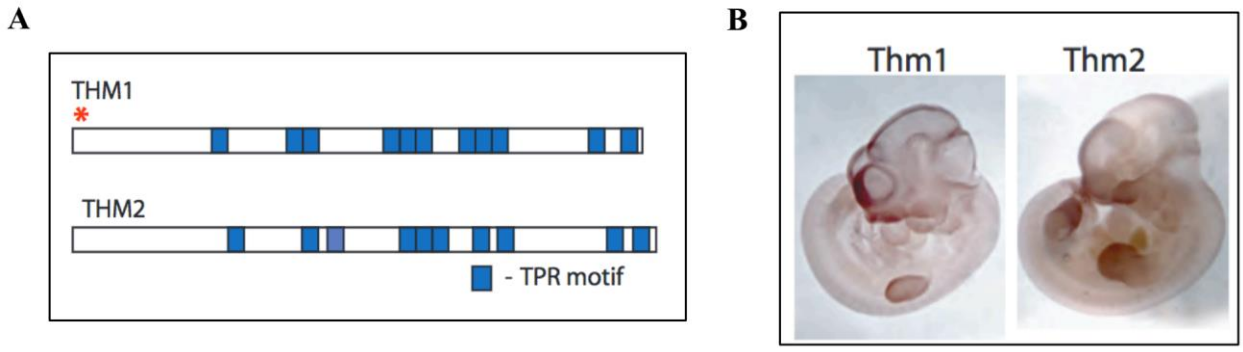

Figure 1.12 Predicted protein structure and embryonic RNA expression of *Thm1* and *Thm2*
(A) Predicted protein structure of THM1 and THM2 with multiple TPR motifs. (B) Whole-mount in situ hybridization shows similar expression patterns of *Thm1* and *Thm2* at E10.5. Reprinted with permission from Tran, P.V., et al., THM1 negatively modulates mouse sonic hedgehog signal transduction and affects retrograde intraflagellar transport in cilia. *Nat Genet*, 2008. 40(4): p. 403-410.

1.7 Study significance

ADPKD causes development of fluid-filled renal cysts and is the most common fatal monogenic kidney disorder. Deficiency of polycystins, which localize to primary cilia, causes ADPKD. On a normal background, the disruption of primary cilia can lead to cystic kidney disease, but on a PKD background, the disruption of primary cilia can attenuate cystogenesis. Therefore, greater understanding of the molecular mechanisms connecting cilia dysfunction to renal cystic disease is needed. To bridge this knowledge gap, using cellular and mouse models, I have investigated the role of *Thm1* and *Thm2* in renal and hepatic cystogenesis and in cilia function. In Chapter Two, I investigate the role of *Thm1* deficiency in PKD severity in juvenile and adult ADPKD mouse models. In Chapter Three, I examine the effect of *Thm1* deficiency in polycystic liver disease (PLD) in *Pkd2* cko mice. In Chapter Four, using mouse embryonic fibroblasts (MEF), I investigate the roles of *Thm1*, and its paralog, *Thm2*, in cilia assembly and disassembly, ciliary protein trafficking, and signaling. These studies uncover cell type- and maturation-dependent roles for IFT-A deficiency in polycystic kidney and liver diseases of ADPKD mouse models. These studies also reveal a novel role for *Thm1* alone in biliary development. Further, these investigations reveal novel interactions between *Thm1* and *Thm2* in regulation of cilia structure, length, and function. Taken together, the work documented in this dissertation uncovers multiple novel facets of IFT-A function in ciliary homeostasis and signaling, and in renal and hepatic ciliopathies, providing essential groundwork for identifying therapeutic strategies against ADPKD.

Chapter Two: Intraflagellar transport-A deficiency ameliorates ADPKD renal cystogenesis in a renal tubular- and maturation-dependent manner

2.1 Abstract

Primary cilia are sensory organelles that are built and maintained by intraflagellar transport (IFT) multi-protein complexes. Deletion of certain ciliary genes in Autosomal Dominant Polycystic Kidney Disease (ADPKD) mouse models markedly attenuates PKD severity, indicating that a component of cilia dysfunction may have critical therapeutic potential. We have ablated the *Ift-A* gene, *Thm1*, globally in juvenile and adult mouse models of ADPKD. Relative to juvenile *Pkd2* conditional knock-out mice, deletion of *Thm1* together with *Pkd2* resulted in a complex phenotype, with reduced kidney weight/body weight (KW/BW) ratios, reduced cortical collecting duct-derived cysts, but increased proximal tubular and glomerular dilations, and similar blood urea nitrogen (BUN) levels. Additionally, primary cilia of cortical collecting duct epithelia were lengthened in *Pkd2* conditional knock-out kidneys, as well as in *Pkd2;Thm1* double knock-out kidneys. In contrast, *Thm1* deletion in adult ADPKD mouse models markedly reduced multiple disease parameters, including KW/BW ratios, collecting duct- and loop of Henle-derived cysts, proximal tubular dilations, and BUN levels. Further, primary cilia lengths of cortical collecting duct epithelia were increased in *Pkd1* and *Pkd2* conditional knock-out mice, but similar to control in *Pkd1;Thm1* and *Pkd2;Thm1* double knock-out mice. These data reveal that during kidney development, *Thm1* both promotes and inhibits different aspects of ADPKD renal cystogenesis in a tubule-dependent manner; however, during adult kidney homeostasis, *Thm1* promotes virtually all features of ADPKD renal cyst growth. These findings suggest that differential factors between tubules and between developing versus mature renal microenvironments influence cilia dysfunction and ADPKD pathobiology.

2.2 Introduction

Autosomal Dominant Polycystic Kidney Disease (ADPKD) is among the most common, fatal monogenetic diseases, affecting 1:1000 individuals worldwide. ADPKD is characterized by the growth of large fluid-filled renal cysts, which cause injury and fibrosis and can lead to end-stage renal disease by the 6th decade of life. Tolvaptan is the only FDA-approved therapy, but has variable effectiveness and aquaresis side effects[158, 159]. Thus, the need to discover additional underlying disease mechanisms and design new therapeutic strategies continues.

Primary cilia are small, antenna-like sensory organelles that play an important role in ADPKD pathobiology via mechanisms that remain unclear. ADPKD is caused by mutations in *PKD1* (≥80% of cases) or *PKD2* (≥10% of cases), which encode polycystin 1 (PC1) and polycystin 2 (PC2), respectively[87, 160]. PC1 and PC2 form an ion-channel receptor complex that functions at the primary cilium. While PC1 and PC2 also localize to other subcellular compartments, analyses of human ADPKD primary renal epithelial cells, of mouse models harboring human ADPKD mutations, and of an ethylnitrosourea (ENU)-induced *Pkd2* mouse mutation that causes ciliary exclusion of PC2, indicate that deficiency of PC1 or PC2 from the cilium is sufficient to cause ADPKD[113, 114, 161].

Primary cilia are synthesized and maintained via intraflagellar transport (IFT), which is the bi-directional transport of protein cargo along a microtubular axoneme. Two multiprotein complexes mediate IFT. The IFT-B complex interacts with the kinesin motor and mediates anterograde IFT, while the IFT-A complex together with cytoplasmic dynein mediates retrograde IFT. IFT-A proteins are also required for ciliary import of membrane and signaling molecules[11, 162, 163]. In mice, deletion of *Ift-A* or *-B* genes either perinatally or in the embryonic kidney results in renal cystic disease[164-166]. However, these mutants differ from ADPKD models in

manifesting generally smaller renal cysts and greater fibrosis relative to cyst size[167, 168]. Additionally, *Ift-A* and *–B* mutants differ in cilia phenotype, showing in general shortened and absent cilia, respectively, and can also show opposing signaling phenotypes, reflecting the differing functional roles of IFT-A and -B[50, 51, 165, 169]. Intriguingly, deletion of *Ift-B* genes, *Kif3a, Ift20*, and of an IFT-A adaptor gene, *Tulp3*, in *Pkd1* or *Pkd2* conditional knock-out (cko) mice reduces severity of the PKD phenotype[116, 170, 171]. The mechanisms underlying this rescue remains elusive, but the impressive attenuation of PKD severity in these *Pkd; cilia* double knock-out (dko) mice indicates that a component of cilia dysfunction has potential therapeutic value.

A commonly mutated *IFT* gene is *THM1* (TPR-containing Hedgehog modulator 1; also termed *TTTC21B).* Causative and modifying mutations in *THM1* have been identified in 5% of patients with ciliopathies, including nephronophthisis, Bardet Biedl syndrome, Meckel syndrome and Jeune syndrome[167]. *THM1* encodes an IFT-A component, and its deletion impairs retrograde IFT, causing accumulation of proteins in bulb-like distal tips of shortened primary cilia[50]. *Thm1* loss also impairs cilia entry of membrane-associated proteins, delays and reduces ciliogenesis, and promotes cilia disassembly[172]. In mice, *Thm1* deletion recapitulates many of the clinical manifestations of ciliopathies[50, 143, 173]. Perinatal global deletion of *Thm1* results in renal cystic disease[143]. Deletion of *Thm1* in adult mice does not result in a renal phenotype by 3 months of age, consistent with the developmental time-frame that determines whether loss of a cystogenic gene will cause rapid- or slow-progressing renal cystic disease[174]. Here we have examined the role of IFT-A deficiency in ADPKD by deleting *Thm1* in juvenile and adult ADPKD mouse models. We observe that during postnatal kidney development, *Thm1* loss both attenuates and exacerbates different features of ADPKD, while in the adult kidney, *Thm1* loss markedly

attenuates most aspects of ADPKD renal cystogenesis. These data reveal renal tubular- and maturation-dependent roles for IFT-A in ADPKD.

2.3 Methods

2.3.1 Generation of mice

Pkd1$^{flox/flox}$, *Pkd2*$^{flox/flox}$ and *ROSA26-Cre* mice were obtained from the Jackson Laboratories (Stock numbers 010671, 017292 and 004847, respectively). Generation of *Thm1* cko mice has been described previously[143]: *Thm1*$^{aln/+}$; *ROSA26Cre*$^{ERT+}$ male mice were mated to *Thm1*$^{flox/flox}$ females. *Pkd1* floxed alleles were introduced into the colony to generate *Thm1*$^{flox/flox}$*;Pkd1*$^{flox/flox}$ or *Thm1*$^{flox/flox}$*;Pkd1*$^{flox/+}$ females and *Pkd1*$^{flox/flox}$*; Thm1*$^{aln/+}$, *ROSA26-Cre*$^{ERT/+}$ males, which were mated. Similarly, *Pkd2* floxed alleles were introduced into the colony to generate *Thm1*$^{flox/flox}$*;Pkd2*$^{flox/flox}$ or *Thm1*$^{flox/flox}$*;Pkd2*$^{flox/+}$ females and *Pkd2*$^{flox/flox}$*; Thm1*$^{aln/+}$, *ROSA26-Cre*$^{ERT/+}$ males. To generate early-onset *Pkd2* models, *Thm1*$^{flox/flox}$*;Pkd2*$^{flox/flox}$ or *Thm1*$^{flox/flox}$*;Pkd2*$^{flox/+}$ nursing mothers mated to *Pkd2*$^{flox/flox}$*; Thm1*$^{aln/+}$, *ROSA26-Cre*$^{ERT/+}$ males were injected intraperitoneally with tamoxifen (10mg/40g; Sigma) at postnatal day 0 (P0) to induce gene deletion. Offspring were analyzed at P21. To generate late-onset *Pkd2* models, offspring from matings between *Thm1*$^{flox/flox}$*;Pkd2*$^{flox/flox}$ or *Thm1*$^{flox/flox}$*;Pkd2*$^{flox/+}$ females and *Pkd2*$^{flox/flox}$*; Thm1*$^{aln/+}$, *ROSA26-Cre*$^{ERT/+}$ males were injected intraperitoneally with tamoxifen (10mg/40g) at P28. To generate late-onset *Pkd1* models, offspring from matings between *Thm1*$^{flox/flox}$*;Pkd1*$^{flox/flox}$ or *Thm1*$^{flox/flox}$*;Pkd1*$^{flox/+}$ females and *Pkd2*$^{flox/flox}$*; Thm1*$^{aln/+}$, *ROSA26-Cre*$^{ERT/+}$ males were injected intraperitoneally with tamoxifen (10mg/40g) at P35. Mice were analyzed at 6 months of age. All mouse lines were maintained on a pure C57BL6/J background (backcrossed 10 generations). All

animal procedures were conducted in accordance with KUMC-IACUC and AAALAC rules and regulations.

2.3.2 Kidney and body weight measurements

Kidneys were dissected and weighed using a standard laboratory weighing scale. The kidney weight/body weight (KW/BW) ratio was calculated as the total kidney weights divided by body weight for each mouse.

2.3.3 Western blot

Passive Lysis Buffer (Promega) containing proteinase inhibitor cocktail (Pierce) was used to generate protein extracts from frozen kidney tissue. Tissue was homogenized by using 0.5 mm zirconium oxide PINK beads (Next Advance) and a Bullet Blender Storm (Next Advance) set at Speed 10 for approximately 5 minutes. Lysates were centrifuged at 4^0C at maximum speed for 1 minute and supernatant was collected. Protein concentrations were determined using the bicinchoninic acid protein (BCA) assay reagents (Pierce). Western blot was performed as described [143], using primary antibodies for P-STAT3 (Cell Signaling Technology, 9145), STAT3 (Cell Signaling Technology, 9139), P-ERK (Cell Signaling Technology, 4370), ERK (Cell Signaling Technology, 4696). SuperSignal West Femto Chemiluminescent Substrate (Pierce) was used to detect signal. ImageJ was used to quantify Western blot signals.

2.3.4 qPCR

RNA was extracted using Trizol (Life Technologies), then reverse transcribed into cDNA using Quanta Biosciences qScript cDNA mix (VWR International). qPCR for *Ccl2* was performed

using Quanta Biosciences Perfecta qPCR Supermix (VWR International) in a BioRad CFX Connect Real-Time PCR Detection System. Primers used were *mCcl2* (Forward: 5'-AAGCTCAACCCTGACTTCTTAC-3'; Reverse: 5'-CAACGTCTGAGAACTGGAGAAA-3'). qPCR was performed in duplicate using RNA lysates from five samples per genotype.

2.3.5 Histology

Kidneys were halved transversely, fixed in 10% formalin for several days, then processed in a tissue processor and embedded in paraffin. Tissue sections (7μm) were obtained with a microtome. Sections were deparaffinized, rehydrated through a series of ethanol washes, and stained with hematoxylin and eosin (H&E). Images were taken with a Nikon 80i microscope equipped with a Nikon DS-Fi1 camera. Cystic areas of H&E-stained sections were quantified using ImageJ.

2.3.6 Immunofluorescence

Following deparaffinization and rehydration, tissue sections were subjected to an antigen retrieval protocol, which consisted of steaming sections for 25 minutes in Sodium Citrate Buffer (10 mM Sodium Citrate, 0.05% Tween 20, pH 6.0). Sections were blocked with 1% BSA in PBS for 1 hour at room temperature, and then incubated with primary antibodies against acetylated-α tubulin (1:4000; Sigma, T7451), IFT81 (1:200; Proteintech, 11744-1-AP), αSMA (1:500; Abcam, ab5694) and PCNA (1:300; Cell Signaling Technology, 13110), DBA (1:100; Vector Laboratories, FL-1031), LTL (1:300, Vector Laboratories, FL-1321), THP (1:100; Santa Cruz Biotechnology, sc-271022) overnight at 4°C. Sections were washed three times in PBS, and then incubated with secondary antibodies conjugated to Alexa Fluor 488 (1:500; Invitrogen, A-11001 (anti-mouse) or

A-11034 (anti-rabbit)) or Alexa Fluor 594 (1:500; Invitrogen, A-11005 (anti-mouse) or A-11012 (anti-rabbit)) for 1 hour at room temperature. After three washes of PBS, sections were mounted with Fluoromount-G containing 4′,6-diamidino-2-phenylindole (DAPI) (Electron Microscopy Sciences). Staining was visualized and imaged using a Nikon 80i microscope with a photometrics camera or a Nikon Eclipse TiE attached to an A1R-SHR confocal, with an A1-DU4 detector, and LU4 laser launch.

2.3.7 Blood urea nitrogen measurements

Mouse trunk blood was collected in Microvette CB 300 Blood Collection System tubes (Kent Scientific), and centrifuged at 1800g at room temperature for 10 minutes to collect serum. Blood urea nitrogen (BUN) was measured using the QuantiChrom Urea Assay Kit (BioAssay Systems) according to the manufacturer's protocol.

2.3.8 ADPKD and normal human kidney sections

Normal human kidneys (NHK) and ADPKD kidneys were obtained from the PKD Biomarkers, Biomaterials, and Cellular Models Core in the Kansas PKD Center. The protocol for the use of discarded human tissues complied with federal regulations and was approved by the Institutional Review Board at KUMC. Paraffin-embedded de-identified NHK, n=3 (K357, K402, K419), and ADPKD, n=3 (K386, K408, K423) tissues were sectioned. Sections were deparaffinized and rehydrated, steamed in Sodium Citrate Buffer (10 mM Sodium Citrate, 0.05% Tween 20, pH 6.0) for antigen retrieval, and immunostained for ARL13B (1:300; Proteintech, 17711-1-AP).

2.3.9 Statistics

Statistical significance ($P < 0.05$) was determined using a one-way ANOVA followed by Tukey's test for comparing more than two groups or an unpaired t-test for only two groups. GraphPad Prism 8 software was used to perform these analyses.

2.4 Results

2.4.1 Perinatal deletion of *Thm1* in *Pkd2* cko mice reduces cortical cystogenesis, but does not improve kidney function

To examine the effect of IFT-A deficiency in an early-onset, rapidly progressing ADPKD mouse model, we deleted *Thm1* together with *Pkd2* at postnatal day (P) 0, and examined the renal phenotypes of control, *Thm1* cko, *Pkd2* cko and *Pkd2;Thm1* dko mice at P21. At this stage, *Thm1* cko kidneys appear mostly intact morphologically[143], with some tubular dilations observed in the cortex and with kidney weight/body weight (KW/BW) ratios similar to control (Figures 2.1A and 2.1B). Yet, BUN levels are elevated about 2-fold (Figure 2.1C). In *Pkd2* cko mice, renal cysts are present in both cortex and medulla, and KW/BW ratios and BUN levels are increased 5-fold and 3-fold, respectively. In *Pkd2;Thm1* dko mice, renal cysts are also present in the cortex and medulla, and KW/BW ratios and BUN levels are increased 4-fold and 3-fold, respectively. Thus relative to *Pkd2* cko mice, *Pkd2;Thm1* dko mice have reduced KW/BW ratios, but similar kidney function. *Pkd2;Thm1* dko kidneys also show decreased percent cystic index (Figure 2.1D), due to reduced cystogenesis in the cortex (Figure 2.1E), while percent cystic index in the medulla is similar (Figures 2.1F).

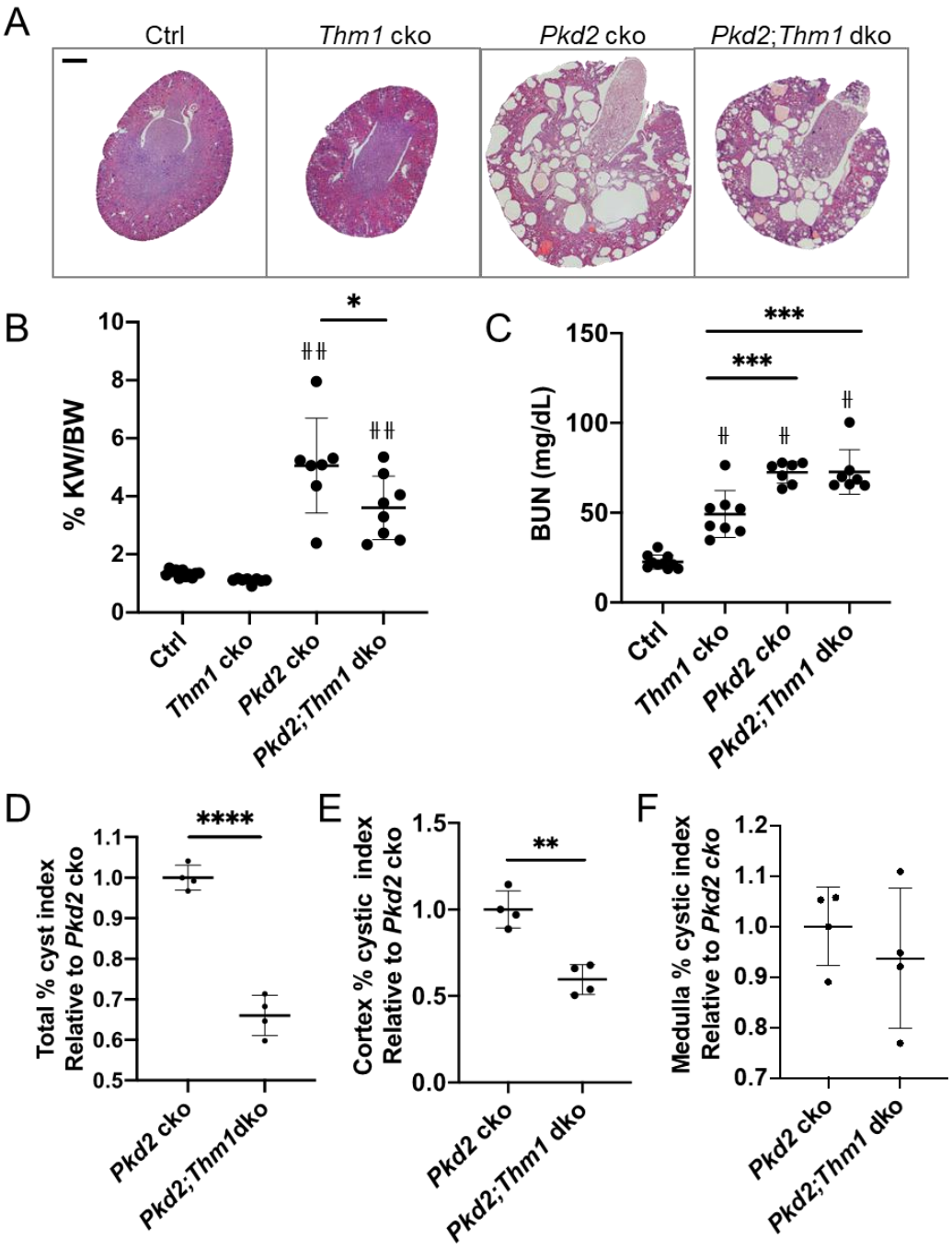

Figure 2.1 Early onset *Pkd2;Thm1* dko mice have reduced cortical cystic index, but not improved kidney function relative to *Pkd2* cko mice

(A) Haemotoxylin and eosin staining of P21 kidney sections. Scale bar - 500 m, (B) Percent kidney weight/body weight (KW/BW) ratios, (C) Blood urea nitrogen (BUN) levels, (D) Percent cystic index, (E) Percent cortical cystic index, and (F) Percent medullary cystic index. Pkd2 cko percent cystic indices are set at 1. Bars represent mean SD. In (B) and (C), statistical significance was determined by one-way ANOVA followed by Tukey's test. *p<0.05; ****p<0.00005; ǂ p<0.0005 compared to Ctrl; ǂǂ p<0.00005 compared to Ctrl. In (E) and (F), statistical significance was determined by unpaired two-tailed t-test. **p<0.005

2.4.2 Perinatal deletion of *Thm1* in *Pkd2* cko mice reduces cortical collecting duct cystogenesis, but increases proximal tubular and glomerular dilations

Since cystogenesis was reduced in the cortex of *Pkd2;Thm1* dko kidneys relative to *Pkd2* cko kidneys, subsequent analyses focused on the cortex. At P21 in the *Thm1* cko renal cortex, we observed some dilations, most of which were LTL+, marking proximal tubules, and fewer that were THP+ or DBA+, marking loop of Henle and collecting duct, respectively (Figure 2.2A). In *Pkd2* cko renal cortex, LTL+ dilations, THP+ cysts, and multiple, large DBA+ cysts were observed. In *Pkd2; Thm1* dko cortex, LTL+ dilations were increased relative to those of *Pkd2* cko and *Thm1* cko kidneys (Figures 2.2A and 2.2B,); THP+ cysts were similar in size to those of *Pkd2* cko kidneys (Figure 2.2C), and DBA+ cysts were decreased in size relative to those of *Pkd2* cko kidneys (Figure 2.2D). Thus, we observed a tubular-specific effect of deleting *Thm1* in juvenile *Pkd2* cko mice. *Thm1* deletion worsened LTL+, but attenuated cortical DBA+ cystogenesis.

Histology revealed that glomerular dilations were present across the mutant genotypes (Figure 2.2E). We observed a reduced number of glomeruli per cross-section in *Pkd2* cko kidneys (28.3 vs 45.0), but a restored number of glomeruli per cross-section in *Pkd2;Thm1* dko kidneys (46.5; Figure 2.2F). In *Pkd2* cko kidneys, while the area of Bowman's space was not significantly altered, the ratio of the area of Bowman's space to the area of Bowman's capsule was increased, indicating presence of glomerular dilations (Figures 2.2G and 2.2H). In *Pkd2;Thm1* dko kidneys, area of Bowman's space and also the ratio of Bowman's space to area of Bowman's capsule were increased, and this ratio was increased to a greater extent relative to *Pkd2* cko kidneys, indicating that additional loss of *Thm1* exacerbates the glomerular dilations (Figures 2.2G and 2.2H).

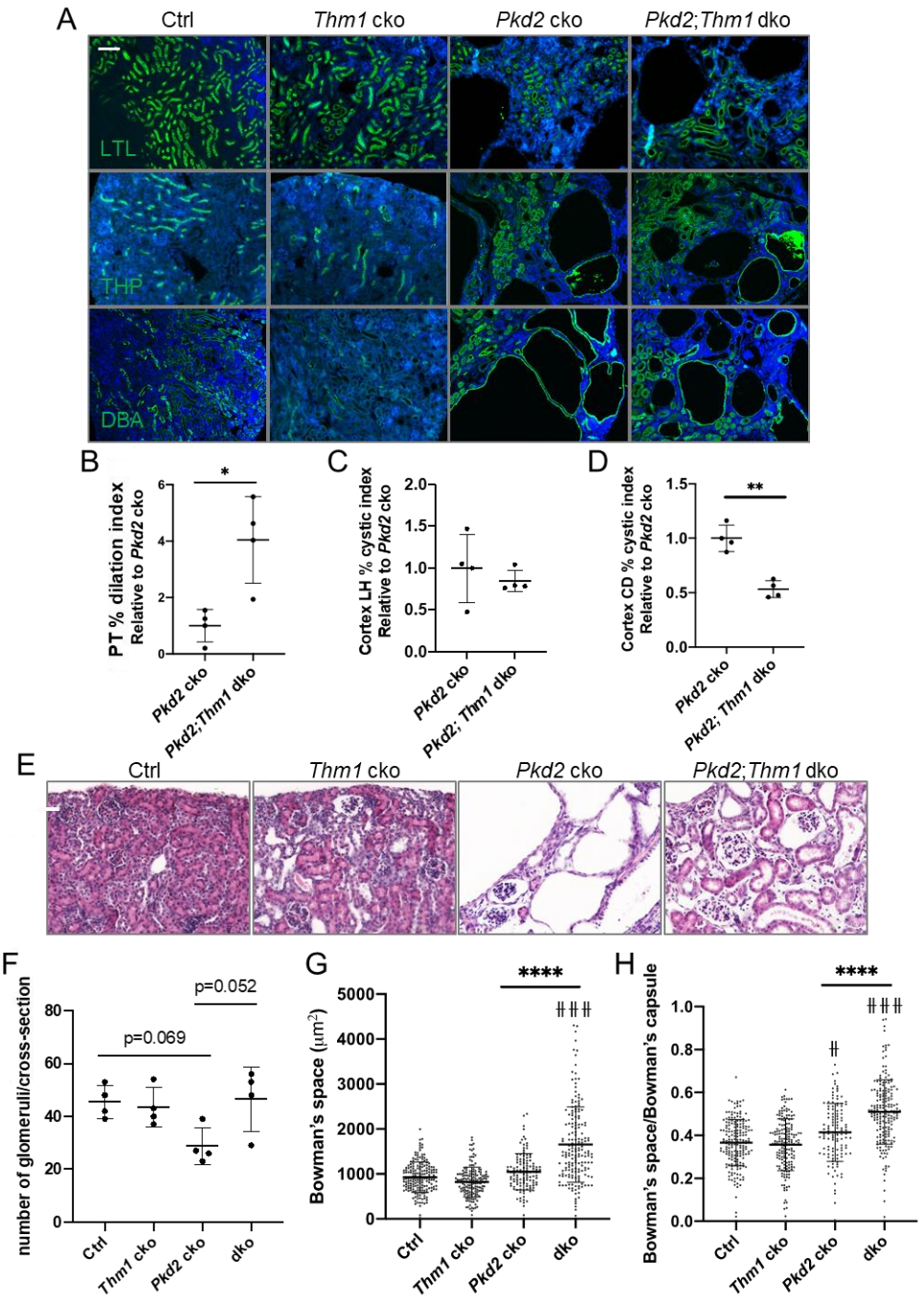

Figure 2.2 Early onset *Pkd2;Thm1* dko mice have reduced cortical collecting duct cysts, but increased proximal tubule and glomerular dilations

A) Staining of kidney cortex with LTL, THP and DBA. Scale bar - 100μm (B) Percent LTL+ dilations (C) Percent THP+ cystic index (D) Percent DBA+ cystic index in renal cortex. *Pkd2* cko percent cystic indices are set at 1. Bars represent mean ± SD. Statistical significance was determined by unpaired two-tailed t-test. *p<0.05; **p<0.005. (E) Haemotoxylin and eosin staining. Scale bar - 50μm (F) Number of glomeruli (G) Area of Bowman's space (H) Area of Bowman's space/area of Bowman's capsule. Bars represent mean ± SD. Statistical significance was determined by one-way ANOVA followed by Tukey's test. ****p<0.00005; ǂ p<0.005 compared to Ctrl; ǂǂǂ p<0.00005 compared to Ctrl

2.4.3 Deletion of *Pkd2* increases proliferation of renal tubular epithelia

We next examined cell proliferation, a driver of ADPKD renal cystogenesis, by immunostaining for PCNA together with proximal tubule and collecting duct markers, LTL and DBA, respectively. Similar levels of PCNA staining were observed in normal LTL+ and DBA+ tubules across the various genotypes - control, *Thm1* cko, *Pkd2* cko and *Pkd2;Thm1* dko kidneys (Figures 2.3A and 2.3B). However, in *Pkd2* cko kidneys, PCNA+ cells were increased in dilated LTL+ tubules relative to normal LTL+ tubules (Figure 2.4), and in *Pkd2* cko and *Pkd2;Thm1* dko kidneys, PCNA+ cells were increased in dilated DBA+ tubules relative to normal DBA+ tubules (Figure 2.3B). These data support that increased proliferation is an early event in ADPKD renal cystogenesis.

2.4.4 Perinatal deletion of *Thm1* causes fibrosis

Cyst growth compresses surrounding parenchyma, leading to injury and fibrosis in ADPKD. To assess fibrosis, we immunostained kidney sections for presence of myofibroblasts, which label with alpha smooth muscle actin (αSMA). In *Thm1* cko kidneys, we observed αSMA+ cells around glomeruli and tubular dilations (Figure 2.3C). In *Pkd2* cko kidneys, more αSMA+ labelling was observed than in *Thm1* cko kidneys, and in *Pkd2;Thm1* dko kidneys, levels of αSMA+ labelling were similar to those in *Pkd2* cko kidneys. Thus, deletion of *Thm1* alone causes fibrosis, but *Thm1* deletion in *Pkd2* cko mice does not exacerbate fibrosis at P21.

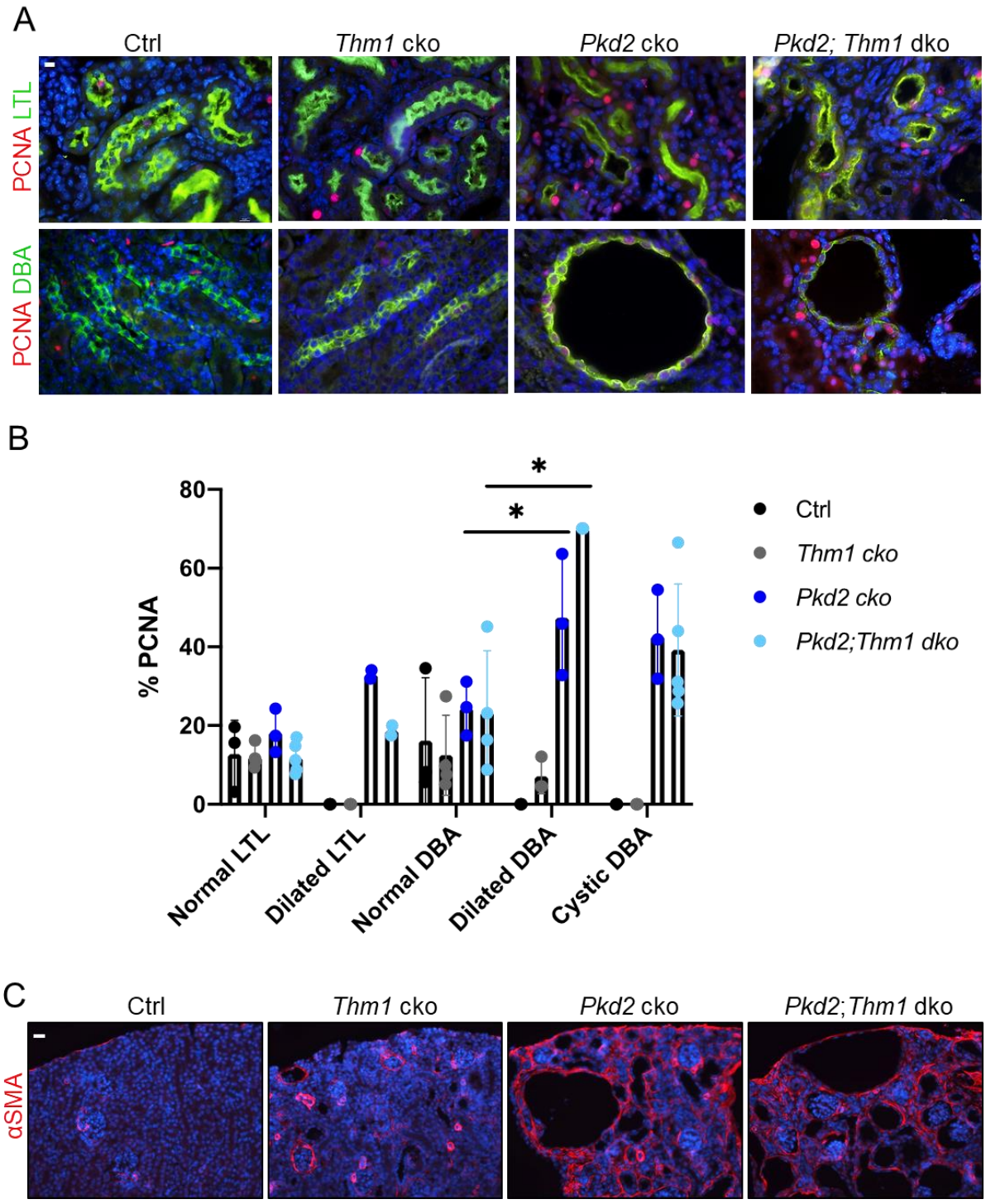

Figure 2.3 Early onset *Pkd2* cko mice show increased proliferation in dilated cortical collecting ducts (A) Immunostaining of kidney cortex for PCNA (red) together with LTL or DBA (green). Scale bar - 10μm (B) Percent PCNA+ cells per tubule. Bars represent mean ± SD. Statistical significance was determined by two-way ANOVA followed by Tukey's test. *$p<0.05$. Note: Control and *Thm1* cko LTL+ dilations, control DBA+ dilations, and control and *Thm1* cko DBA+ cysts were not observed in sections analyzed. (C) Immunostaining of kidney cortex for αSMA (red). Scale bar - 50μm.

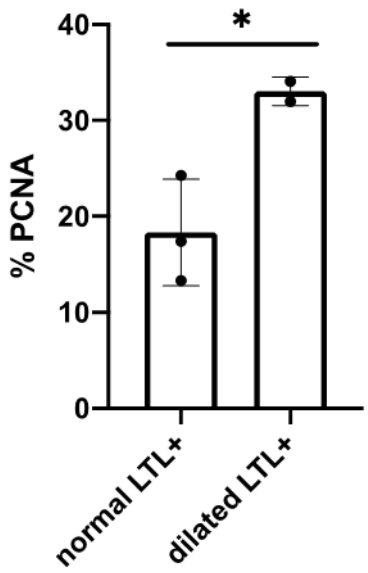

Figure 2.4 Proliferation of *Pkd2* cko proximal tubular cells
Quantification of PCNA+ cells in normal and dilated LTL+ tubules of *Pkd2* cko kidneys. Bars represent mean ± SD. Statistical significance was determined by unpaired two-tailed t-test. *$p<0.05$

2.4.5 Perinatal deletion of *Thm1* in *Pkd2* cko mice increases STAT3 signaling

We have observed that perinatal deletion of *Thm1* increases STAT3 activation in kidneys prior to cyst formation (data not shown). STAT3 signaling is also increased in ADPKD mouse models and pharmacological inhibition of STAT3 signaling attenuates ADPKD in mouse models[175]. ERK signaling is also increased during early cystic kidney disease of *Thm1* cko mice (data not shown) and this pathway is elevated in ADPKD[176, 177]. We therefore examined these pathways using Western blot analyses. In *Thm1* cko and *Pkd2* cko kidneys, STAT3 activation was increased (Figures 2.5A and 2.5B), and in *Pkd2;Thm1* dko kidneys, STAT3 activation was further increased (Figures 2.5B). Additionally, in *Pkd2* cko and *Pkd2;Thm1* dko kidneys, there was a trend toward increased ERK activation (Figure 2.5C). Thus, *Pkd2* cystic disease causes increased STAT3 and ERK signaling consistent with previous reports[178, 179], and deletion of *Thm1* in *Pkd2* cko mice further increases STAT3 activation.

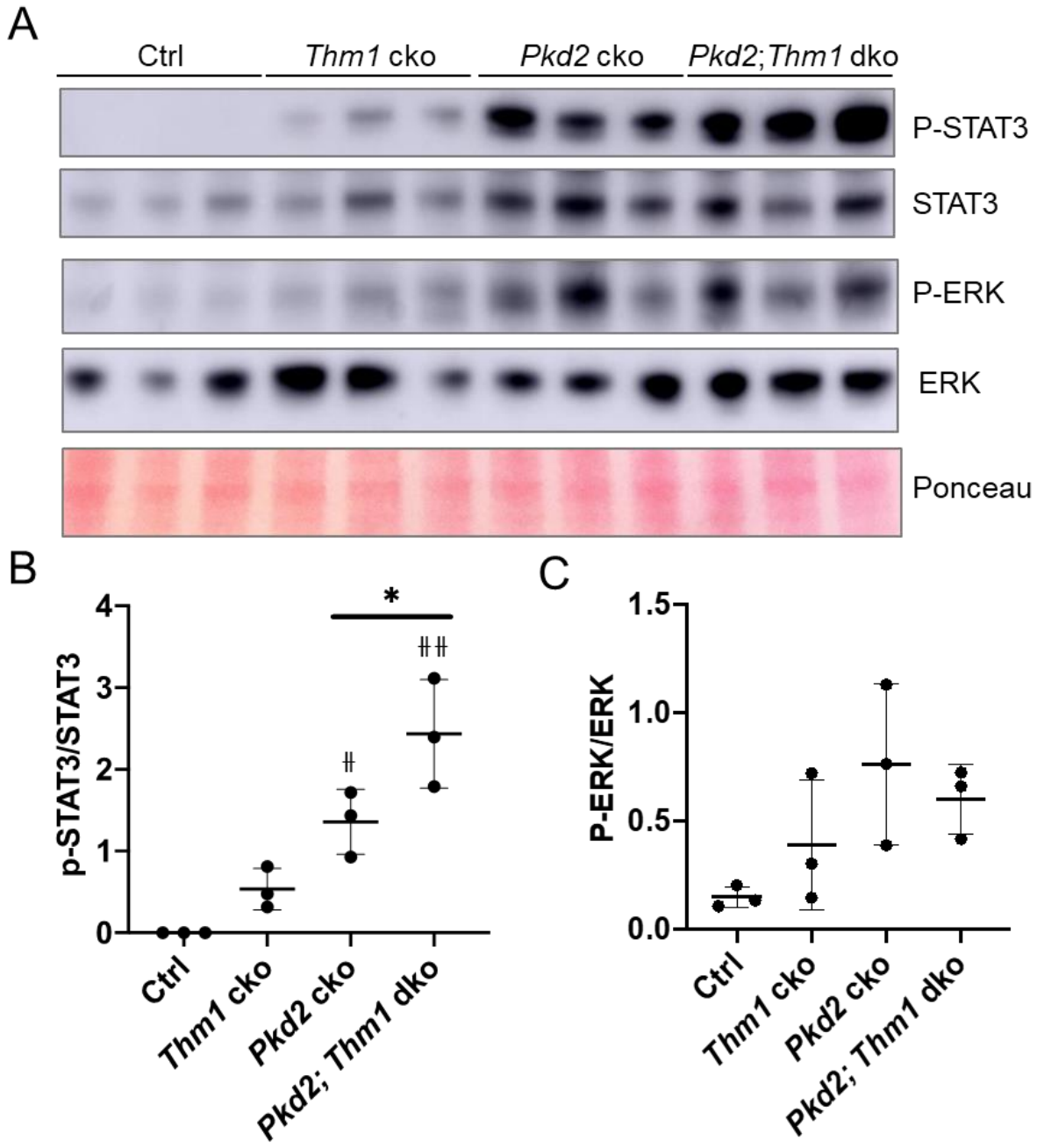

Figure 2.5 Early onset *Pkd2*;*Thm1* dko kidneys have increased STAT3 activation
(A) Western blot analysis of kidney extracts. (B) Quantification of P-STAT3/STAT3 and (C) P-ERK/ERK. Statistical significance was determined by one-way ANOVA followed by Tukey's test. *p<0.05; # p<0.05 compared to Ctrl; ## p<0.005 compared to Ctrl
.

2.4.6 Deletion of *Pkd2* increases cilia length on renal epithelia

We examined cilia length on renal tubular epithelia by co-immunostaining for acetylated, α-tubulin together with lectins, LTL and DBA. In control kidneys, average cilia lengths were 3.0μm and 2.1μm for LTL+ and DBA+ cells, respectively (Figures 2.6A and 2.6B). We also noted qualitative differences between LTL+ and DBA+ primary cilia, with the former cilia appearing thinner and longer, and the latter being thicker and more rod-like. Cilia lengths were increased in both *Pkd2* cko LTL+ and DBA+ tubules. However, relative to *Pkd2* cko tubules, cilia lengths were further increased in *Pkd2;Thm1* dko LTL+ tubules, but similar in *Pkd2;Thm1* dko DBA+ tubules. These differences reveal tubular-specific effects on cilia length.

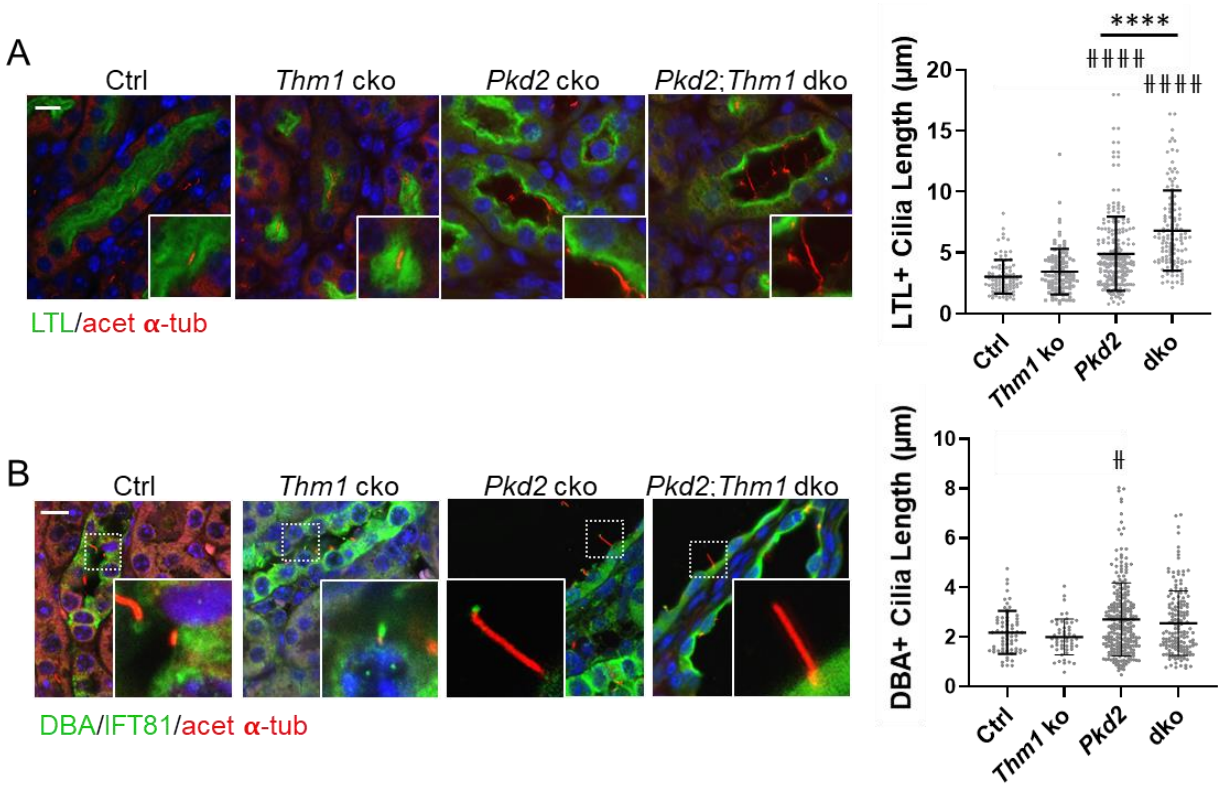

Figure 2.6 *Pkd2* cko mice have longer renal epithelial primary cilia
(A) Immunostaining of kidney cortex for acetylated α-tubulin (red) together with LTL (green). Scale bar - 10μm. Quantification of cilia length of LTL+ cells. (B) Immunostaining of kidney cortex for acetylated α-tubulin together with DBA. Scale bar - 10μm. Quantification of cilia length of cortical DBA+ cells. Bars represent mean ± SD. Statistical significance was determined by one-way ANOVA followed by Tukey's test. ****p<0.00005; # p<0.05 compared to Ctrl; #### p<0.00005 compared to Ctrl

2.4.7 Deletion of *Thm1* in adult *Pkd2* or *Pkd1* cko mice markedly attenuates ADPKD renal cystogenesis

We next examined the effect of IFT-A deficiency in late-onset, slowly progressive adult ADPKD mouse models. We deleted *Thm1* together with *Pkd2* at P28 and examined the renal phenotypes of control, *Thm1* cko, *Pkd2* cko and *Pkd2;Thm1* dko mice at 6 months of age. *Thm1* cko kidneys have similar morphology and BUN levels to those of control mice (Figures 2.7A and 2.7B). *Pkd2* cko mice show renal cysts mostly in the cortex, with the largest cysts being DBA+, and smaller cysts being LTL+ or THP+ (Figure 2.8A). In contrast, in *Pkd2;Thm1* dko mice, the *Pkd2* cko cystic phenotype is largely corrected morphologically. KW/BW ratios are unchanged in *Pkd2* cko mice, reflecting the mild disease induced in adulthood. BUN levels show a trend toward a slight elevation in *Pkd2* cko mice, but the average BUN value is still within the range of normal renal function. BUN levels of *Pkd2;Thm1* dko mice were similar to those of *Pkd2* cko mice. In ADPKD, pro-inflammatory cytokines, such as *Ccl2*, are elevated[180]. In *Pkd2* cko kidney extracts, expression of *Ccl2* showed an increasing trend, while in *Pkd2; Thm1* dko extract, *Ccl2* levels were similar to control, suggesting reduced inflammation (Figure 2.10A).

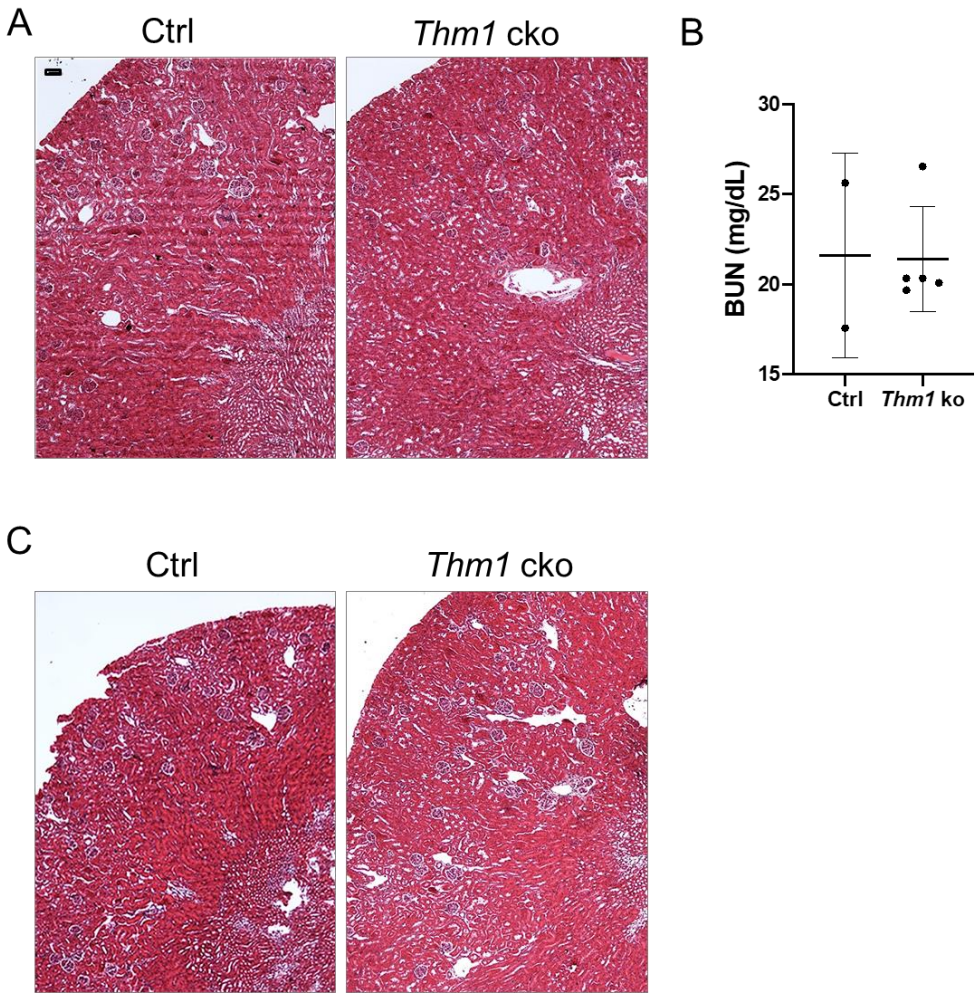

Figure 2.7 Renal histology of late onset *Thm1* cko mice
(A) Haemotoxylin and eosin staining, and (B) BUN levels of 6-month-old *Thm1* cko kidneys following *Thm1* deletion at P28. Scale bar - 50μm. (C) Haemotoxylin and eosin staining of 6-month-old *Thm1* cko kidneys following *Thm1* deletion at P35.

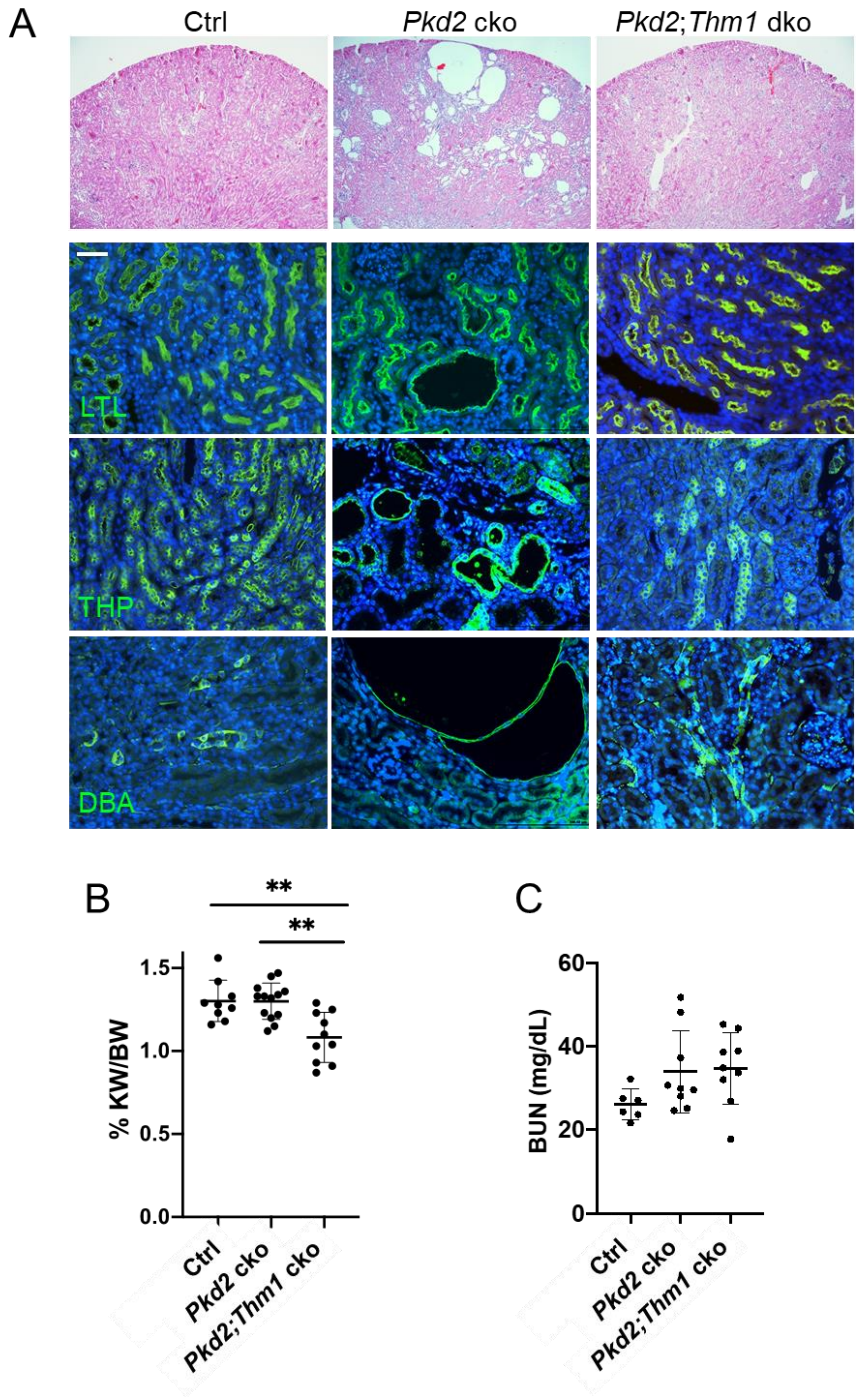

Figure 2.8 *Thm1* deletion rescues ADPKD in late-onset *Pkd2* model
(A) Histology and immunostaining of kidney sections for LTL, THP and DBA. Scale bar - 100μm (B) KW/BW ratios (C) BUN levels. Bars represent mean ± SD. Statistical significance was determined by one-way ANOVA followed by Tukey's test. **p<0.005

We also deleted *Thm1* together with *Pkd1* at P35 and examined the renal phenotypes at 6 months of age (Figure 2.9A). *Thm1* cko kidneys have morphology resembling control kidneys (Figure 2.7C), similar to *Thm1* deletion at P28. Like *Pkd2* cko adult models, *Pkd1* cko renal cysts were mostly in the cortex, with the largest and most abundant cysts being DBA+. Fewer cysts were THP+, and only dilations, not cysts, were observed that were LTL+ (Figure 2.9A). Notably, all these features were reduced in *Pkd1; Thm1* dko kidneys. KW/BW ratios were elevated in *Pkd1* cko mice, and corrected in *Pkd1;Thm1* dko mice (Figure 2.9B). Additionally, BUN levels were elevated in *Pkd1* cko mice, although the average value was still within the range of normal kidney function, while BUN levels in *Pkd1;Thm1* dko mice were similar to control. Further, while expression of *Ccl2*, and activation of STAT3 and ERK were increased in kidney extracts of *Pkd1* cko mice, these parameters were normalized in kidneys of *Pkd1; Thm1* dko mice, consistent with attenuation of disease severity (Figures 2.10B-2.10D).

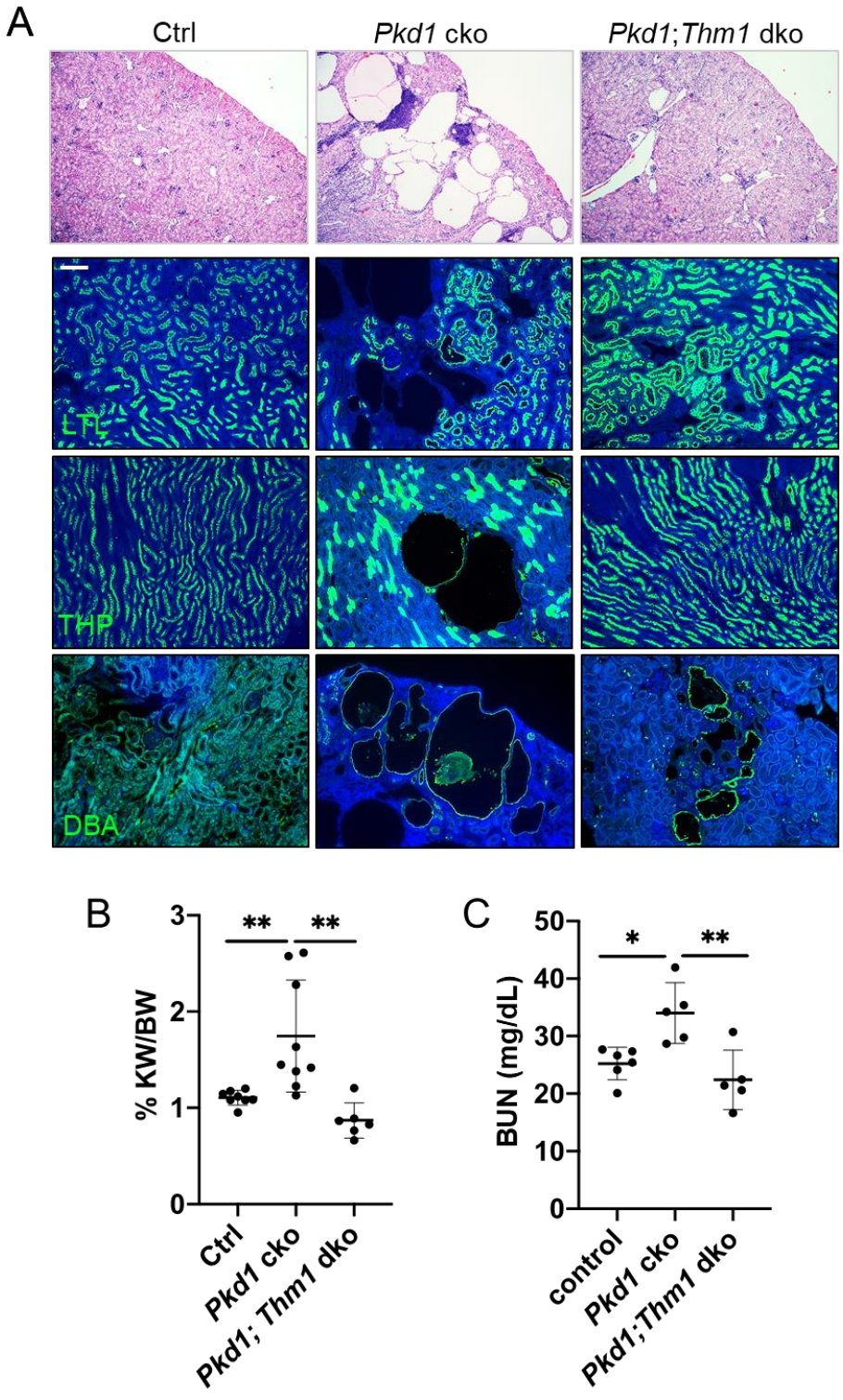

Figure 2.9 *Thm1* deletion rescues ADPKD in late-onset *Pkd1* model
Histology and immunostaining of kidney sections for LTL, THP and DBA. Scale bar - 100μm. (B) KW/BW ratios (C) BUN levels. Bars represent mean ± SD. Statistical significance was determined by one-way ANOVA followed by Tukey's test. *p<0.05; **p<0.005

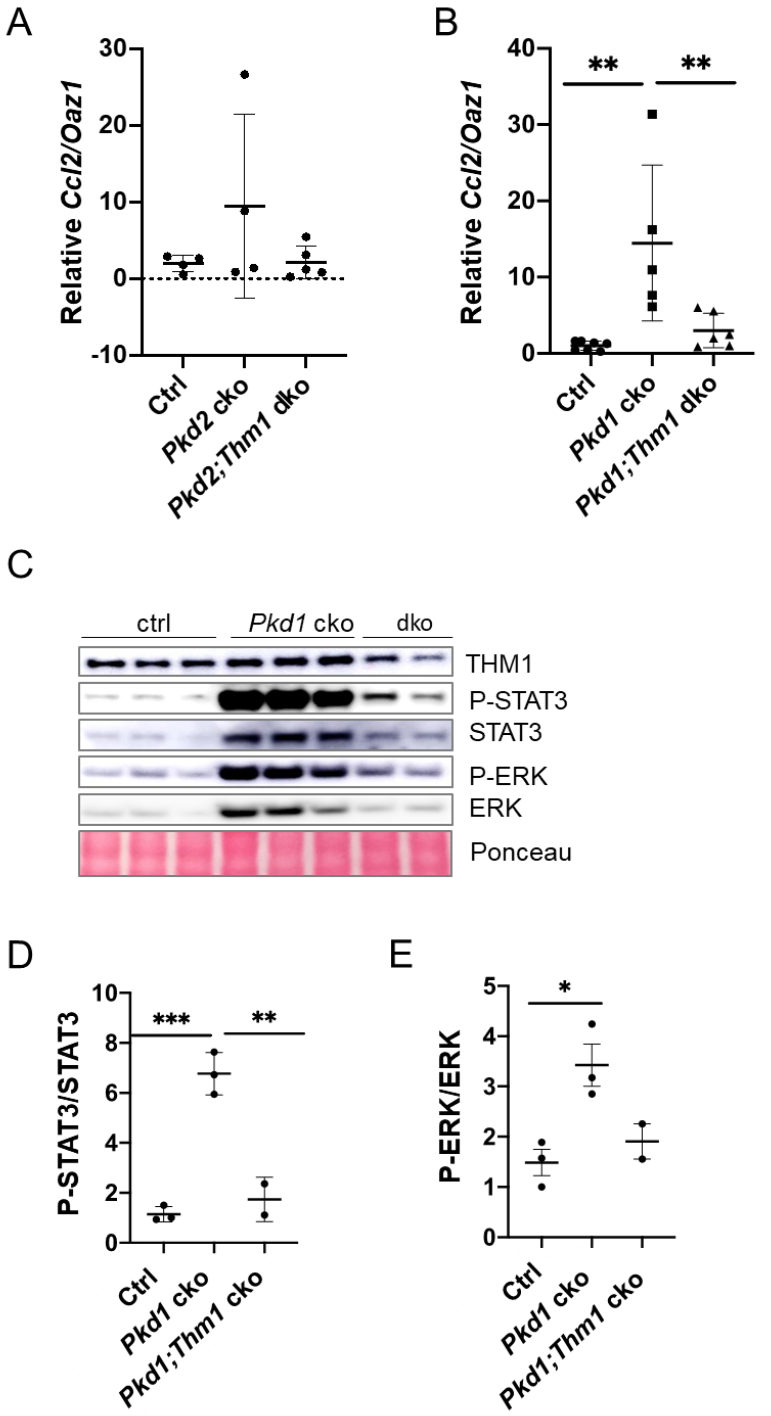

Figure 2.10 *Thm1* deletion in late onset ADPKD models decreases signaling
(A) qPCR for *Ccl2* in renal extracts of *Pkd2* cko and *Pkd2;Thm1* dko mice and (B) of *Pkd1* cko and *Pkd1;Thm1* dko mice. (C) Western blot analysis of *Pkd1* cko and *Pkd1;Thm1* dko kidney extracts. (D) Quantification of P-STAT3/STAT3 and (E) P-ERK/ERK. Bars represent mean ± SD. Statistical significance was determined by one-way ANOVA followed by Tukey's test. *p<0.05; **p<0.005; ***p<0.0005

2.4.8 Cilia length is increased on cortical renal epithelia of mouse and human ADPKD kidneys

We examined cilia length on renal tubular epithelia of adult ADPKD mouse models by co-immunostaining for acetylated, α-tubulin together with DBA. Similar to juvenile ADPKD models, cilia lengths were increased in *Pkd1* cko and *Pkd2* cko DBA+ adult tubules. However, in contrast to juvenile models, cilia lengths were normalized in *Pkd1;Thm1* and *Pkd2;Thm1* dko DBA+ tubules (Figures 2.11A and 2.11B). These differences suggest maturation-dependent effects on cilia length.

Further, we examined cilia lengths on renal cortical sections of normal human kidney (NHK) and ADPKD samples. Human ADPKD sections had longer cilia than NHK sections (Figure 2.11C), suggesting that increased cilia length is also a feature of the human disease.

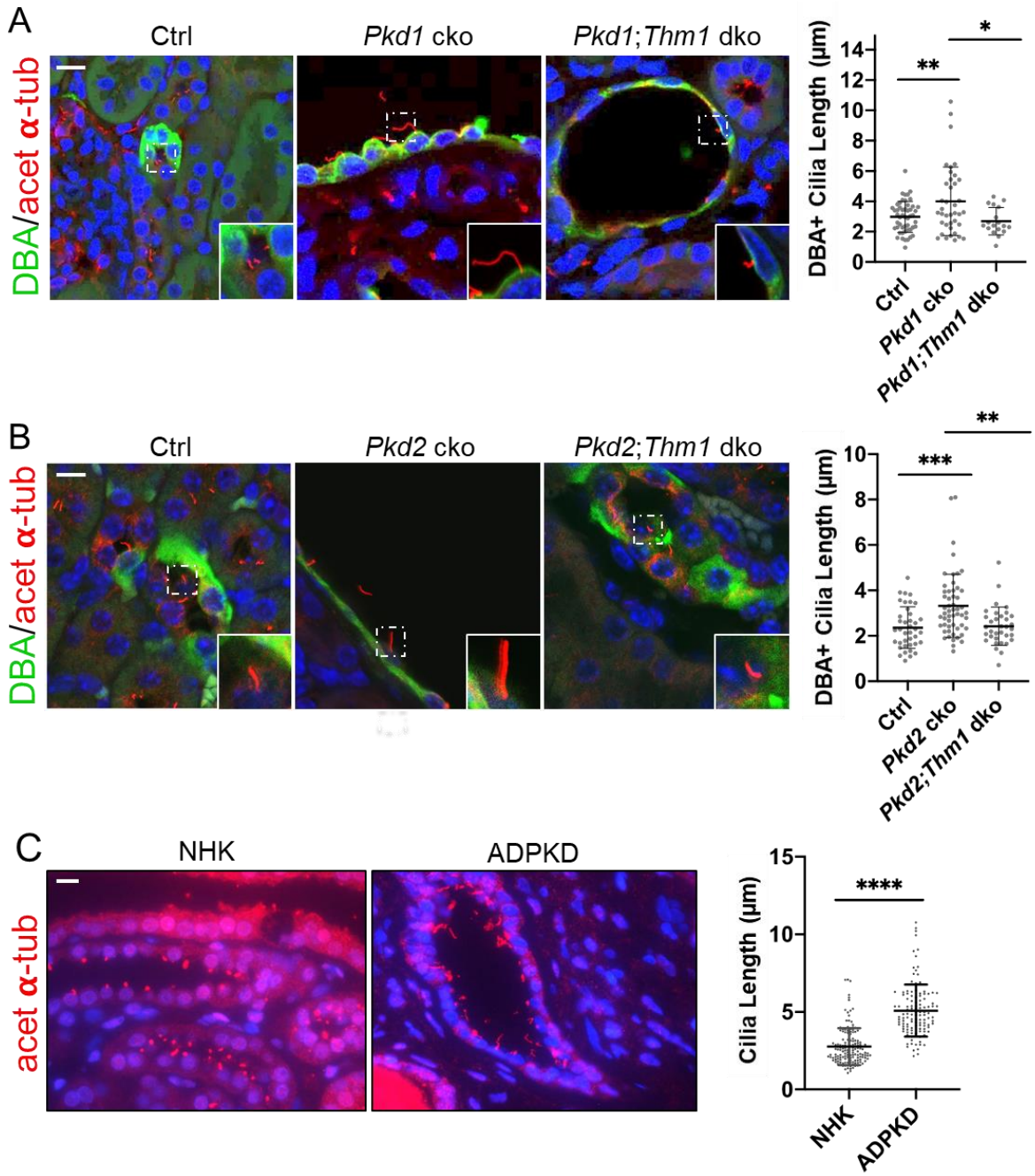

Figure 2.11 Cilia length is increased on cortical renal epithelial cells of mouse and human ADPKD kidneys.

(A) Immunostaining for acetylated α-tubulin together with DBA of *Pkd1* cko kidney cortex, and quantification of cilia lengths. Scale bar - 10μm. (B) Immunostaining for acetylated α-tubulin together with DBA of *Pkd2* cko kidney cortex, and quantification of cilia lengths. Scale bar - 10μm. (C) Immunostaining for ARL13B of normal human kidney (NHK) and ADPKD renal sections. Scale bar - 10μm. Quantification of cilia length. Bars represent mean ± SD. Statistical significance was determined by one-way ANOVA followed by Tukey's test. *p<0.05; **p<0.005; ***p<0.0005; ****p<0.00005

2.5 Discussion

This study demonstrates differential effects of IFT-A deficiency in early- versus late-onset ADPKD mouse models, highlighting differences in developing versus mature renal microenvironments (Table 1). These data also show that deleting *Thm1* in an early-onset ADPKD model has tubule-specific effects: partially protecting cortical collecting duct structure, but worsening the decline of proximal tubular structural integrity; and restoring glomerular number, but increasing glomerular dilation.

Table 1. Role of *Thm1* loss in PKD of ADPKD mouse models

Relative to *Pkd2* or *Pkd1* cko		Juvenile	Adult
KW/BW		↓	↓
BUN		-	↓(*Pkd1*); - (Pkd2)
Cystic index	**Glomeruli**	↑	N/A
	Proximal tubule	↑	↓
	Loop of Henle	-	↓
	Collecting duct	↓	↓
Cilia length	**Proximal tubule**	↑	N/A
	Collecting duct	-	↓
STAT3		↑	↓
ERK		-	↓

"N/A" Not available; "-" not affected.

In *Pkd2;Thm1* dko juvenile mice, STAT3 activation was increased. Since cortical collecting duct cystogenesis was reduced, this suggests that STAT3 signaling may contribute to other disease processes. *Pkd2;Thm1* dko kidneys showed increased proximal tubular and glomerular dilations, and increased STAT3 activation could potentially drive these dilations. STAT3 signaling may also be involved in fibrosis. However, while STAT3 activation was increased in *Pkd2;Thm1* dko mice, staining of αSMA, a marker of myofibroblasts, was not. In contrast to studies suggesting a pathogenic role for increased STAT3 signaling, a recent study has shown that tubular STAT3 activation restricts immune cell infiltration in *Pkd1* cko mice[181]. Genetic deletion of *Stat3* together with *Pkd1* in renal tubular cells slightly reduced cystic burden, but did not ameliorate kidney function and increased interstitial inflammation. Thus, STAT3 activation in *Pkd2;Thm1* dko mice could potentially serve a protective role against inflammation.

In several ADPKD mouse models, $PKD1^{RC/RC}$, *Pkd1* and *Pkd2* cko mice, renal primary cilia are lengthened[182, 183]. Our data showing increased cilia length in both *Pkd2* juvenile and adult mouse models and in *Pkd1* adult mouse models are consistent with these studies. Additionally, the increased cilia length in ADPKD tissue sections suggest that similar ciliary mechanisms may be relevant to the human disease. We observed a range of cilia lengths within a genotype. This could result from limitations of quantifying immunostained tissue sections. Additionally, multiple factors influence renal cilia length and could also contribute to this variability. Our data suggest that in addition to genotype, cilia length varied by renal tubule and age, suggesting that factors within a tubule's microenvironment affect cilia length. Cilia length is determined by the ratio of cilia assembly and disassembly. As well, intracellular Ca^{2+} and cAMP, oxidative stress, cytokines, and fluid flow influence ciliary length of renal epithelial cells[184-186]. These multiple factors indicate that cilia length regulation may be fine-tuned in order to

maintain renal tubular structure and function. In support of this, genetic and pharmacological inhibition of cilia disassembly in *Pkd1* cko mice increased renal cilia length and exacerbated ADPKD[187]. In the *jck* non-orthologous ADPKD mouse model, renal primary cilia are also lengthened, and pharmacological shortening of primary cilia in *jck* mutant mice was associated with an attenuation of the ADPKD phenotype[116, 188]. Moreover, cilia length is altered also in acute kidney injury and chronic kidney disease[189-192]. Thus, to understand mechanisms of renal tubule homeostasis, the connections between cilia length and cilia function, and renal disease require deeper study.

Thus far, the effects of deleting Ift-B genes, *Kif3a* and *Ift20*, and of the IFT-A adaptor, *Tulp3*, in ADPKD mouse models have been demonstrated. Ift-B gene deletion attenuates PKD severity in both tubular-specific juvenile and adult models of ADPKD[116]. In contrast, *Tulp3* deletion did not rescue renal cystic disease in a tubular-specific juvenile model of ADPKD, but did in an adult model[171, 193]. Similarly, global deletion of *Thm1* in a juvenile ADPKD model results in a complex phenotype, but in an adult model, rescues most aspects of the renal cystic disease. Perinatal loss of *Thm1* results in cystic kidney disease[143], indicating that *Thm1* is required for kidney maturation, which might account for the lack of rescue in juvenile models. However, perinatal deletion of *Kif3a* and mutation of *Tulp3* also causes renal cystic disease[171, 194], suggesting these genes are required as well for kidney differentiation and maturation. Thus, there may be functional differences between IFT-B and IFT-A and *Tulp3* that result in attenuated disease in juvenile *Pkd;Ift-B* dko mice, but not in *Pkd;Thm1* or *Pkd;Tulp3* dko mice. These differences could include differential roles in IFT, cilia length regulation, and/or ciliary-mediated signaling. For instance, *Ift-B* genes are required for anterograde IFT, unlike *Thm1* and *Tulp3*.

While IFT-B and IFT-A regulate cilia length, a role for *Tulp3* in altering cilia length has not been reported. Further, IFT-B and IFT-A mutants have shown opposing signaling phenotypes.

We noted that in the late-onset models, BUN levels were similar between *Pkd2* cko and *Pkd2;Thm1* dko mice, while in contrast, BUN levels in *Pkd1;Thm1* dko mice were reduced relative to those of *Pkd1* cko mice, suggesting *Thm1* deletion might confer greater protection in *Pkd1* cko mice than in *Pkd2* cko mice. We deleted *Pkd2* one week earlier than *Pkd1*, since *Pkd1* deficiency results in a more severe ADPKD phenotype than *Pkd2* deficiency. Importantly, *Thm1* deletion at P28 resulted in BUN levels similar to those of control mice at 6 months of age, and *Thm1* deletion at either P28 or P35 resulted in kidney morphology resembling control. Thus, the BUN data may suggest a functional difference between *Pkd2;Thm1* dko and *Pkd1;Thm1* dko mice.

The mechanisms by which *Pkd; cilia* dko mice attenuate ADPKD severity are still obscure. Reducing *Ccl2* signaling and altering lipid composition of the ciliary membrane have been proposed[170, 171, 193]. Primary cilia are designed to detect both chemical and mechanical cues in the extracellular environment. While mechanosensing by primary cilia and the polycystins has been controversial, recent studies have renewed interest in a potential mechanosensory role for the polycystins, particularly regarding tissue microenvironment stiffness[195, 196]. If sensing physical forces in the tissue microenvironment is essential to maintaining renal tubular function, then other mechanical cues that would change with cyst growth include shear stress and intraluminal pressure. Cilia length could then also be a possible contributing factor in PKD severity. Further, by extrapolating findings of cilia studies from the cancer field[197], cilia of not only renal tubular epithelial cells, but of interstitial cells might also affect signaling and disease severity.

In summary, our data demonstrate for the first time the role of IFT-A in an ADPKD context in developing versus mature kidneys. Defining the mechanisms by which IFT-A deficiency attenuates ADPKD in adult models will be critical to identifying potential therapeutic targets.

Chapter Three: Role of *Thm1* in liver cystogenesis of ADPKD mouse models

3.1 Abstract

Polycystic liver disease (PLD) is a genetic disorder characterized by the growth of numerous hepatic cysts. Hepatic cysts can be found in up to 94% of ADPKD patients older than 35 years of age. In mice, loss of *Pkd1* or *Pkd2* also causes PLD, but interestingly, deletion of certain *Ift-B* genes together with *Pkd1* reduces PLD severity. Here, I examined the role of IFT-A deficiency in PLD of early- and late-onset *Pkd2* conditional knock-out (cko) mice. Perinatal deletion of *Pkd2* causes PLD by postnatal day (P) 21. In contrast, perinatal deletion of *Thm1* causes a ductular reaction, characterized by abnormal proliferation of cholangiocytes, increased number of biliary ducts, and increased biliary fibrosis in the liver portal area, without cysts. *Thm1* cko juvenile mice also show increased proliferation of hepatocytes. Perinatal deletion of *Thm1* in *Pkd2* cko mice increases liver weight/body weight (LW/BW) ratio, hepatocyte proliferation, liver necrosis and STAT3 activation, suggesting that *Thm1* deletion exacerbates PLD in juvenile ADPKD mice. In addition, primary cilia were lengthened in livers of *Pkd2* cko mice, and normalized in *Pkd2*;*Thm1* double knock-out (dko) mice, with some cilia showing a bulb-like structure at the distal tip, indicating a retrograde IFT defect caused by *Thm1* loss. Deletion of *Pkd2* at 4 weeks of age results in PLD at 6 months of age. In contrast, deletion of *Thm1* at 4 weeks of age does not cause liver cysts nor a ductular reaction. Loss of *Thm1* together with *Pkd2* at 4 weeks of age does not ameliorate PLD in *Pkd2*;*Thm1* dko females, but reduces LW/BW ratios in *Pkd2*;*Thm1* dko males at 6 months of age. These data reveal novel roles for IFT-A in biliary development and disease.

3.2 Introduction

Polycystic liver disease (PLD) is a genetic disorder characterized by numerous (>20) fluid-filled cysts in the liver[119]. PLD can be divided into two distinct hereditary disorders: PLD in association with Autosomal Dominant Polycystic Kidney disease (ADPKD) and PLD in the absence of renal impairment. In humans, PLD occurs as an extrarenal manifestation in up to 94% of ADPKD patients who are older than 35 years of age[124]. Clinical manifestations including pain, digestive disorders and respiratory discomfort may be due to hepatomegaly or cyst complications such as hemorrhage or infection[122]. Treatments are insufficient and surgical means are the main interventions to reduce pain and discomfort in symptomatic PLD patients. Therefore, there is strong interest in exploring mechanisms promoting hepatic cystogenesis to find potential therapies for PLD.

Primary cilia are sensory organelles proposed to play key roles in the pathobiology of hepatic cystogenesis. Hepatic cysts derive from bile ducts, which are lined with ciliated cholangiocytes. Primary cilia on cholangiocytes are found to be abnormal in PLD animal models and ADPKD patients with liver symptoms[134-136]. In addition, liver cysts are frequently observed in ciliopathies, a group of diseases caused by dysfunction of primary cilia. Furthermore, mutations in PLD-associated genes lead to aberrant expression and subcellular localization of polycystin 1 (PC1), which is encoded by *PKD1* and is translocated to primary cilia to fulfil its function[132].

Primary cilia are built and maintained by intraflagellar transport (IFT), which mediates the bi-directional transport of protein cargos along the ciliary axoneme. IFT can be divided into two protein subcomplexes: IFT complex B (IFT-B) and IFT complex A (IFT-A). IFT-B interacts with the kinesin motor to mediate anterograde IFT, while IFT-A together with cytoplasmic dynein is

required for retrograde IFT, and ciliary entry of membrane and signaling molecules [162]. Mutations in *IFT-B* genes have been reported in families with biliary ciliopathies[198]. In mice, mutation of *Ift-B* genes alone causes rapid expansion of the biliary regions with an increased number of cholangiocytes and periportal fibrosis[199]. While loss of ADPKD orthologous genes, *Pkd1* and *Pkd2* in mice causes polycystic liver disease[200], interestingly, deletion of *Ift-B* genes in adult-onset *Pkd1* mouse models ameliorates bile duct-derived liver cyst formation[201]. Mutations in the *Ift-A* and *Ift–B* genes often cause contrasting ciliary phenotypes and can also result in opposing signaling phenotypes, suggesting differing roles for IFT-A and IFT–B in the pathobiology of ciliopathies [50, 51, 165, 169]. Thus, study of *Ift-A* mutants is essential for understanding the molecular mechanisms underlying hepatic cystogenesis.

Tetratricopeptide repeat–containing hedgehog modulator-1 (*Thm1;* also known as *Ttc21b,* an orthologue of *Chlamydomonas reinhardtii Fla17*/*Ift139*) encodes an IFT-A protein [50]. Deletion of *Thm1* results in various ciliopathy phenotypes, including cystic kidney disease [143] and obesity[144, 145]. Here we have investigated the role of *Thm1* in polycystic liver disease in a *Pkd2*-null mouse model of ADPKD. The goal of this study is to better define the contribution and importance of IFT-A in cystic liver disease. Importantly, these are the first studies to investigate the role of IFT-A in PLD in an ADPKD mouse model.

3.3 Methods

3.3.1 Animals

Pkd2$^{flox/flox}$ and *ROSA26-Cre* mice were obtained from the Jackson Laboratories (Stock numbers 017292 and 004847, respectively). Generation of *Thm1* cko mice has been previously described [143]: *Thm1*$^{aln/+}$; *ROSA26Cre*$^{ERT+}$ male mice were mated with *Thm1*$^{flox/flox}$ females.

ROSA26-Cre$^{ERT/+}$ and *Pkd2* floxed alleles were introduced into the colony to generate *Thm1*$^{flox/flox}$*;Pkd2*$^{flox/flox}$ or *Thm1*$^{flox/flox}$*;Pkd2*$^{flox/+}$ females and *Pkd2*$^{flox/flox}$*; Thm1*$^{aln/+}$, *ROSA26-Cre*$^{ERT/+}$ males, which subsequently were crossed. To generate early-onset models of ADPKD, nursing mothers were injected intraperitoneally at postnatal day 0 (P0) with tamoxifen (10mg/40g; Sigma) to induce gene deletion. Mice were sacrificed at P21. To generate late-onset models, offspring of matings between *Thm1*$^{flox/flox}$*;Pkd2*$^{flox/flox}$ or *Thm1*$^{flox/flox}$*;Pkd2*$^{flox/+}$ females with *Pkd2*$^{flox/flox}$*; Thm1*$^{aln/+}$, *ROSA26-Cre*$^{ERT/+}$ males were injected intraperitoneally at P28 with tamoxifen (10mg/40g). Mice were sacrificed at 6 months of age. All mouse lines were maintained on a pure C57BL6/J background (backcrossed 10 generations).

3.3.2 Liver and body weight measurements

Livers were dissected and weighed using a standard laboratory weighing scale. The liver weight (LW) / body weight (BW) ratio was calculated as the liver weight divided by body weight for each mouse.

3.3.3 Histology analysis

The left lobe of the liver was fixed in 10% formalin for several days and then processed in a tissue processor and embedded in paraffin. Tissue sections (7μm) were obtained with a microtome. Sections were deparaffinized, rehydrated through a series of ethanol washes and stained with hematoxylin and eosin (H&E) or picrosirius red according to standard protocols[202]. Images were taken with a Nikon 80i microscope equipped with a Nikon DS-Fi1 camera. ImageJ was used to quantify cystic area and necrotic area in H&E-stained sections.

3.3.4 Immunofluorescence

Following deparaffinization and rehydration described above, tissue sections were subjected to antigen retrieval, performed by steaming sections for 25 minutes in Sodium Citrate Buffer (10 mM Sodium Citrate, 0.05% Tween 20, pH 6.0). Sections were blocked with 1% BSA in PBS for 1 hour at room temperature, and then incubated with primary antibodies against acetylated-α tubulin (1:4000; Sigma), IFT81 (1:200; Proteintech), αSMA (1:500; Abcam) and PCNA (1:300; Cell Signaling) overnight at 4°C. Sections were washed three times in PBS, and then incubated with secondary antibodies conjugated to Alexa Fluor 488 or Alexa Fluor 594 (1:500; Invitrogen by Thermo Fisher Scientific) for 1 hour at room temperature. After three washes of PBS, sections were mounted with Fluoromount-G containing 4′,6-diamidino-2-phenylindole (DAPI) (Electron Microscopy Sciences). Staining was visualized and imaged using a Nikon 80i microscope with a photometrics camera or a Nikon Eclipse TiE attached to an A1R-SHR confocal, with an A1-DU4 detector, and LU4 laser launch.

3.3.5 Western blot

Passive Lysis Buffer (Promega) containing proteinase inhibitor cocktail (Pierce) was used to generate protein extracts from frozen liver tissue. Tissue was homogenized by using 0.5 mm zirconium oxide PINK beads (Next Advance) and a Bullet Blender Storm (Next Advance) set at Speed 8 for approximately 3 minutes. Lysates were centrifuged at 4^0C at maximum speed for 1 minute and the supernatant was collected. Protein concentrations were determined using the bicinchoninic acid protein (BCA) assay reagents (Pierce). Western blot was performed as described [143], using primary antibodies for P-STAT3, STAT3, P-ERK, ERK, (Cell Signaling).

SuperSignal West Femto Chemiluminescent Substrate (Pierce) was used to detect signal. ImageJ was used to quantify Western blot signal.

3.3.6 Statistics

Statistical significance ($P < 0.05$) was determined using one-way ANOVA followed by Tukey's test or unpaired t-test for comparison of more than two groups or of two groups, respectively. GraphPad Prism 8 software was used to perform these analyses.

3.4 Results

3.4.1 *Thm1* loss alone causes a ductular reaction and exacerbates severity of polycystic liver disease in *Pkd2* cko juvenile mice

Recent data indicate that mutation of *Ift-B* genes in mice causes rapid expansion of the biliary region[199]. To explore the role of Ift-A deficiency in the liver, we deleted *Thm1* alone, and together with *Pkd2* in mice at P0, and examined the liver phenotypes of control, *Thm1* cko, *Pkd2* cko, and *Pkd2;Thm1* dko mice at P21. At this stage, *Thm1* cko mice had similar LW/BW ratios as those of control mice. Liver histology revealed expansion of the biliary region with increased number of cholangiocytes and bile ducts - a phenotype defined as a ductular reaction (Figure 3.1A) [203]. Deletion of *Pkd2* perinatally led to an early onset, rapidly progressing polycystic liver disease, with increased LW/BW ratios compared to control mice (Figure 3.1A and 3.1B). Loss of *Thm1* in *Pkd2;Thm1* dko mice does not alter hepatic cystogenesis relative to *Pkd2* cko mice *(*Figure 3.1A and 3.1C), but does increase severity of the liver disease, causing increased LW/BW ratios and multifocal necrosis (Figure 3.1A and 3.1D).

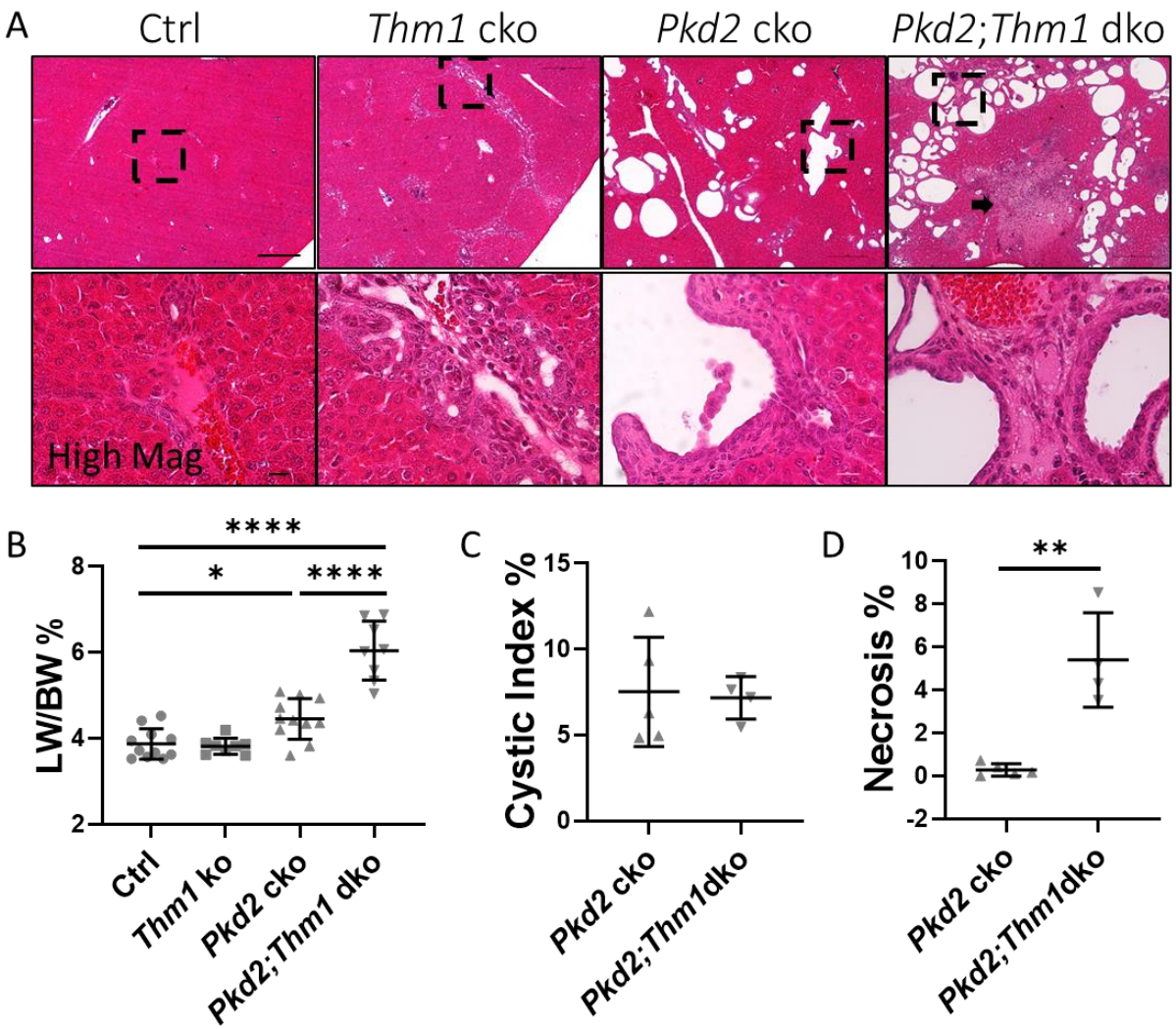

Figure 3.1 Biliary defects and liver cyst in *Thm1* cko, *Pkd2* cko, and *Pkd2;Thm1* dko mice at P21
(A) Representative low-magnification (4x, top) and high-magnification (40x, bottom) images of H&E-stained liver sections from 3-week-old control, *Thm1* cko, *Pkd2* cko and *Pkd2;Thm1* dko mice. Scale bar = 200 μm (top), and 10 μm (bottom). (B) LW/BW ratios of 3-week-old control, *Thm1* cko, *Pkd2* cko and *Pkd2;Thm1* dko mice. (C) Liver cyst index and (D) percentage of necrosis of *Pkd2* cko and *Pkd2;Thm1* dko mice. Statistical significance was determined by ANOVA or t-test. *P<0.05; **P<0.01; ****P< 0.0001.

3.4.2 *Thm1* loss alone causes biliary fibrosis

We next examined liver fibrosis, which is a common feature of severe PLD and presents in more than half of PLD patients[204]. Liver sections were immunostained for αSMA to detect myofibroblasts and also stained using picrosirius red to label collagen fibers (Figure 3.2). In *Thm1* cko livers, fibrosis was present in the periportal regions (Figure 3.2). In *Pkd2* cko and *Pkd2; Thm1* dko livers, similar levels of fibrosis were observed around hepatic cysts (Figure 3.2). These data suggest that perinatal loss of *Thm1* induces biliary fibrosis, yet does not exacerbate fibrosis in early-onset PLD mouse models at P21.

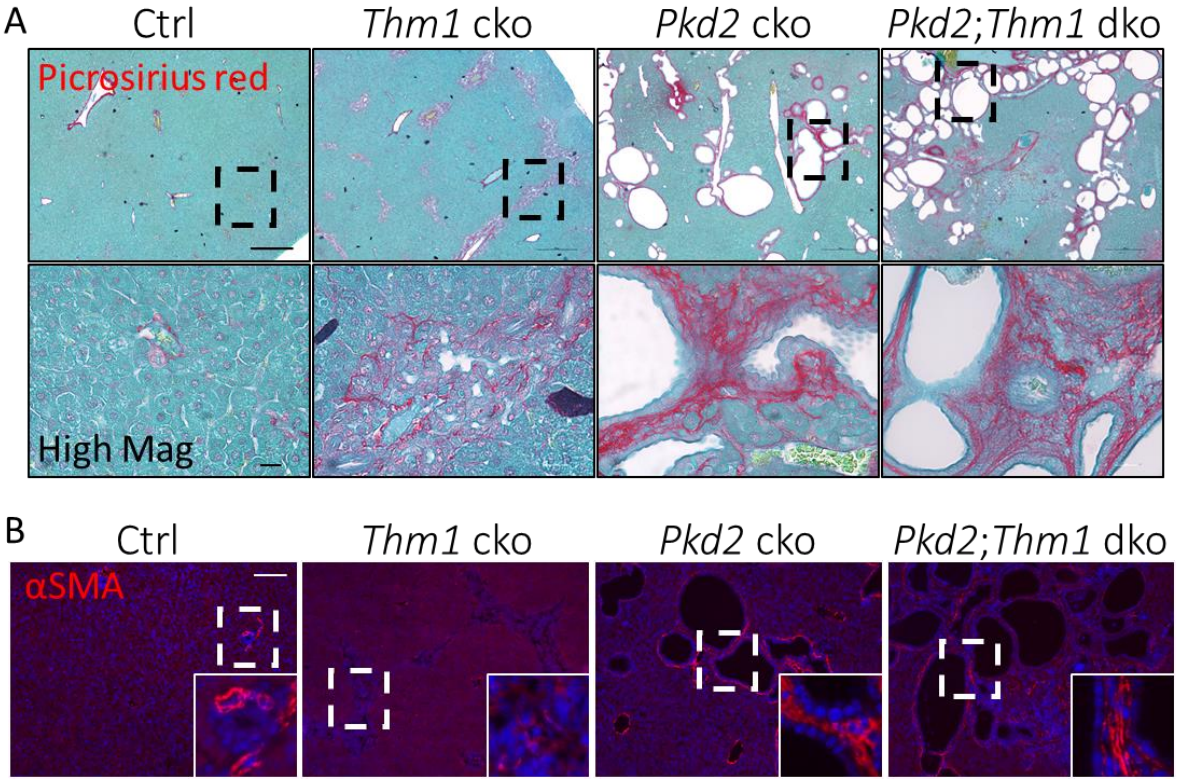

Figure 3.2 *Thm1* cko, *Pkd2* cko and *Pkd2;Thm1* dko mice develop liver fibrosis at P21
(A) Representative low- (4x, top) and high-magnification (20x, bottom) images of picrosirius red-stained liver sections from 3-week-old control, *Thm1* cko, *Pkd2* cko and *Pkd2;Thm1* dko mice. Scale bar = 200 μm (top), and 10 μm (bottom) (B) Immunostaining of αSMA (red) and DAPI (blue) in liver sections from 3-week-old control, *Thm1* cko, *Pkd2* cko and *Pkd2;Thm1* dko mice. Scale bar = 100 μm.

3.4.3 *Thm1* loss increases proliferation of hepatocytes and cholangioctyes

A major mechanism underlying hepatic cystogenesis is enhanced proliferation of cyst-lining epithelial cells. Thus, we immunostained liver sections for PCNA to assess proliferation. In control livers, PCNA was not observed in the biliary regions, but was observed in hepatocytes of the liver parenchyma, consistent with the liver still undergoing maturation at P21. In contrast, PCNA+ cells were observed in the biliary regions of *Thm1* cko livers and lining cysts of *Pkd2* cko and *Pkd2*; *Thm1* dko livers (Figure 3.3). There was no difference in the number of PCNA+ cells between *Pkd2* cko and *Pkd2*; *Thm1* dko sections. In *Thm1* cko and *Pkd2*;*Thm1* dko livers, there was an increased number of PCNA+ hepatocytes relative to control and *Pkd2* cko livers (Figure 3.3), indicating more proliferation of hepatocytes in the absence of *Thm1*.

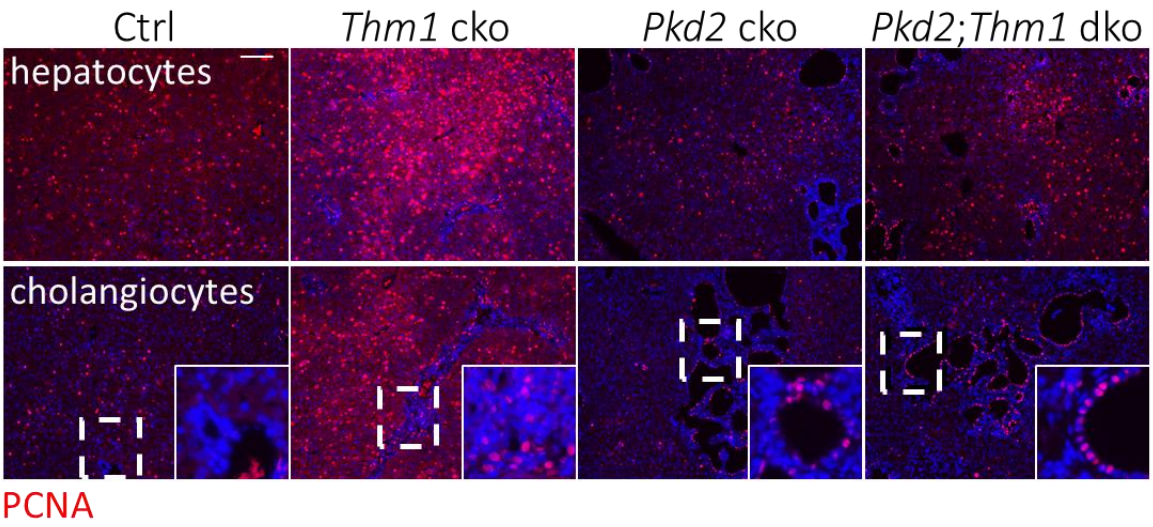

Figure 3.3 Proliferation of hepatocytes and cholangiocytes in control, *Thm1* cko, *Pkd2* cko and *Pkd2;Thm1* dko mice

Representative images for PCNA (red) and DAPI (blue) in hepatocytes (top) and cholangiocytes (bottom) from 3-week-old control, *Thm1* cko, *Pkd2* cko and *Pkd2;Thm1* dko mice. Scale bar = 100 μm.

3.4.4 P-STAT3 levels are increased in *Pkd2*;*Thm1* dko livers

We have observed that STAT3 activation is increased in *Pkd2*;*Thm1* dko kidneys (Figure 2.8). Using Western blot analysis, we observed increased STAT3 activation in *Pkd2* cko livers at P21, and further STAT3 activation in *Pkd2*;*Thm1* dko livers (Figure 3.4A and 3.4B). In cholangiocytes, ERK signaling is the main pathway that drives proliferation and is significantly increased in cyst-lining epithelia[200]. However, we did not observe significant differences in ERK signaling in the livers of the various genotypes (Figure 3.4A and 3.4B). P-ERK might be expressed only in cholangiocytes, but the liver extracts may have been derived from tissue with a high content of hepatocytes. Thus, immunostaining for P-ERK in liver sections will be required to determine if P-ERK is increased in cholangiocytes. Similarly, immunostaining for P-STAT3 in liver sections will be required to determine which cell types express P-STAT3.

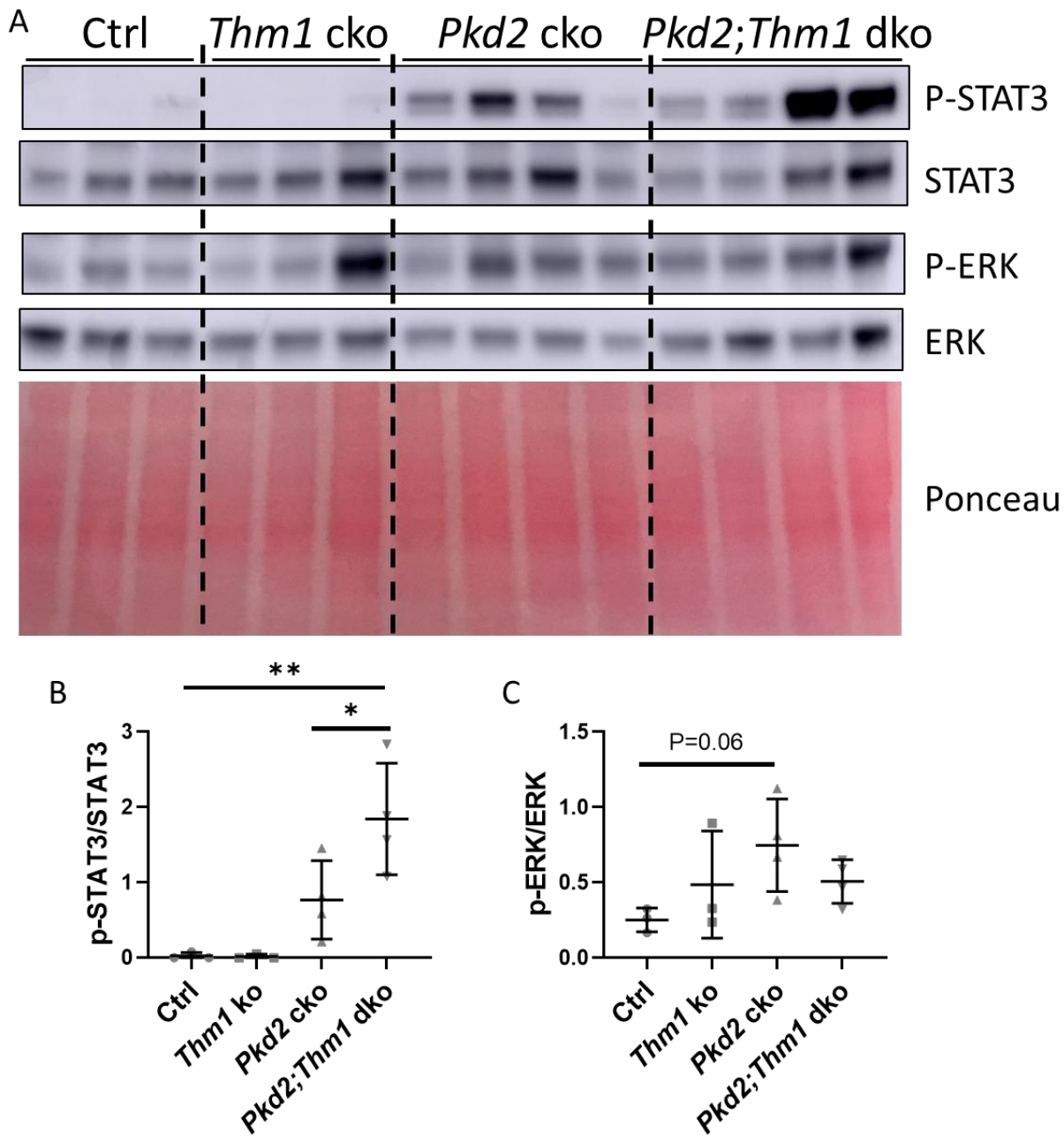

Figure 3.4 STAT3 and ERK signaling in control, *Thm1* cko, *Pkd2* cko and *Pkd2*;*Thm1* dko mice at P21

(A) Western blot of whole liver extracts. (B) and (C) Western blot quantifications show increased activation of P-STAT3 signaling in *Pkd2*;*Thm1* dko livers (B) and slightly increased p-ERK signaling in *Pkd2* cko livers (C). Western blot was quantified using ImageJ. Statistical significance was determined by ANOVA. *P<0.05; **P<0.01.

3.4.5 *Pkd2;Thm1* double mutants have shortened primary cilia with a bulb like structure at the tip

At P21, primary cilia are present only on cholangiocytes lining the bile ducts, and are not present on hepatocytes[205]. We next examined cilia length of cholangiocytes by co-immunostaining liver sections for acetylated α-tubulin, a marker of the ciliary axoneme, and for IFT81, a component of the IFT-B complex. We observed increased cilia length in *Pkd2* cko cholangiocytes relative to control (Figure 3.5). In *Pkd2;Thm1* dko cholangiocytes, cilia length was not different from control, and shorter than those of *Pkd2* cko, suggesting that cilia length is normalized with additional loss of *Thm1* in *Pkd2* cko cholangiocytes (Figure 3.5). In addition, IFT-81 accumulated at the tip of several primary cilia forming a bulb-like structure, indicating retrograde IFT defects in some *Pkd2*;*Thm1* dko cilia (Figure 3.5A).

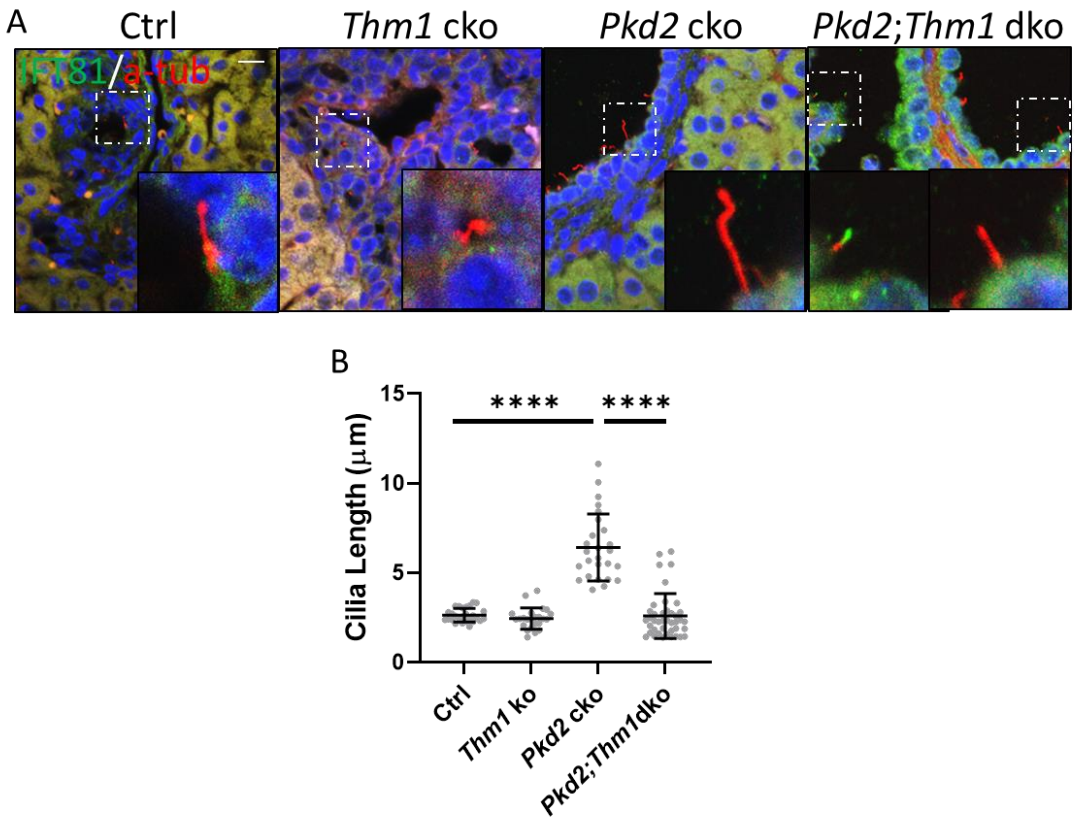

Figure 3.5 Primary cilia of cholangiocytes in control, *Thm1* cko, *Pkd2* cko and *Pkd2*;*Thm1* dko mice
(A) Representative immunostaining images of acetylated α-tubulin (red), IFT81 (green) and DAPI (blue) in cholangiocytes from 3-week-old control, *Thm1* cko, *Pkd2* cko and *Pkd2;Thm1* dko mice. Scale bar = 10 μm. (B) Quantification of cilia length shows elongated primary cilia in *Pkd2* cko mice. Cilia lengths were quantified by ImageJ. Statistical significance was determined by ANOVA. ****P< 0.0001.

3.4.6 *Thm1* loss in adult male mouse models of ADPKD attenuates severity of polycystic liver disease

Cilia ablation by *Ift-B* deficiency ameliorates bile duct-derived liver cyst formation in adult *Pkd1* mouse models[201]. To examine the effect of IFT-A deficiency in adult, slowly progressive PLD mouse models, we deleted *Thm1* together with *Pkd2* at P28, and examined the liver phenotypes of control, *Thm1* cko, *Pkd2* cko and *Pkd2;Thm1* dko mice at 6 months of age. In human ADPKD, female patients are associated with more severe PLD[74]. However, in *Pkd2* cko mice at 6 months of age, we did not observe sex differences for liver weight/body weight (LW/BW) ratios (Figure 3.6A). In *Pkd2*;*Thm1* dko mice, LW/BW ratios were reduced in males (Figure 3.6B and 3.6H), and remained similar in females (Figure 3.6C), relative to those of *Pkd2* cko mice. We have shown that global deletion of *Thm1* at P35 causes obesity[145]. Loss of *Thm1* together with *Pkd2* at P28 also caused obesity in both males and females at 6 months of age (Fig 3.6D and 3.6E). *Pkd2;Thm1* dko liver weight was increased in females but not in males when compared with *Pkd2* cko liver weight, which might contribute to the decreased LW/BW ratios in *Pkd2;Thm1* dko males.

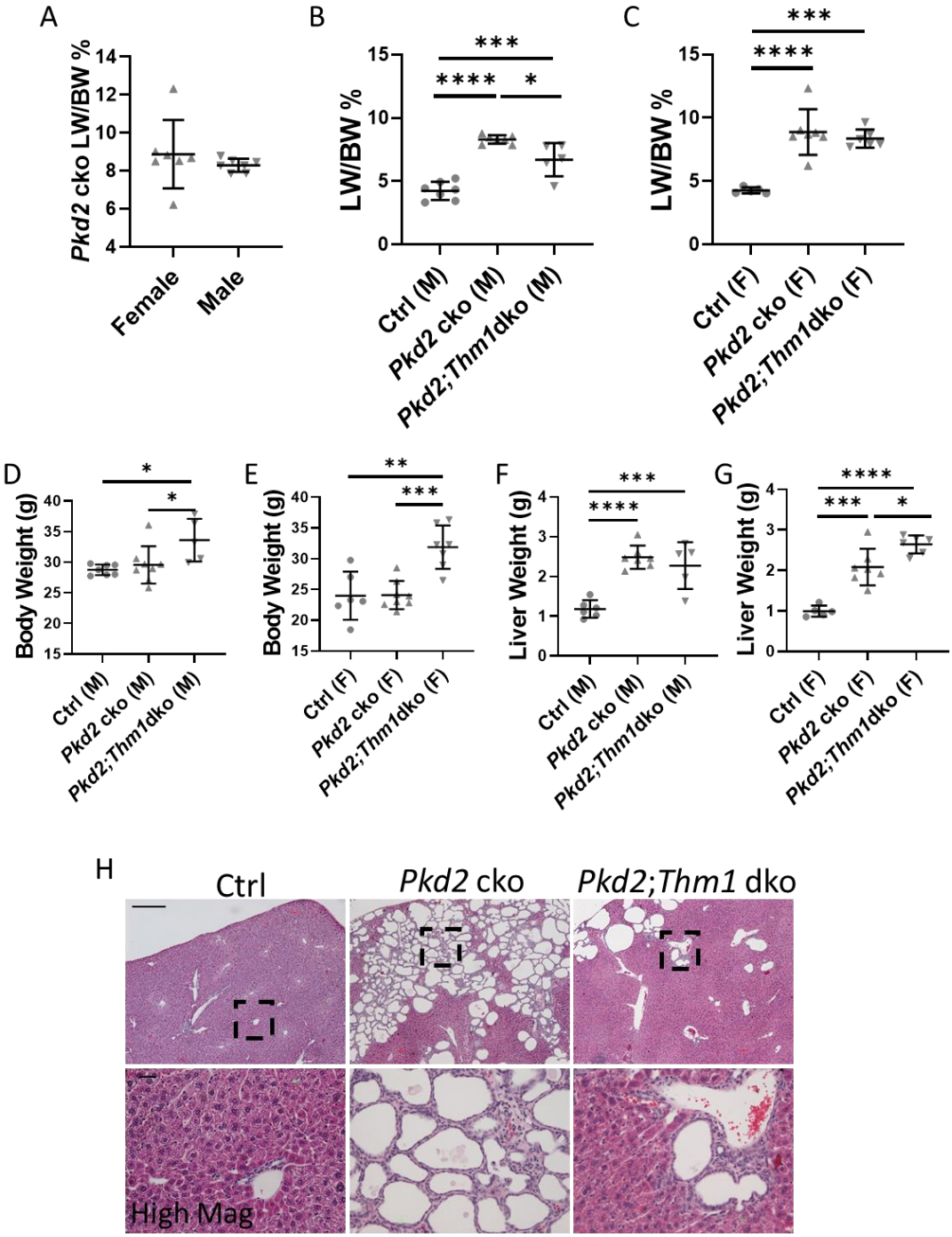

Figure 3.6 Adult onset loss of *Thm1* attenuated severity of polycystic liver disease in *Pkd2* cko males
LW/BW ratios (A-C), body weight (D and E), liver weight (F and G) of 6 months old control, *Pkd2* cko and *Pkd2;Thm1* dko male and female mice. Statistical significance was determined by ANOVA or t-test. *P<0.05; **P<0.01; ***P< 0.001; ****P< 0.0001. (H) Representative low-magnification (4x, top) and high-magnification (20x, bottom) images of H&E-stained liver sections from 6 months old control, *Pkd2* cko and *Pkd2;Thm1* dko male mice. Scale bar = 200 μm (top), and 20 μm (bottom).

3.5 Discussion

We deleted an *Ift-A* gene, *Thm1*, together with *Pkd2* perinatally and in adulthood to induce rapidly progressing and slowly progressing PLD mouse models, respectively. Our data reveal that perinatal deletion of *Thm1* together with *Pkd2* increases severity of liver disease, causing increased LW/BW ratios and areas of necrosis. In contrast, loss of *Thm1* in adult models of ADPKD ameliorates liver cystogenesis in males at 6 months of age with decreased LW/BW ratios. In addition, our data reveal a novel role for IFT-A in biliary development. Perinatal loss of *Thm1* alone causes a ductular reaction characterized by abnormal proliferation of cholangiocytes, increased numbers of biliary ducts, and biliary fibrosis in the liver portal area. These data are the first to demonstrate a role for IFT-A deficiency in liver-associated ciliopathies.

Ductular reaction is characterized by the proliferation of bile ducts induced by liver injury and is commonly observed in biliary diseases, such as primary biliary cholangitis, primary sclerosing cholangitis, and biliary atresia[203]. The mechanism underlying ductular reaction induced by liver injury is unknown. Several experimental models to investigate ductular reaction have been proposed, including mice with bile duct ligation (a surgical model), *Rhesus* rotavirus type A (RRV)-treated mice (an infective model), and *Mdr2* knockout mice (a genetic model)[206]. Here, our novel finding that deletion of *Thm1* induces ductular reaction links primary cilia to biliary abnormalities and provides a new genetic model to study biliary disease.

We observed enhanced proliferation of cholangiocytes in the biliary region, and loss of *Thm1* may have a direct impact on cholangiocytes. In the liver, primary cilia are present on cholangiocytes to sense fluid flow and regulate intracellular Ca^{2+} and cAMP levels[146]. Disruption of cilia on cholangiocytes can significantly increase intracellular cAMP levels[22], which is a major stimulus of proliferation[137]. Previous studies have shown that loss of *Thm1*

results in a shortened primary cilium with proteins accumulating at the distal tip, indicating retrograde IFT defects[50, 146, 147]. However, since ductular reaction is generally induced by liver injury, we cannot rule out the possibility that the abnormal proliferation of cholangiocytes is a response to unknown liver injuries caused by *Thm1* loss. We observed increased proliferation of hepatocytes in *Thm1* cko livers, which could be due to a delay of liver development or regeneration of the hepatocyte pool in response to liver injury. In mice, the liver grows in size and differentiates during the first 4 weeks after birth[207]. We did not observe differences in liver weight, body weight and LW/BW ratios between control and *Thm1* cko mice, indicating liver growth is at a similar stage and the difference in proliferation is more likely coming from a potential unknown liver injury caused by *Thm1* loss. In addition, we did not observe ductular reaction when *Thm1* is deleted at 5 weeks of age (data not shown), suggesting that a developmental window is important to inducing the ductular reaction.

Perinatal loss of *Thm1* does not cause liver cysts. In addition, in *Pkd2*;*Thm1* dko mice, additional loss of *Thm1* does not enhance hepatic cystogenesis. These data suggest that unlike the role of *Thm1* in the kidney, *Thm1* may not be involved in the pathogenesis of hepatic cystogenesis in the early-onset model, indicating tissue-specificity in the roles of *Thm1*. However, the PLD severity is increased in *Pkd2*;*Thm1* dko mice, resulting in increased LW/BW ratios and increased areas of necrosis, indicating that mechanisms, other than cyst-promoting, contribute to this disease. A possible mechanism is inflammatory cell infiltration. Ductular reaction is often observed with inflammatory cell infiltration[208]. In *Ift-B* mutated mice, accumulation of immune cells was observed in the periportal area[199]. In pre-cystic kidneys of *Thm1* cko mice, there is also increased expression of the cytokine, *Ccl2* (Luci Silva, pers. comm.). These data suggest that additional loss of *Thm1* might recruit more immune cells to *Pkd2* cko livers and thereby increase

severity of the disease. In addition, we also observed increased activation of STAT3 signaling in *Pkd2*;*Thm1* dko livers. The role of STAT3 signaling in PLD remains unclear. Since the degree of hepatic cystogenesis is not altered in *Pkd2*;*Thm1* dko mice, STAT3 signaling likely does not contribute to hepatic cystogenesis. In many tumors, STAT3 has been reported to be consistently activated to induce transcription of cytokines, chemokines and growth factors, which is associated with macrophage activation and inflammatory responses[209]. Cancer cells and cyst-lining cells share similarities such as enhanced proliferation. Thus, there is a possibility that STAT3 activation may play a critical role in the inflammatory microenvironment in cystic liver disease.

A previous study showed that disruption of primary cilia with *Ift-B* deletion at 4 weeks of age dramatically ameliorates hepatic cystogenesis at 4 months of age in a *Pkd1* cko adult mouse model of ADPKD. Here we did not observe a consistent decrease in cystogenesis in adult onset *Pkd2*;*Thm1* dko mice at 6 months of age. At most, we observed slightly decreased LW/BW ratios in adult onset *Pkd2*;*Thm1* dko males at 6 months of age. The difference between the *Ift-B;Pkd1* results and our data might reflect differing roles of IFT-A and IFT-B in hepatic cystogenesis. We have observed that cystogenesis is reduced in *Pkd2*;*Thm1* dko mice (n=2) at 4 months of age when compared with that of *Pkd2* cko mice (n=3) (data not shown). There is also a lot of variability in LW/BW ratios of *Pkd2*;*Thm1* dko males at 6 months of age. These data suggest that adult loss of *Thm1* might slow liver cystic disease progression as shown in mice at 4 months of age but does not alter the final outcome of PLD in mice at 6 months of age.

In summary, our work identifies a novel role for IFT-A in liver development and homeostasis.

Chapter Four: Genetic interaction of mammalian IFT-A paralogs regulates cilia loss, ciliary entry of membrane protein, Hedgehog signaling, and embryogenesis

This chapter was previously published and is reprinted here with permission, including verbiage edits. Wang W., et al., *Genetic interaction of mammalian IFT-A paralogs regulates cilia disassembly, ciliary entry of membrane protein, Hedgehog signaling, and embryogenesis.* FASEB j, 2020. **34**(5): p. 6369-6381. doi.org/10.1096/jf.201902611R. [172]

4.1 Abstract

Primary cilia are sensory organelles that are essential for eukaryotic development and health. These antenna-like structures are synthesized by intraflagellar transport protein complexes, IFT-B and IFT-A, which mediate bidirectional protein trafficking along the ciliary axoneme. Here using mouse embryonic fibroblasts (MEF), we investigate the ciliary roles of two mammalian orthologues of *Chlamydomonas* IFT-A gene, *IFT139*, namely *Thm1* (also known as *Ttc21b*) and *Thm2 (Ttc21a)*. *Thm1* loss causes perinatal lethality, and *Thm2* loss allows survival into adulthood. At E14.5, the number of *Thm1;Thm2* double mutant embryos is lower than that for a Mendelian ratio, indicating deletion of *Thm1* and *Thm2* causes mid-gestational lethality. We examined the ciliary phenotypes of mutant MEF. *Thm1*-mutant MEF show decreased ciliogenesis, shortened primary cilia, misregulated ciliary localization of IFT and BBS proteins, and reduced ciliary entry of membrane-associated proteins. *Thm1*-mutant cilia also show increased ciliary localization of the Hedgehog transducer, Smoothened, and an impaired response to Smoothened agonist, SAG. *Thm2*-null MEF show normal ciliary dynamics and Hedgehog signaling, but additional loss of a *Thm1* allele impairs response to SAG. Further, *Thm1;Thm2* double-mutant MEF show enhanced serum-induced cilia loss, and increased impairment of INPP5E ciliary import. Thus, *Thm1* and *Thm2* have unique and redundant roles in MEF. *Thm1* regulates ciliogenesis alone and, together with *Thm2*, regulates serum-induced cilia loss, ciliary entry of membrane-associated protein, Hedgehog signaling, and embryogenesis. These findings shed light on mechanisms underlying *Thm1*-, *Thm2*- or IFT-A-mediated ciliopathies.

4.2 Introduction

Cilia are evolutionarily-conserved organelles present in most eukaryotic organisms from *Chlamydomonas reinhardtii to vertebrates* [210]. These microtubular organelles can confer motility or act as sensory organelles. In the latter role, a singular cilium, termed a primary cilium, extends from the apical surface of a cell, where it detects and transduces extracellular signals. Primary cilia regulate cell cycle, cell differentiation and cell-cell communication [45].

Mutations that disrupt cilia function cause multi-system disorders, termed ciliopathies [64]. Clinical manifestations can include craniofacial and neural tube defects, retinal degeneration, skeletal dysplasia, fibrocystic diseases of the kidney, liver, and pancreas, obesity, and male infertility [211]. Understanding the role of ciliary proteins in mediating ciliary processes can provide insight into cellular mechanisms underlying these various defects.

The primary cilium consists of a microtubule-based ciliary axoneme, ensheathed in a ciliary membrane. Extension and maintenance of the axoneme is dependent on multiple protein complexes [212]. The IFT-B complex, comprised of approximately 15 proteins, and the kinesin motor mediate anterograde transport, moving protein cargo from the base to the tip of the primary cilium. The IFT-A complex, comprised of approximately 7 proteins, together with the dynein motor mediate retrograde transport, returning cargo from the tip to the base of the primary cilium. IFT-A proteins also mediate ciliary entry of signaling and membrane-associated proteins [11, 162, 213]. Another protein complex, the BBSome, traffics signaling molecules to the cilium and throughout the cilium where it acts as an adaptor between the IFT complexes and the protein cargoes[214]. Despite that these ciliary proteins assemble into complexes, mutations in ciliary genes that encode proteins of the same ciliary complex can result in different phenotypes [215]. Thus, individual ciliary proteins likely have cell-specific roles.

Previously, we identified the mammalian IFT-A gene, *Thm1* (TPR-containing Hedgehog Modulator 1; also known as *Ttc21b*), an orthologue of *Chlamydomonas reinhardtii fla17*/*ift139* [50, 216]. In mouse, early embryonic loss of *Thm1* misregulates Hedgehog (Hh) signaling and causes perinatal lethality, polydactyly, and defects of the skeleton, forebrain, palate, and neural tube [50, 139, 217]. Additionally, in mice, *Thm1* deletion in the perinatal period causes renal cystic disease [143], and its deletion in adulthood causes obesity [173]. These phenotypes recapitulate the clinical features present in individuals with ciliopathies who have *THM1* mutations. Causative mutations in *THM1* have been identified in patients with nephronophthisis, a renal fibrocystic disease, while modifying mutations in *THM1* have been found in patients with Bardet Biedl Syndrome, which manifests obesity as a cardinal clinical feature [149].

Loss or deficiency of *Thm1* impairs retrograde IFT, resulting in accumulation of IFT proteins and signaling molecules at the ciliary distal tip [50, 146]. In some cells, such as mesenchymal cells of the developing limb bud, *Thm1* depletion causes shortened cilia [50], while in cultured RPE cells, cilia length was not affected [146]. In *Chlamydomonas ift139-null* mutants, levels of other IFT-A proteins were reduced, indicating that in the green alga, IFT139 is required for assembly of the IFT-A complex [218].

While there is only one *ift139* gene in *Chlamydomonas*, evolution has generated two vertebrate orthologues, which we have called *Thm1* and *Thm2*. THM1 and THM2 proteins are both 50% identical to *Chlamydomonas* IFT139 [50, 216]. Additionally, the murine *Thm1* and *Thm2* sequences are 50% homologous and encode proteins that have very similar predicted protein structures with multiple (10-11) tetratricopeptide repeat (TPR) domains. At embryonic day (E) 10.5, *Thm1* and *Thm2* also show very similar RNA expression patterns in whole mouse embryos. Recently, *THM2* mutations were identified in adult males with subfertility, and *Thm2* knock-out

male mice have been reported to be subfertile [156]. Still the role of *Thm2* in ciliogenesis and development remains uncharacterized. By generating a *Thm2*-null mouse and using *Thm1*- and *Thm2*-null derived mouse embryonic fibroblasts (MEF), here we show a role for *Thm1* in ciliogenesis, and an interaction between *Thm1* and *Thm2* in serum-induced cilia loss, ciliary entry of membrane-associated protein, Hh signaling and embryogenesis.

4.3 Methods

4.3.1 Generation of *Thm2* knockout (*Thm2*$^{-/-}$) mouse

Thm2-null mice were generated using CRISPR/Cas9 genome editing. Two guide RNAs (gRNAs)—one targeting exon 4 (target sequence CATACTCCCTGGCCTTGTCGTGG) and the other in intron 8 (target sequence AACCTGACCGACAGCCCACCTGG)—were designed to delete exons 4-8 and ultimately cause a premature stop codon. gRNAs were generated and validated by the Washington University Genome Engineering and iPSC Center). Pro-nuclear injections of 20 ng/μL of each in vitro transcribed gRNA and 50 ng/μL of Cas9 mRNA of 317 F1 embryos derived from FVB oocyte donors and C57BL6/J males yielded 42 founders. Genomic DNA of founders was amplified and sequenced to determine exon 4-8 deletion and a resulting premature stop codon. Founders carrying a large deletion and stop codon were then crossed to FVB mice to expand the *Thm2*$^{-/-}$ lines.

4.3.2 Genotyping of NHEJ events following CRISPR/Cas9 genome editing

Three PCR primer sets were designed to characterize the deletions generated by nonhomologous end joining (NHEJ) following CRISPR/Cas9 genome editing. Two sets of primers were designed around the exon 4 gRNA, and one set of primers was designed to flank the entire

region between exon 4 and intron 8. The first primer set surrounding exon 4 included F-Thm2ex4p (5′-TAC TAC GCC AGC CTC TTC CT-3′) and R-Thm2ex4p (5′-CCC TCC TGT ACC TCT TTG GA-3′) and was expected to produce a WT band of 107 bp. The second primer set surrounding exon 4 included F-Thm2ex4r (5′-TGT CTG AAG CCA ACA GAG AGG-3′) and R-Thm2ex4r (5′-GTT CAA GGC CAC CTT TGC T-3′) and was expected to produce a WT band of 1000 bp. PCR amplicons with a lower molecular weight indicate evidence of NHEJ in exon 4. Primers designed to detect the large exon 4-8 deletion flank exon 4 and intron 8 include F-Thm2ex4b (5′-GGA GAG CAG CTT GAA GGA AA-3′) and R-Thm2ex4b (5′-GTC ACG GCT GGT GTG ATT C-3′). A PCR amplicon was expected of approximately 216 bp, only in the event of NHEJ. To detect the presence of a WT allele, a separate PCR reaction was performed using primers within exon 6, F-WT (5-AAC TTC CTG CCC GCT TTA GT-3′) and R-WT (5′-GTG TCA GAT ACC CTG GAA CCA GAG-3′). In the presence of a WT allele, this PCR reaction yields an amplicon of approximately 461 bp.

4.3.3 Sequencing of *Thm2* knockout alleles

PCR products were run on an agarose gel, excised, and extracted using the Qiaex II DNA extraction kit (Qiagen, 20021). Samples were sequenced by Genewiz. Sequencing results were analyzed to determine the presence or absence of stop codons resulting from NHEJ events. A line harboring a deletion from exon 4 to intron 8, producing a stop codon in exon 4 was chosen, with the allele designation of *Ttc21a*$^{\Delta 4\text{-}8}$. The founder of this line was mated to FVB mice to expand the line. This line was maintained on a C57BL6/J/FVB mixed genetic background.

4.3.4 Analysis of mouse embryos and generation of mouse embryonic fibroblasts

Timed matings were performed between *Ttc21a*$^{\Delta 4\text{-}8/+}$; *Thm1*$^{aln/+}$ mice. The *aln* allele of *Thm1* results in absence of protein, and thus acts like a null allele[50]. Visualization of a vaginal plug was designated as embryonic day (E) 0.5. Mouse embryos were dissected at E10.5, E12.5, and E14.5 using a Leica dissection microscope. Tails of mouse embryos were collected for genomic DNA extraction and genotyping. To generate MEF, embryos were eviscerated. In a fresh 10-cm cell culture plate, an individual carcass was minced with a razor in 0.25% trypsin-EDTA, then media (DMEM containing 10% FBS and penicillin-streptomycin antibiotics) was added. Cells were grown to confluency, then trypsinized and plated for an experiment. Cells were passaged maximally up to two times.

4.3.5 qPCR

RNA was extracted using Trizol (Life Technologies), then reverse transcribed into cDNA using Quanta Biosciences qScript cDNA mix (VWR International). qPCR for *Gli1* was performed using Quanta Biosciences Perfecta qPCR Supermix (VWR International) in a BioRad CFX Connect Real-Time PCR Detection System. Primers used were *mThm1* (Forward: 5′-AAGCTCAACCCTGACTTCTTAC-3′; Reverse: 5′-CAACGTCTGAGAACTGGAGAAA-3′), *mThm2* (Forward: 5′-CCCCACAATCCAAACCTACA-3′; Reverse: 5′-GCTCACAAGCCGATGGAC-3′), and m*Gli1* (Forward: 5′-CTGACTGTGCCCGAGAGTG-3′; Reverse: 5′-CGCTGCTGCAAGAGGACT-3′). qPCR was performed in duplicate using RNA lysates from three samples per genotype.

4.3.6 Ciliogenesis and serum-induced cilia loss assays

Cells were plated on 12-mm poly-L-lysine-coated coverslips in a 24-well plate with DMEM medium containing 10% FBS and pen/strep antibiotics. Two days after cells reached 100% confluency, medium was replaced with serum-free medium for 6 and 24 hours to assess early and late ciliogenesis, respectively. Cells were fixed, immunostained for ciliary markers, imaged, and quantified for the presence of cilia.

To measure serum-induced cilia loss, cells were plated on 12-mm poly-lysine-coated glass coverslips in a 24-well plate with complete medium containing 10% FBS. Two days after cells reached 100% confluence, media was replaced with serum-free media for 24 hours to bring cells to G0 and induce ciliogenesis. Following 24-hour serum starvation, cells were cultured in media containing 10% FBS for 2 and 6 hours to induce cilia loss[219]. Cells were fixed, immunostained for ciliary markers, imaged, and quantified for presence of cilia.

4.3.7 Immunofluorescence

Cells were washed with PBS, then fixed with 4% paraformaldehyde/0.2% triton X-100 in PBS for 10 minutes at room temperature. Cells were washed again with PBS and blocked with 1% BSA in PBS for 1 hour. Cells were then incubated with antibodies against SMO (Abcam), IFT52, IFT81, IFT88, IFT140, BBS2, BBS5 (Proteintech), ARL13B and INNP5E (Proteintech), α-tubulin and acetylated α-tubulin (Sigma), and polyglutamylated tubulin (Adipogen) overnight at 4°C. Following three washes in PBS, cells were incubated with anti-rabbit AF488 and anti-mouse AF594 (InVitrogen Technologies) for 30 minutes at room temperature. Cells were washed 3X in PBS, and mounted with Vectashield containing 4,6-diamidino-2-phenylindole (DAPI) (Vector

Laboratories). Immunolabeled cells were viewed and imaged using a Leica TCS SPE confocal microscope configured on a DM550 Q upright microscope.

4.4 Results

4.4.1 *Thm2* interacts with *Thm1* in embryogenesis

Timed matings of *Thm2*$^{\Delta 4\text{-}8/+}$;*Thm1*$^{aln/+}$ intercrosses were performed. At E10.5, E12.5, and E14.5, pregnant females were dissected and their embryos analyzed. *Thm2*-null (*Thm2*$^{\Delta 4\text{-}8/\Delta 4\text{-}8}$) and *Thm2*-null;*Thm1*$^{+/-}$ (*Thm2*$^{\Delta 4\text{-}8/\Delta 4\text{-}8}$;*Thm1*$^{aln/+}$) embryos were normal, while *Thm1*-null (*Thm1*$^{aln/aln}$) and *Thm1*; *Thm2* double knock-out (*Thm2*$^{\Delta 4\text{-}8/\Delta 4\text{-}8}$;*Thm1*$^{aln/aln}$) embryos showed polydactyly and occasional exencephaly. At E10.5 and E12.5, the number of *Thm1*-null mutants and *Thm1; Thm2* double knock-outs (dko) was consistent with a Mendelian inheritance pattern, but at E14.5, the frequency of *Thm1;Thm2* dko embryos was reduced (Table 2). *Thm1* deletion causes perinatal lethality[50]. Thus, the reduced number of *Thm1; Thm2* double mutants at E14.5 suggests that additional loss of *Thm2* exacerbates the *Thm1*-null developmental phenotype causing mid-gestational lethality.

Table 2. Frequency of live *Thm1;Thm2* double knock-out embryos

	$Thm1^{aln/+}; Thm2^{\Delta 4\text{-}8/+}$ x $Thm1^{aln/+}; Thm2^{\Delta 4\text{-}8/+}$			
	Expected % frequency	**Observed % frequency (no.)**		
Genotype		**E10.5**	**E12.5**	**E14.5**
$Thm1^{aln/aln}$	25	32 (13)	22 (4)	27 (7)
$Thm1^{aln/aln}; Thm2^{\Delta 4\text{-}8/+}$	50	46 (19)	44 (8)	69 (18)
$Thm1^{aln/aln}; Thm2^{\Delta 4\text{-}8/\Delta 4\text{-}8}$	25	22 (9)	33 (6)	4 (1)*

Fisher's Exact Test was applied to analyze differences between expected and observed numbers of *Thm1*-null (including $Thm1^{aln/aln}$ and $Thm1^{aln/aln}; Thm2^{\Delta 4\text{-}8/+}$) and *Thm1:Thm2* double knock-out embryos; *$p<0.05$.

4.4.2 *Thm1* regulates ciliogenesis

We derived mouse embryonic fibroblasts (MEF) from E12.5 control, *Thm2* ko, *Thm2*-null;*Thm1*$^{+/-}$ (triple allele mutant), *Thm1*-null (ko), and *Thm1*; *Thm2* double-knockout (dko) mice. Using qPCR, we examined levels of *Thm1* and *Thm2* transcripts in control MEF and observed mean Cq values of 23 and 30, respectively (Figure 4.1A). Using serial dilutions of cDNA template made from MEF RNA for *Thm1* and testis RNA for *Thm2*, the R^2 value for both the *Thm1* and *Thm2* qPCR reactions was approximately 99%, indicating similar efficiency for the *Thm1* and *Thm2* qPCR reactions (Figure 4.1B). Therefore, the lower Cq values for *Thm1* indicate that *Thm1* is expressed at higher levels than *Thm2* in MEF. Further, *Thm2*-null MEF showed almost depleted levels of *Thm2* expression (Figure 4.1C). Following 24 hours of serum starvation, *Thm1* ko cells exhibited shorter ciliary length (mean length of 3.5µm) than control cells (*Thm2*+/-; mean length of 5.2µm), while the loss of *Thm2* did not alter cilia length (*Thm2*-null and *Thm2*-null;*Thm1*+/- mutants; mean lengths of 5.3µm and 5.2µm, respectively; Figures 4.2A and 4.2B).

We next assessed capacity of mutant cells to undergo ciliogenesis. At 6 and 24 hours of serum starvation, percentage of ciliated cells and cilia length was measured in control (*Thm2*$^{\Delta 4\text{-}8/+}$), *Thm2* ko (*Thm2*$^{\Delta 4\text{-}8/\Delta 4\text{-}8}$), triple allele mutant (*Thm2*$^{\Delta 4\text{-}8/\Delta 4\text{-}8}$;*Thm1*$^{aln/+}$), *Thm1* ko (*Thm1*$^{aln/aln}$) and *Thm1*; *Thm2* dko (*Thm1*$^{aln/aln}$; *Thm2*$^{\Delta 4\text{-}8/\Delta 4\text{-}8}$) MEF at 100% confluency. At 6 hours of serum starvation, approximately 75% of control MEF were ciliated. At 24 hours of serum starvation, the percentage of ciliated control cells was not altered, but cilia length was increased (Figures 4.2C-1D). We posit that under our experimental conditions, early events in cilium formation, such as maturation and docking of the basal body, were completed at 6 hours of serum starvation, and that axoneme elongation occurred from 6 to 24 hours of serum starvation. In *Thm2* ko and in triple allele mutant MEF, the percentage of ciliated cells and cilia lengths were similar to control MEF

(Figure 4.2C, 4.2D, 4.1A, 4.1B). In contrast, the percentage of ciliated *Thm1*-null MEF was lower than control MEF (48% vs. 75%, respectively) at 6 hours serum starvation, and increased (to 64%) at 24 hours of serum starvation, suggesting absence of *Thm1* reduces and delays ciliogenesis. From 6 to 24 hours serum starvation, cilia length did not change in *Thm1*-null MEF, suggesting that events required for axoneme elongation are hindered by *Thm1* loss. A similar percentage of ciliated cells and cilia length was observed in *Thm1;Thm2* dko MEF as in *Thm1*-null MEF, suggesting that *Thm2* does not participate in ciliogenesis.

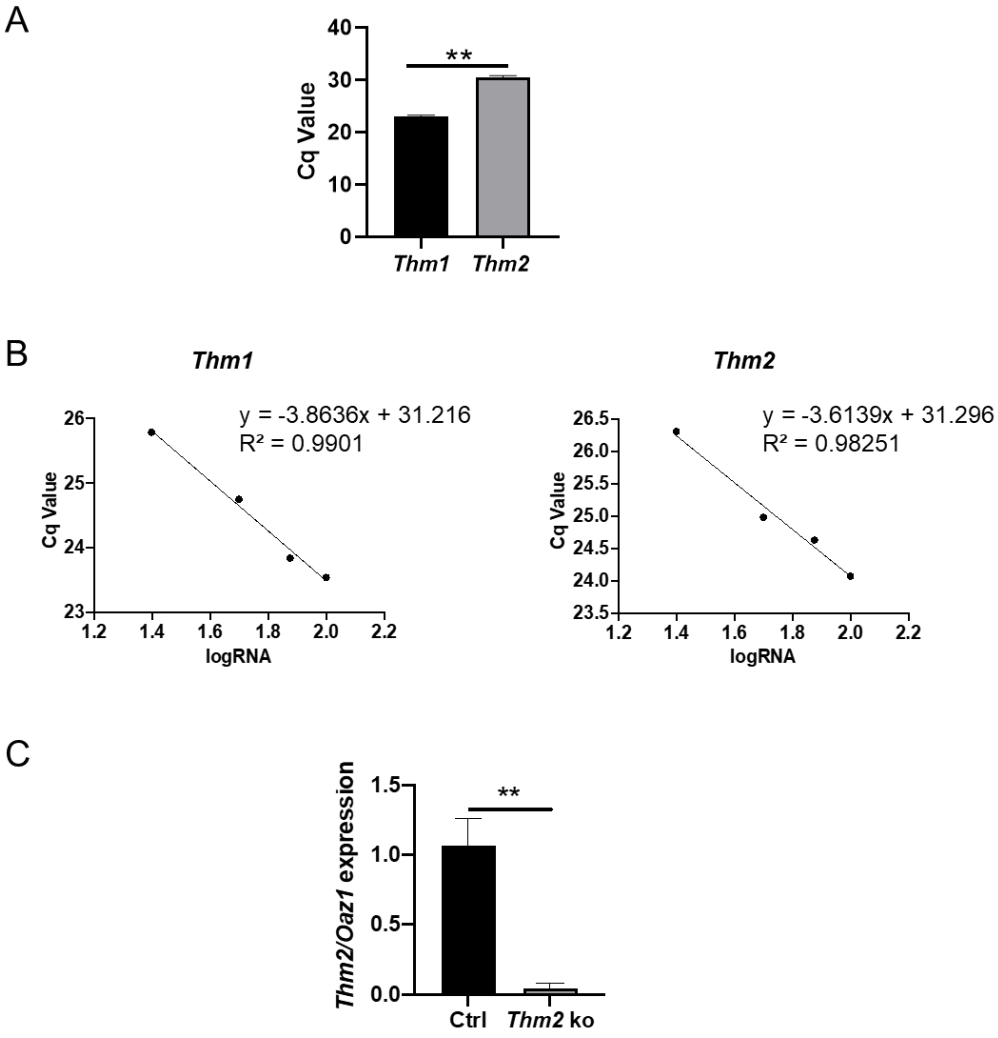

Figure 4.1 *Thm1* and *Thm2* transcript analysis in MEF
(A) Cq values for*Thm1* and *Thm2* in MEF. n=3. (B) Cq values for *Thm1* and *Thm2* using 25ng, 50ng, 75ng and 100ng cDNA made from MEF and testis RNA (for *Thm1* and *Thm2*, respectively). R^2 values of 0.99 for both *Thm1* and *Thm2* indicate similar levels of PCR efficiency. (C) qPCR analysis of *Thm2* relative to housekeeping gene, *Oaz1*, in ctrl and *Thm2* ko MEF. n=3 ctrl and n=3 *Thm2* ko.

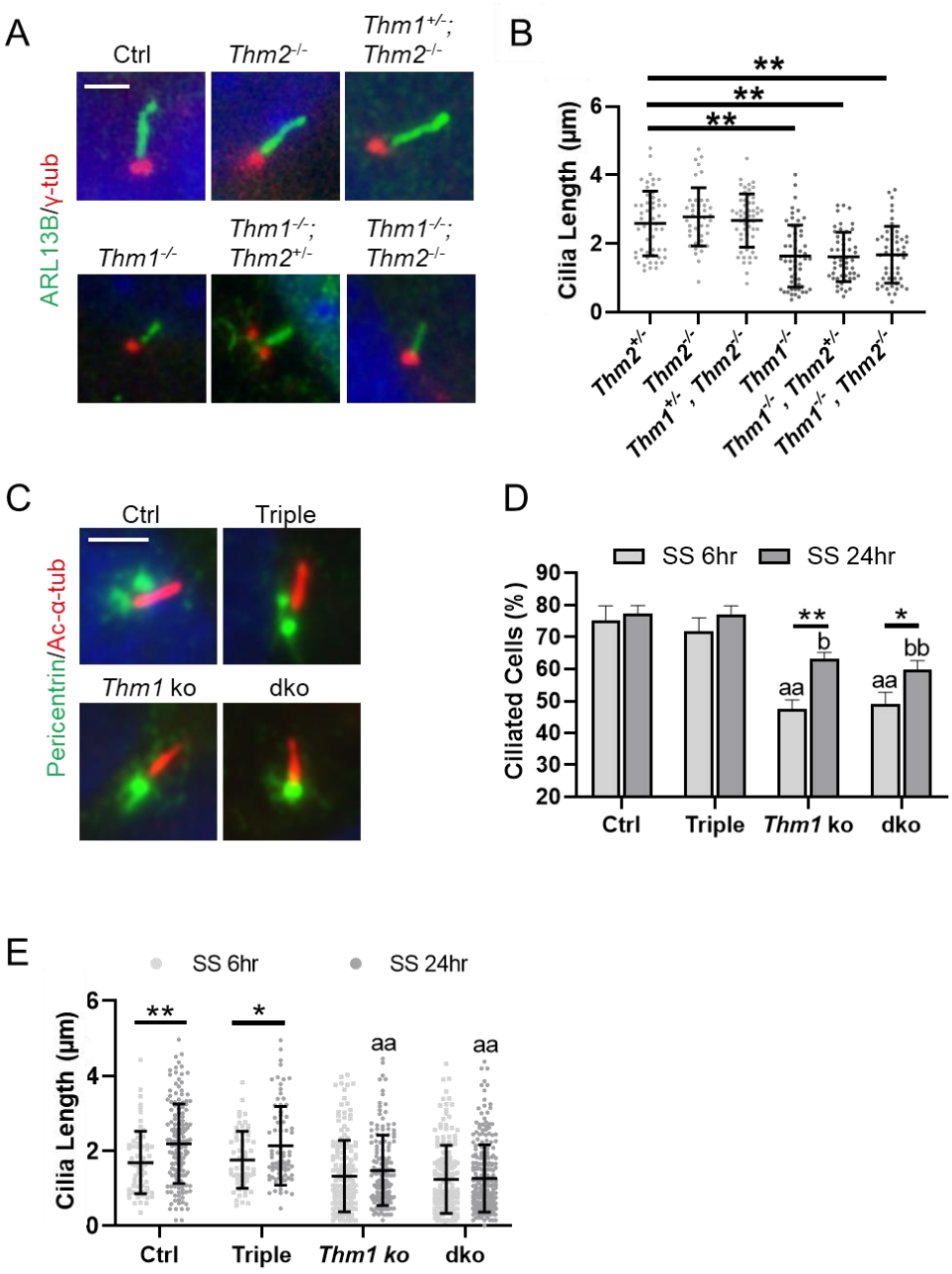

Figure 4.2 *Thm1* regulates early and late ciliogenesis
(A) Immunostaining for ARL13B (green) and γ-tubulin (red). Scale bar = 5 μm. (B) Cilia length. 2-3 cell lines per genotype, and ≥40 cilia/genotype were randomly selected per experiment. Each dot represents an individual cilium length. Bars represent mean ± SD. (C) Immunostaining for acetylated α-tubulin (red) and pericentrin (green). Scale bar = 5 μm. (D) Percentage of ciliated MEF and (E) cilia length following 6hr and 24hr serum starvation (SS). Five-to-ten fields were analyzed per condition per experiment, and included ≥ 65 ciliated cells per condition per genotype. Bars represent mean ± SD from 2-3 independent experiments. Statistical significance was determined by ANOVA followed by Tukey's or Dunnett's test. *p<0.05; ** p<0.01; [aa] p<0.01 compared to Ctrl MEF - 6hr serum starvation; [b] p<0.05; [bb] p<0.0001 compared to Ctrl MEF - 24hr serum starvation.

4.4.3 *Thm2* interacts with *Thm1* to regulate serum-induced cilia loss

Primary cilia undergo ciliogenesis and cilia loss in coordination with the cell cycle, and the cilia assembly:disassembly ratio regulates cilia length [220, 221]. To examine cilia loss, serum was added back to the media for 2 and 6 hours following 24 hours of serum starvation. After 2 hours of serum addition, the percentage of ciliated control, *Thm2* ko, and triple allele mutant MEF was not significantly altered (approximately 78%), but cilia length was decreased (Figures 4.3A, 4.3B, 4.4C, 4.4D). In contrast, the percentage of ciliated *Thm1*-null MEF was reduced (63% vs. 55%) although this did not reach statistical significance, while cilia length was not altered. In *Thm1; Thm*2 dko MEF, 2-hour serum addition significantly reduced the percentage of ciliated cells, but did not modify cilia length. These data suggest that the loss of *Thm1* and *Thm2* promotes cilia loss.

After 6 hours of serum addition, the percentage of ciliated cells across all genotypes was significantly reduced (Figures 4.3A, 4.3B, 4.4C, 4.4D). Moreover, the decrease in the percentage of ciliated cells from 24-hour serum starvation was greater in *Thm1*-null MEF than in control MEF (difference of 35% vs 19%), suggesting that *Thm1* loss alone promotes cilia loss. In *Thm1; Thm*2 dko MEF, 6 hours of serum restimulation also decreased cilia length. Taken together, these results substantiate that IFT-A deficiency promotes cilia loss.

Following 2 hours of serum addition, cells were immunostained for IFT-B protein, IFT81, and for acetylated α-tubulin. This revealed the presence of IFT81 that was separate and distal to its axonemal localization (Figures 4.3C and 4.4C). To ensure that this IFT81 staining is truly distinct from the axoneme, cells were further immunostained for IFT81 together with α-tubulin or polyglutamylated tubulin. Similarly, IFT81 staining was observed that was separate and distal from tubulin (Figure 4.5). These observations may reflect the release of ciliary vesicles from the

distal tip, a phenomenon that is termed decapitation or ectocytosis, and precedes cilia resorption, contributing to cilia loss [222]. In *Thm1*-null and *Thm1*; *Thm2* dko cells, frequency of IFT81 localization that was separate from the axoneme was increased (Figure 4.3D; cilia + dot), suggesting *Thm1* regulates this phenomenon.

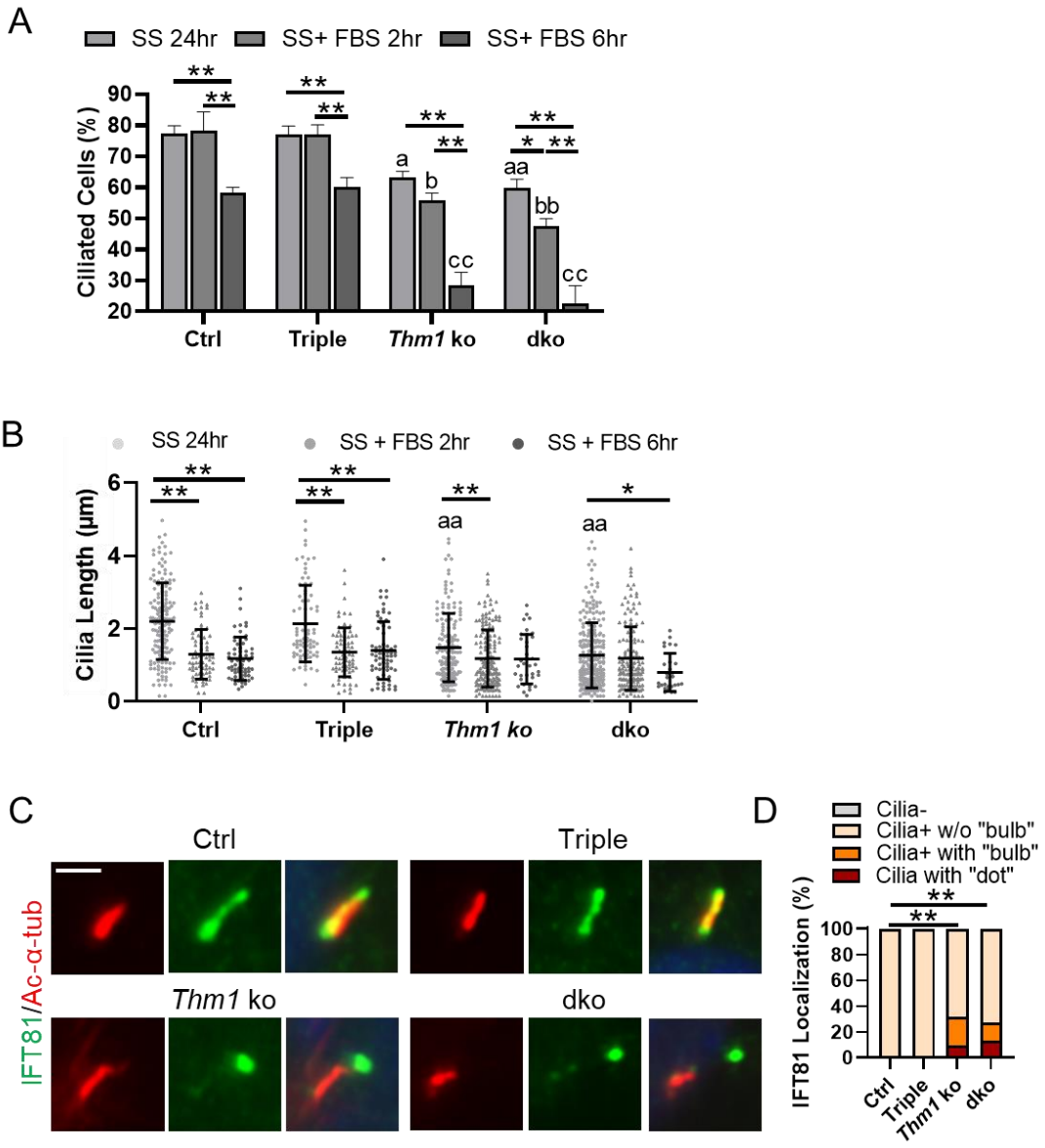

Figure 4.3 *Thm1* and *Thm2* alter stability of pre-established cilia
(A) Percentage of ciliated MEF and (B) cilia length after 24hr serum starvation (SS) alone or followed by 2hr or 6 hr FBS restimulation. Five-to-ten fields were analyzed per condition per experiment, and included ≥ 65 ciliated cells per condition per genotype. Bars represent mean ± SD from 2-3 independent experiments. Statistical significance was determined by ANOVA followed by Tukey's or Dunnett's test. *p<0.05; ** p<0.01; [a] p<0.05; [aa] p<0.01 compared to Ctrl MEF - 24hr serum starvation; [b] p<0.05; [bb] p<0.01 compared to Ctrl MEF - 24hr serum starvation + 2hr FBS; [cc] p<0.01 compared to Ctrl MEF - 24hr serum starvation + 6hr FBS. (C) Immunostaining for IFT81 (green) and acetylated α-tubulin (red) following 24hr serum starvation + 2hr FBS. (D) Quantification of ciliary localization of IFT81, categorized as absent from cilia (Cilia-), present in cilia without a bulbous distal tip (Cilia + w/o bulb), and present in cilia with a bulbous distal tip (Cilia+ with bulb). Stacked bar graphs represent percentage of these occurrences. Total number of Ctrl, Triple, *Thm1* ko and dko cells quantified were 202, 205, 340 and 131, respectively, from 2-3 independent experiments. Statistical significance was determined by χ^2 test. **p<0.01

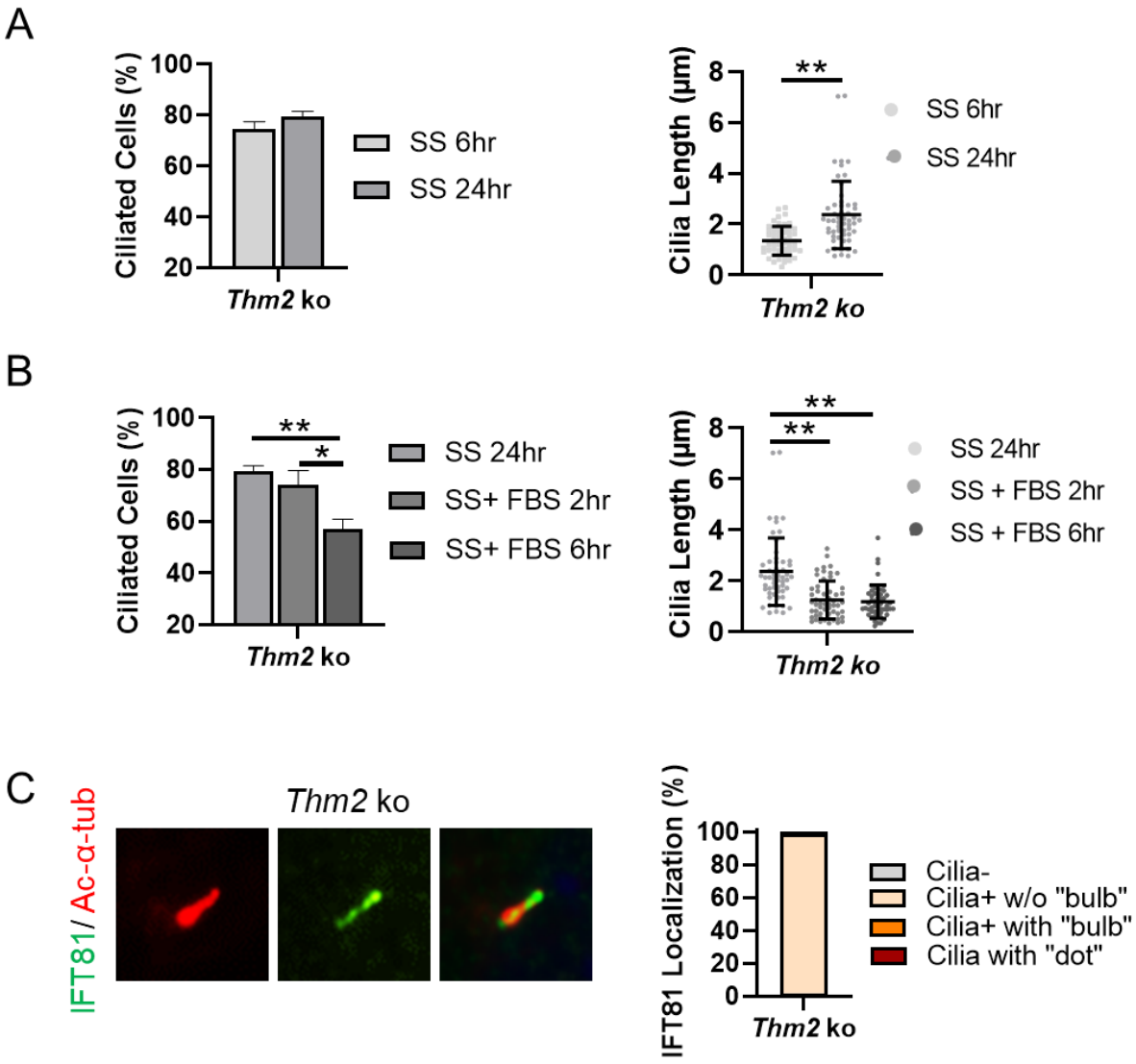

Figure 4.4 Ciliogenesis, cilia disassembly, and analysis of IFT81-positive vesicles in *Thm2* ko MEF
(A) Percentage of ciliated MEF and cilia length following 6hr and 24hr serum starvation (SS). (B) Percentage of ciliated MEF and cilia length after SS alone or followed by 2hr and 6hr FBS restimulation. Statistical significance was determined by t-test in (A) and by ANOVA followed by Tukey's test in (B). *p<0.05; ** p<0.0001. (C) Immunostaining for IFT81 (green) and acetylated **α**-tubulin (red) and quantification of ciliary localization of IFT81 of n=2 *Thm2* ko lines.

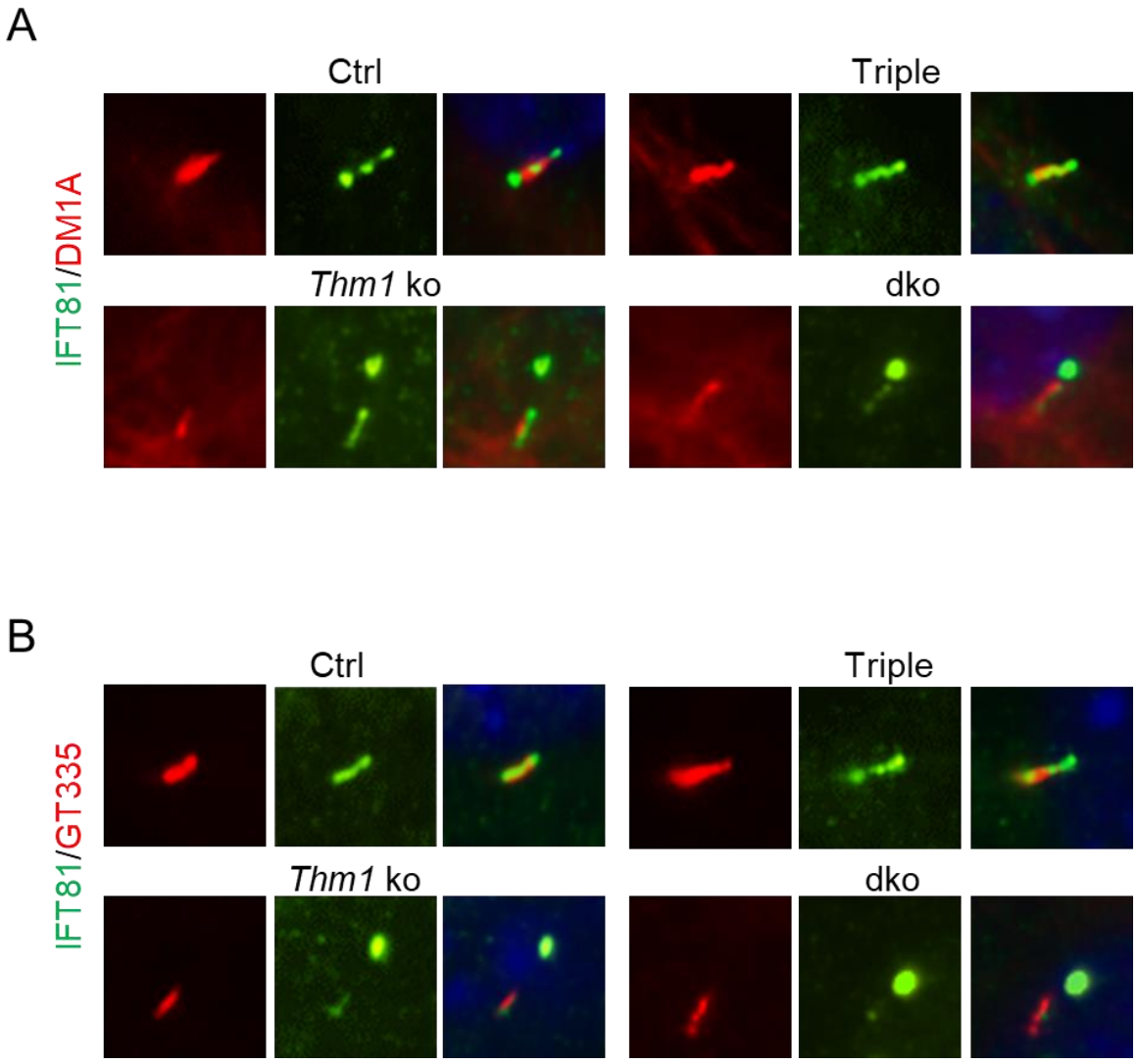

Figure 4.5 Analysis of IFT81-positive vesicles
Cells were serum starved for 24 hours, then restimulated with 2hrs FBS. Immunostaining for (A) IFT81 (green) and **α**-tubulin (DM1A; red) and for (B) IFT81 (green) and polyglutamylated tubulin (GT335; red). n=1 ctrl and triple; n=2 Thm2 ko and dko

4.4.4 Loss of *Thm1* causes accumulation of IFT-B proteins at distal tip

We next investigated the roles of *Thm1* and *Thm2* in ciliary protein transport. Following 24 hours of serum starvation to maximize cilia length, cells were immunostained for IFT-B subunits, IFT81 and IFT52, and for anterograde IFT motor, KIF3A. Ciliary localization of IFT-B proteins was similar between control, *Thm2* ko, and triple allele mutant MEF, while *Thm1*-null and *Thm1;Thm2* dko MEFs exhibited aberrant accumulation of proteins in a bulbous distal tip (Figures 4.6A-4.6C, 4.7). This phenocopies the ciliary phenotype of *Thm1* knock-down IMCD cells expressing IFT88-YFP protein, in which we demonstrated impaired retrograde IFT in live cells[50]. As described previously for IFT-A mutant cells [162], protein localization was classified as either absent in cilia (Cilia-), present in cilia without a bulb (Cilia w/o bulb), or present in cilia with a bulb (Cilia with bulb). Across all genotypes, virtually 100% of cilia showed the presence of IFT81, IFT52 and KIF3A. However, while most control, *Thm2* ko, and triple allele mutant MEF showed localization of IFT81, IFT52 and KIF3A in cilia without a bulb, approximately 50% of *Thm1*-null and *Thm1;Thm2* dko MEF showed localization of IFT81, IFT52 and KIF3A in a bulbous ciliary distal tip. *Thm1*; *Thm2* dko MEF displayed a slightly higher percentage of cells with IFT81 localizing to a ciliary bulbous distal tip than *Thm1*-null MEF (52% vs. 43%; Figure 4.6A). These data indicate that THM1 is required for retrograde transport of IFT-B proteins, and that THM2 may enhance THM1-mediated retrograde transport of IFT81.

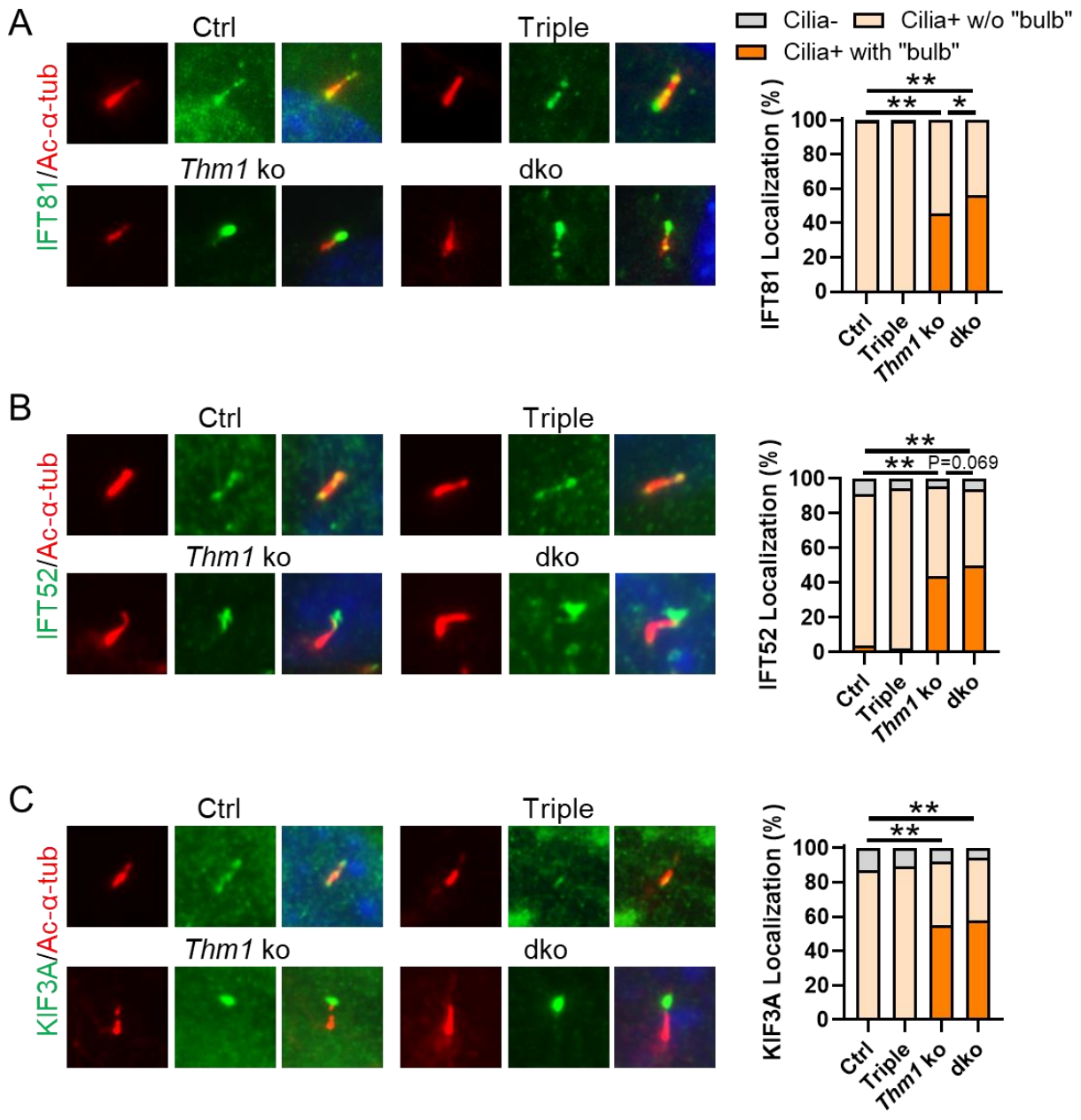

Figure 4.6 Loss of *Thm1* causes accumulation of IFT-B complex at distal tip
Immunostaining and quantification for (A) IFT81 (green); (B) IFT52 (green) and (C) KIF3A (green). Ciliary localization of IFT81, IFT52 and KIF3A was categorized as absent from cilia (Cilia-), present in cilia without a bulbous distal tip (Cilia + w/o bulb), and present in cilia with a bulbous distal tip (Cilia+ with bulb). Stacked bar graphs represent percentage of these occurrences. Total number of Ctrl, Triple, *Thm1* ko and dko cells quantified were 150, 151, 200 and 200, respectively, were IFT81; 220, 244, 407 and 408, respectively, for IFT52; were 220, 244, 407 and 408, respectively, for KIF3A, from 2-3 independent experiments. Statistical significance was determined by χ^2 test. *p<0.05; **p<0.01

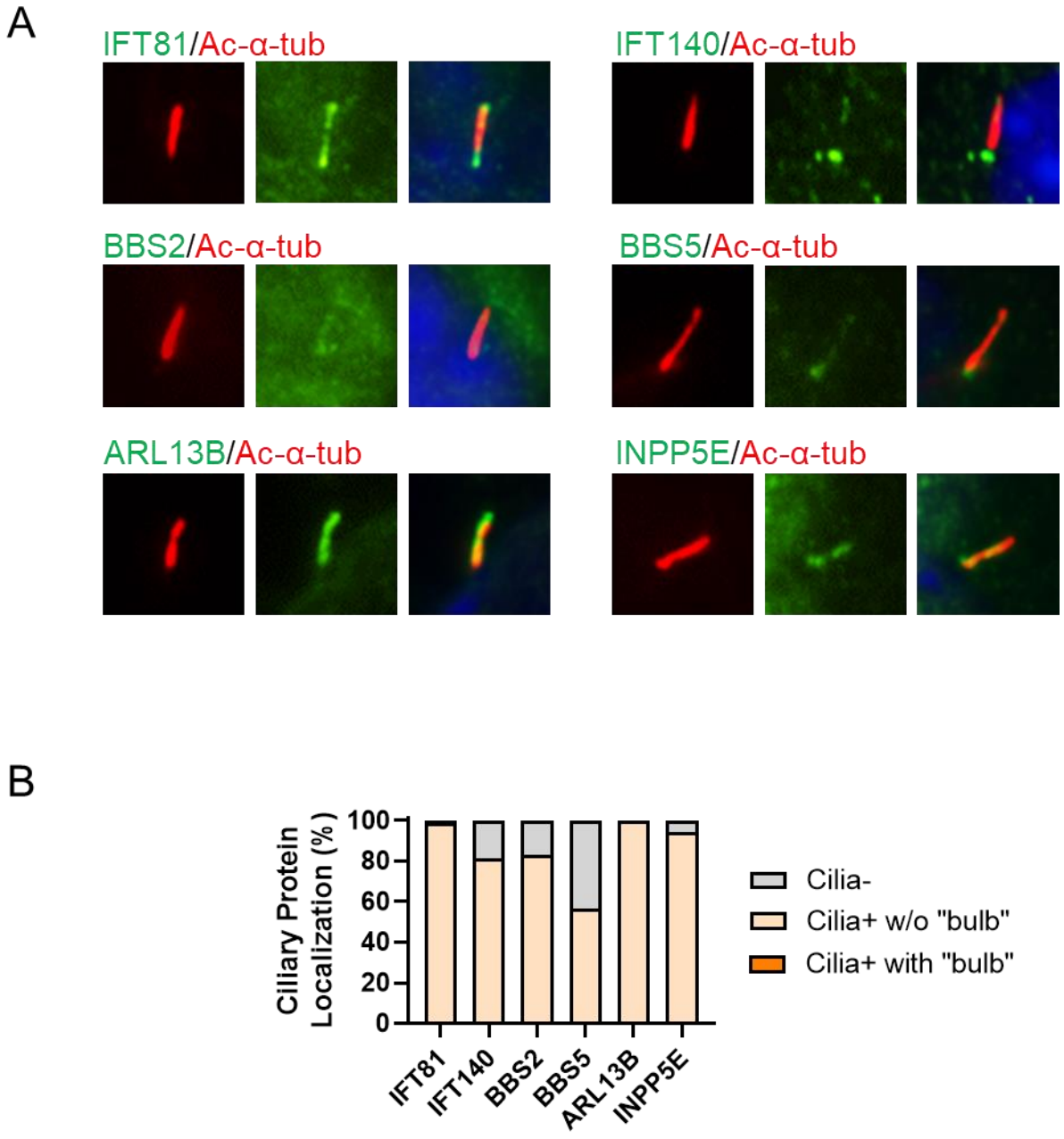

Figure 4.7 Analysis of ciliary localization of IFT, BBS and membrane associated proteins in *Thm2* ko MEF

(A) Immunostaining for IFT81, IFT40, BBS2, BBS5, ARL13B, INPP5E (green) together with acetylated **α**-tubulin (red). B) Quantification of ciliary localization of proteins. n=2 *Thm2* ko lines

4.4.5 Loss of *Thm1* causes accumulation of IFT-A protein, IFT140 at the distal tip, and also reduces its ciliary localization

We next examined ciliary localization of IFT-A component, IFT140. Approximately 80%-90% of cilia of control, *Thm2* ko, and triple allele mutant MEF showed the presence of IFT140, while only 65% of *Thm1*-null and *Thm1*; *Thm2* dko MEF had IFT140-positive cilia (Figures 4.8 and 4.7). To determine whether the reduction in ciliary IFT140 in *Thm1* and *Thm1;Thm2* mutant cells is due to reduced overall IFT140 protein levels, we immunoblotted whole cellular extracts for IFT140. Similar levels of IFT140 between control and the mutant genotypes were observed (Figure 4.9), indicating that unlike in *Chlamydomonas [218]*, loss of *Thm1* in MEF does not affect IFT-A complex stability, and the reduction in ciliary IFT140 in *Thm1*-null and *Thm1;Thm2* dko MEF is due to a defect in ciliary entry. Additionally, approximately 35% of *Thm1*-null and *Thm1*; *Thm2* dko cilia showed IFT140 localization in a bulbous distal tip, indicative of a retrograde defect. Thus, THM1 mediates both ciliary entry and retrograde transport of an IFT-A protein.

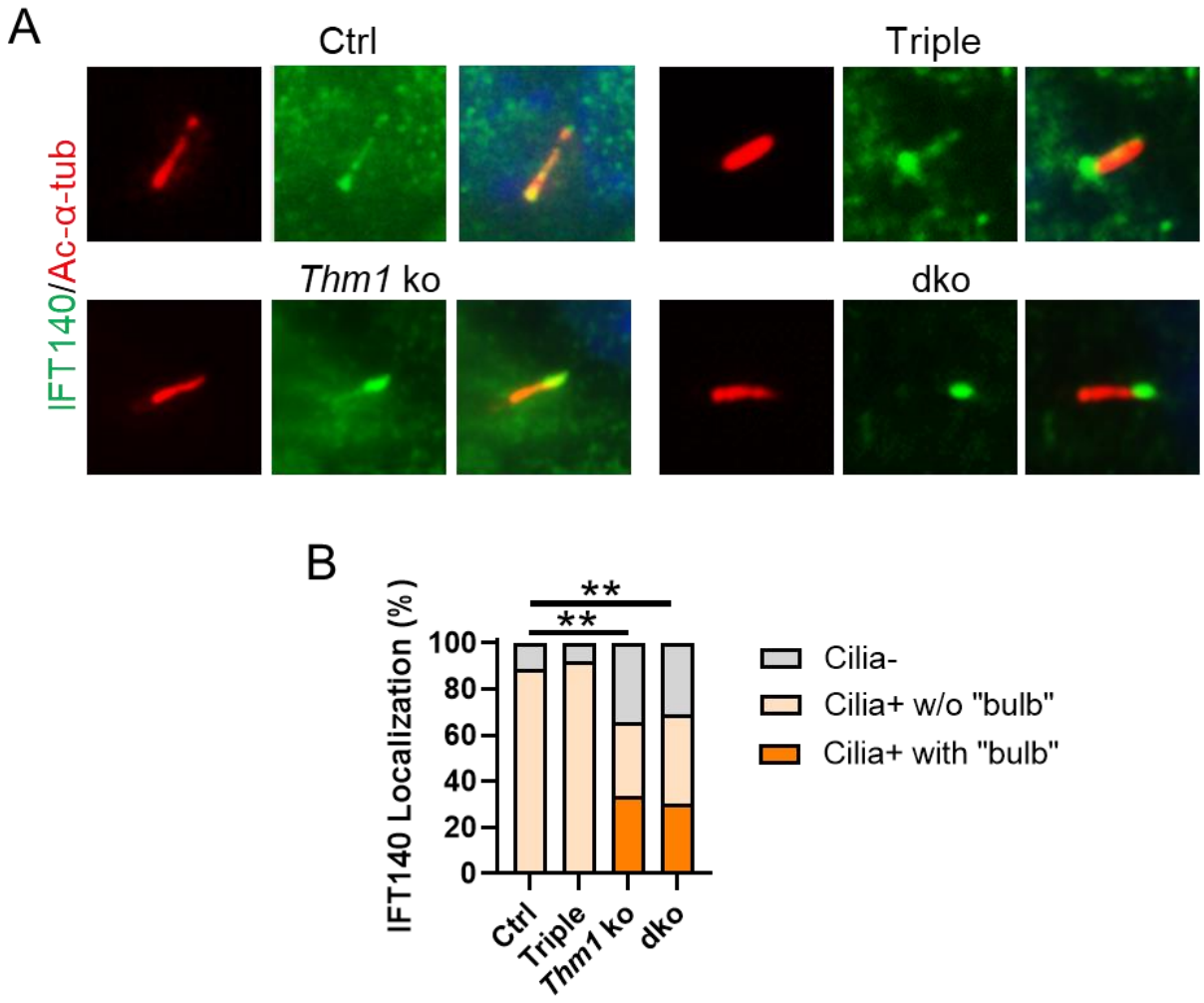

Figure 4.8 Loss of *Thm1* causes accumulation of IFT-A protein, IFT140 at the distal tip, and reduces its ciliary localization

(A) Immunostaining for IFT140 (green) and acetylated-α-tubulin (red). (B) Quantification of IFT140 ciliary localization. Total number of Ctrl, Triple, *Thm1* ko and dko cells quantified were 224, 274, 386 and 385, respectively, from 2-3 independent experiments. Statistical significance was determined by χ^2 test. **p<0.01

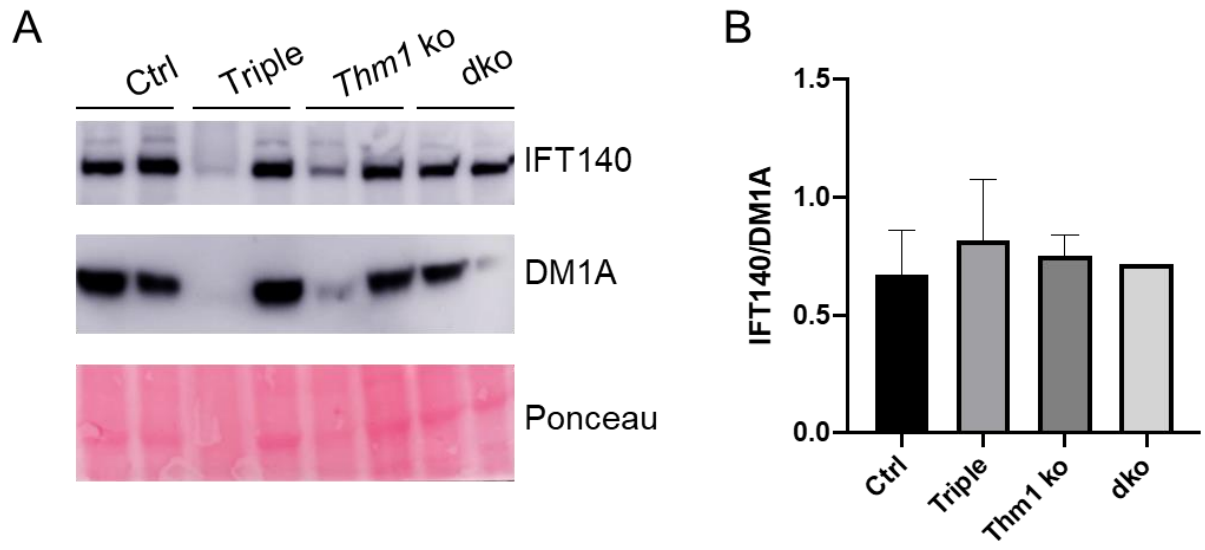

Figure 4.9 IFT140 protein levels in whole cell extracts
(A) Western blot analysis for IFT40 and DM1A (**α**-tubulin) with Ponceau stain. (B) Quantification of IFT140/DM1A. Last lane (dko) was not included in quantification, since DM1A does not reflect protein levels in Ponceau stain.

4.4.6 *Thm1* mediates ciliary exit of BBSome subunits

The BBSome is an 8-subunit complex, which acts like an adaptor between IFT complexes and protein cargo within cilia. BBSome subunits are normally rapidly exported from cilia [162, 223, 224]. Consistent with this, we observed light ciliary staining of BBS2 in approximately 80% of control, *Thm2* ko, and triple allele mutant MEF (Figures 4.10A-4.10C, 4.7) and light ciliary staining of BBS5 in approximately 60% of control, *Thm2* ko, and triple allele mutant MEF (Figures 4.10D-4.10F, 4.7). However, approximately 95% of *Thm1*-null and *Thm1*; *Thm2* dko MEF showed ciliary presence of BBS2 and BBS5, and approximately 20% showed BBS2 and BBS5 localization in bulb-like structures at the distal tip (Figures 4.10B and 4.10E). *Thm1*-null and *Thm1*; *Thm2* dko cilia also showed increased intensity of BBS2 and BBS5 immunofluorescence relative to control cilia (Figures 4.10C and 4.10F). Increased BBS localization at the distal tip suggests defective retrograde IFT of the BBSome, while increased BBS localization throughout the cilium also could suggest a potential gating defect. The latter would be a novel role for IFT-A.

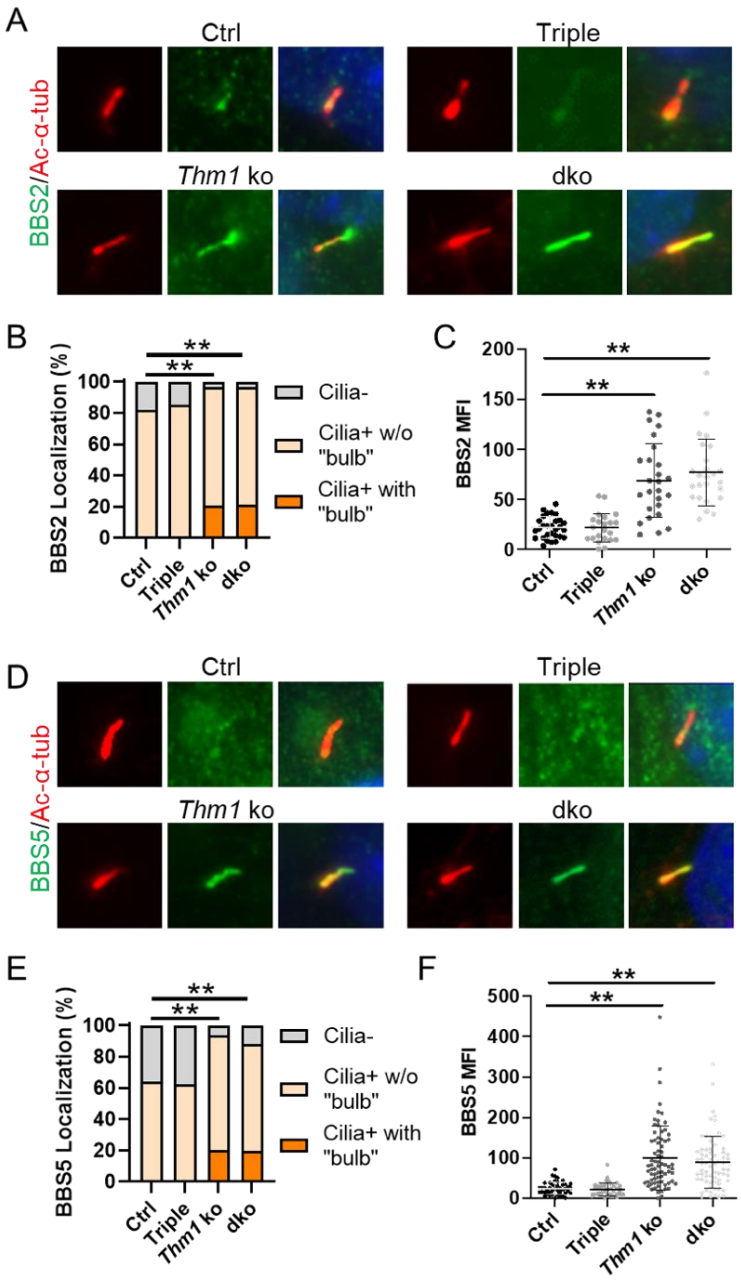

Figure 4.10 BBSome subunits are increased in *Thm1*-null cilia

(A) Immunostaining for BBS2 (green) and ac-α-tubulin (red). (B) Quantification of BBS2 ciliary localization. Total number of Ctrl, Triple, *Thm1* ko and dko cells quantified were 183, 167, 334 and 223, respectively, from 2-3 independent experiments. Statistical significance was determined by χ^2 test. (C) Fluorescence intensity of BBS2 in cilia. Each dot represents an individual cilium. Bars represent mean ± SD. Statistical significance was determined by ANOVA followed by Tukey's test. (D) Immunostaining for BBS5 (green) and ac-α-tubulin (red). (E) Quantification of BBS5 ciliary localization. Total number of Ctrl, Triple, *Thm1* ko and dko cells quantified were 219, 261, 229 and 217, respectively, from 3 independent experiments. Statistical significance was determined by χ^2 test. (E) Fluorescence intensity of BBS5 in cilia. Each dot represents an individual cilium. Bars represent mean ± SD. Statistical significance was determined by ANOVA followed by Tukey's test. **p<0.01

4.4.7 *Thm2* interacts with *Thm1* to mediate ciliary localization of INPP5E

Since the IFT-A complex mediates ciliary entry of membrane-associated proteins [11, 162, 213], we next examined ciliary localization of ARL13B and INPP5E. While 100% of control, *Thm2* ko, and triple allele mutant MEF showed ciliary presence of ARL13B, approximately 90% of *Thm1*-null and *Thm1*; *Thm2* dko cilia were positive for ARL13B (Figures 4.11A, 4.11B, 4.7). Additionally, immunofluorescence intensity was decreased by almost 50% in *Thm1*-null and *Thm1*; *Thm2* dko cilia relative to control (Figure 4.11C). Further, while 95%-100% of control, *Thm2* ko, and triple allele mutant MEF showed ciliary presence of INPP5E, only 50% of *Thm1*-null MEF and 40% of *Thm1*; *Thm2* dko MEF had INPP5E-positive cilia (Figures 4.11D, 4.11E, 4.7). These data suggest *Thm1* regulates ciliary entry of ARL13B and INPP5E, and that *Thm2* enhances *Thm1*-mediated ciliary entry of INPP5E.

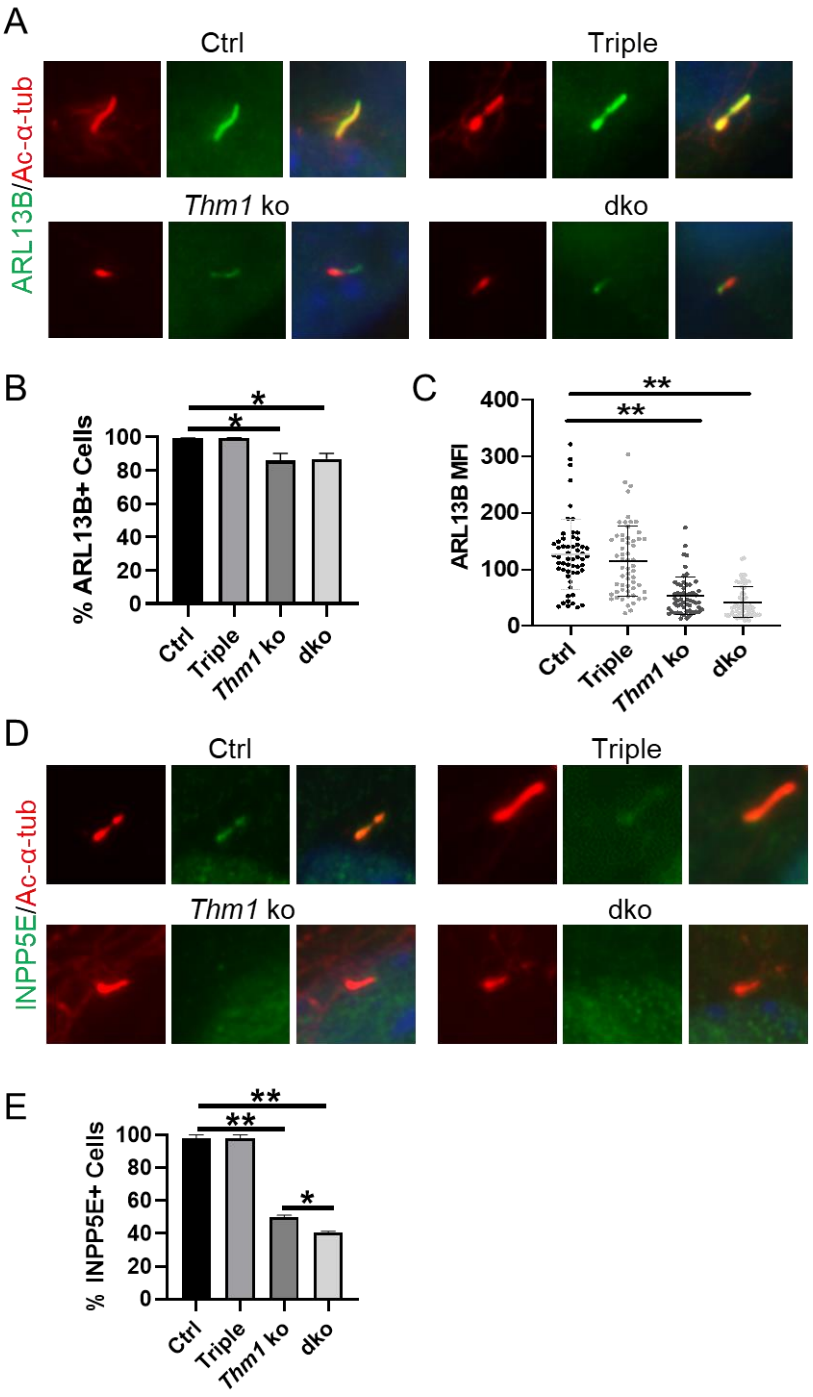

Figure 4.11 *Thm2* interacts with *Thm1* to mediate ciliary localization of ARL13B and INPP5E
(A) Immunostaining for ARL13B (green) and ac-α-tubulin (red). (B) Quantification of ARL13B positive cilia. ≥ 150 cells/genotype from 3 independent experiments were quantified. (C) Fluorescence intensity of Arl13b in cilia. Each dot represents an individual cilium. Bars represent mean ± SD. (D) Immunostaining for INPP5E (green) and ac-α-tubulin (red). (E) Quantification of INPP5E positive cilia. ≥ 150 cells/genotype from 3 independent experiments were quantified. Statistical significance was determined by ANOVA followed by Tukey's test. *p<0.05; **p<0.01

4.4.8 *Thm2* interacts with *Thm1* to regulate Hh signaling

During activation of the mammalian Hedgehog (Hh) signaling pathway, the Smoothened (SMO) signal transducer enriches in the primary cilium [225]. In control MEF, treatment with SMO agonist, SAG, resulted in presence of SMO in 60% of cilia, increased from 20% of cilia in untreated MEF (Figures 4.12A and 4.12B). Treatment with SAG also induced expression of *Gli1*, a transcriptional target and reporter of Hh activity [226]. In triple allele mutant MEF, SAG treatment resulted in a ciliary enrichment of SMO similar to control cells (Figure 4.12B), yet *Gli1* expression was reduced relative to control MEF (Figure 4.12C). In contrast, SAG treatment of *Thm2* ko MEF induced similar levels of *Gli1* expression as control cells (Figure 4.13). In untreated *Thm1*-null and *Thm1*; *Thm2* dko MEF, SMO was present in 90% of cilia, and 20% showed SMO accumulation in a bulbous distal tip (Figure 4.12A). With SAG treatment, approximately 90% of cilia were SMO+, unchanged from untreated cells, but approximately 30% of cilia had SMO localized in a bulbous distal tip (Figure 4.12B). However, despite the increased presence of ciliary SMO in *Thm1*-null and *Thm1*; *Thm2* dko MEF, SAG-induced *Gli1* expression was minimal to almost absent (Figure 4.12C). Thus, consistent with a previous study [146], these data show that *Thm1* regulates retrograde transport of SMO. Further, in MEF, *Thm1* is also required for Hh pathway activation downstream of SMO ciliary localization. Additionally, *Thm2* interacts with *Thm1*, to positively modulate Hh signaling downstream of SMO ciliary localization.

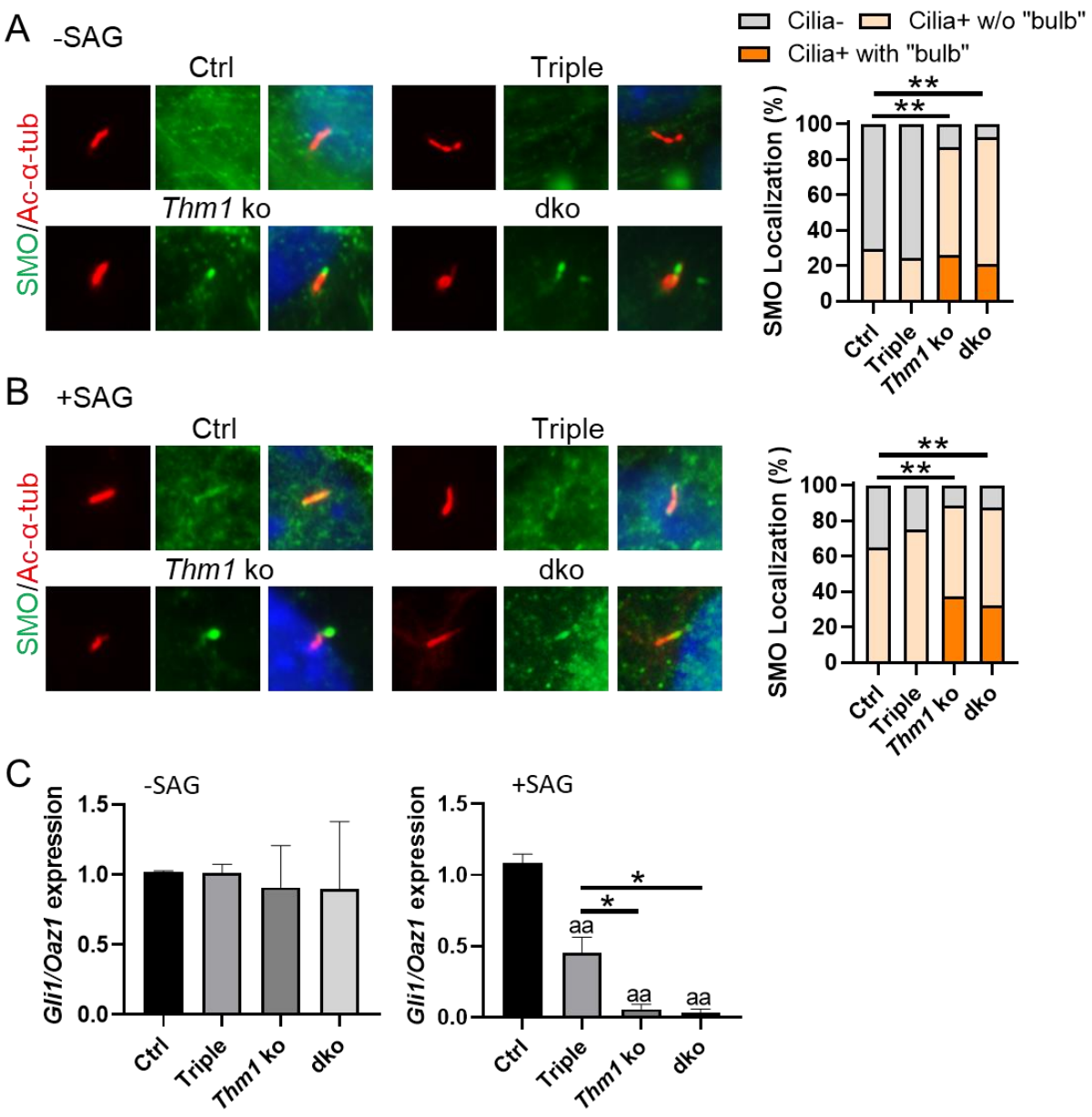

Figure 4.12 *Thm2* interacts with *Thm1* to regulate Hh signaling
Immunostaining for SMO and acetylated-α-tubulin of serum-starved MEF treated with (A) DMSO or (B) SAG for 8 hr, with quantification of SMO ciliary localization. Total number of Ctrl, Triple, *Thm1* ko and dko cells quantified in (A) were 191,135, 235 and 223, respectively, and in (B) were 203, 242, 363 and 200, respectively, from 2-3 independent experiments. Statistical significance was determined by χ^2 test. (C) qPCR for *Gli1* on RNA extracts of MEF cultured in 1% FBS overnight, then treated with DMSO or SAG for 48 h in 1% FBS medium. *Gli1/Oaz1* transcript ratios of control cells were set to 1. Graphs represent mean ± SEM. Three MEF lines per genotype were used. Statistical significance was determined by ANOVA followed by Tukey's test. *p<0.05; **p<0.01; [aa] p<0.01 compared to Ctrl

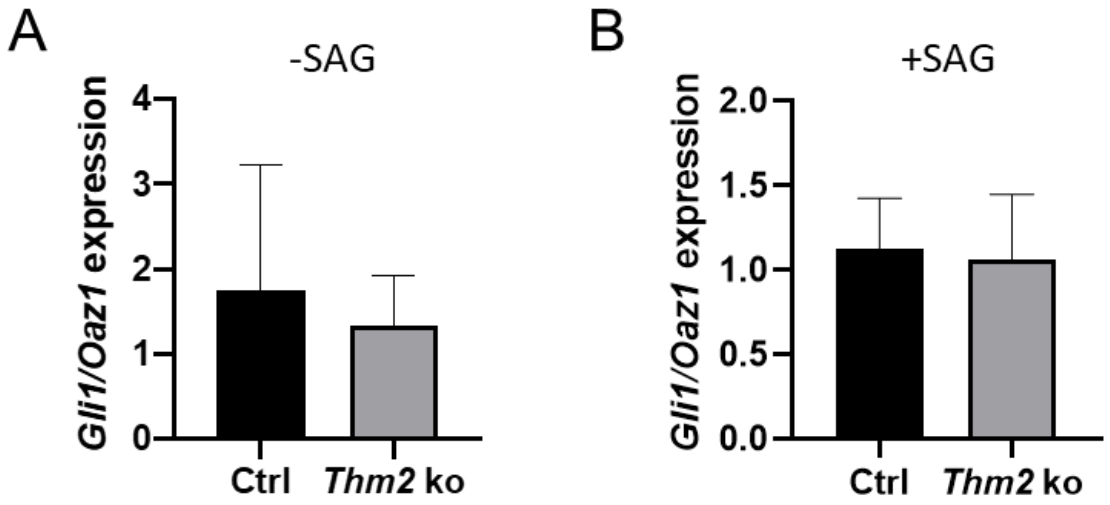

Figure 4.13 Relative *Gli1* transcript levels in *Thm2* ko MEF
qPCR analysis for *Gli1* and *Oaz1* in (A) absence and (B) presence of SAG. n=3 ctrl and n=3 *Thm2* ko

4.5 Discussion

In this study, we reveal that *Thm1* loss decreases ciliogenesis, and that *Thm1* loss alone or together with *Thm2* loss, increases serum-induced cilia loss. Further, in a *Thm1*-dependent manner, *Thm2* also regulates ciliary entry of membrane-associated protein, and Hh signaling activity downstream of SMO ciliary translocation (Figure 4.14).

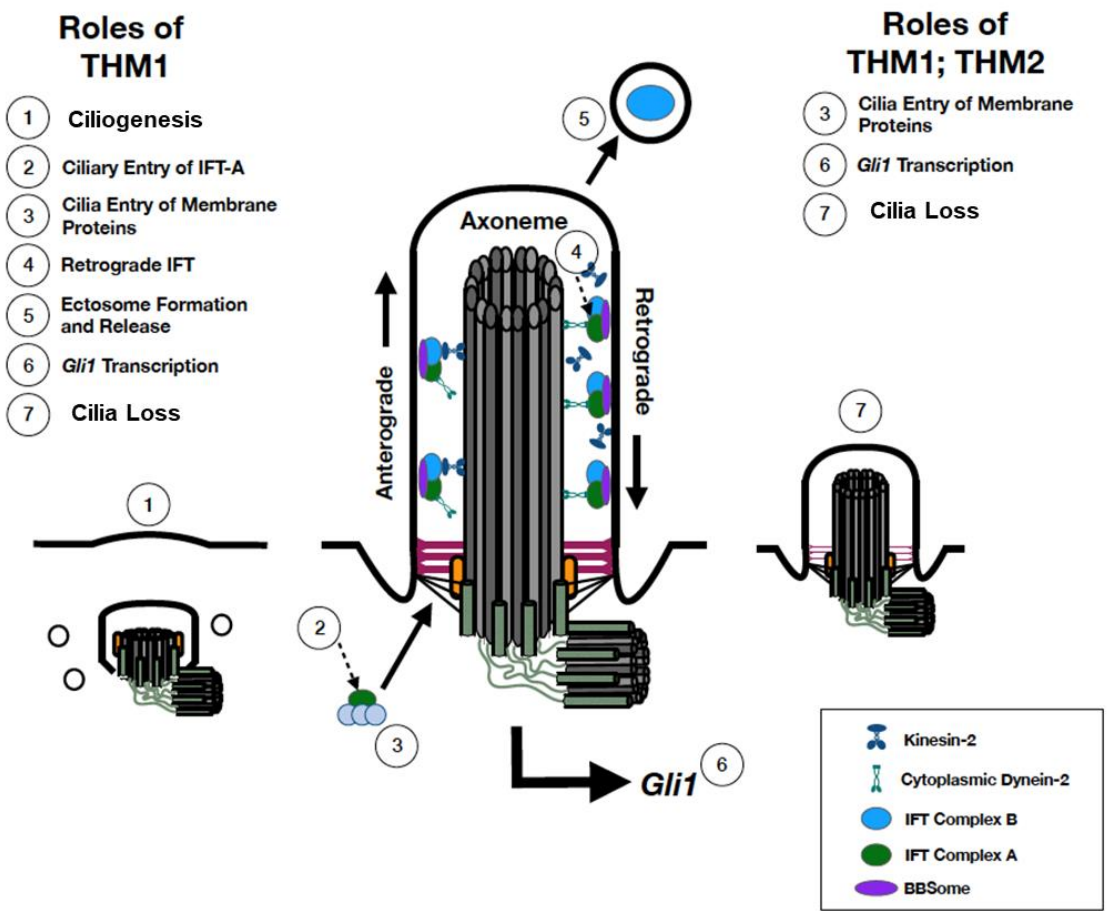

Figure 4.14 Ciliary roles of *Thm1* and *Thm2*
Model for *Thm1*, alone and together with *Thm2*, in regulating ciliogenesis, serum-induced cilia loss, ciliary protein trafficking and Hh signaling in MEF.

This is the first demonstration of a role for IFT-A in serum-induced cilia loss. In control MEF, two hours of serum restimulation following 24 hours of serum starvation did not alter the percentage of ciliated cells, but decreased cilia length. Conversely, in *Thm1; Thm*2 dko cells, two hours of serum restimulation decreased the percentage of ciliated cells, while cilia length was unchanged. This difference between control and mutant cells may indicate that in the presence of dysfunctional IFT-A, the mechanism of cilia loss is shifted. Several mechanisms contribute to cilia loss. These include cilia resorption, which gradually shortens cilia length; complete cilia shedding, which cleaves the entire cilium; and a combination of both mechanisms [227]. The reduction in cilia length in control MEF suggests gradual cilia resorption may be a predominant mechanism within 2 hours of FBS stimulation, whereas the unaltered cilia length together with less ciliated *Thm1; Thm*2 dko MEF may suggest whole cilium shedding may predominate in these mutant cells during this time frame. Additionally, we observed increased frequency of IFT81 localization that was separate and distal to the ciliary axoneme in *Thm1*-null and *Thm1; Thm*2 dko cells after 2 hours of serum addition. This IFT81 localization may present decapitation or ectocytosis [222]. The reduced ciliary INPP5E in *Thm1*-mutant and *Thm1; Thm*2 dko MEF could promote ectocytosis, since *Inpp5e*-null MEF have enhanced ectocytosis [222]. Ectocytosis precedes cilia resorption [222], thus cilia resorption likely also occurs in *Thm1*-null and *Thm1; Thm*2 dko cells. In support of this, after 2 and 6 hours of serum restimulation, *Thm1*-null and *Thm1; Thm*2 dko cells showed shortened primary cilia, respectively. Further studies are required to determine the mechanisms by which IFT-A dysfunction regulates cilia loss.

The IFT-A complex can be subdivided into core and peripheral subcomplexes, comprised of IFT122/IFT140/IFT144 and of IFT42/IFT121/IFT139, respectively [146]. Depletion of core versus peripheral subcomplex components can result in different phenotypes. For instance, *Ift144*-

null RPE cells showed absence of SMO from cilia, suggesting defective ciliary import, while *Ift139*-null RPE cells accumulated SMO in cilia, indicating defective retrograde IFT [146]. These contrasts may reflect differences in cargos carried by the subcomplexes or by the individual IFT-A proteins. As a paralog of *Thm1*, *Thm2* is likely a component of the IFT-A peripheral subcomplex. Consistent with this, *Thm1*-null and *Thm1;Thm2* dko MEF have ciliary protein trafficking defects similar to those of RPE cells depleted of another peripheral subcomplex component, *Ift121/WDR35* [162]. This includes defective retrograde transport of IFT and BBSome proteins and impaired ciliary import of IFT-A protein, IFT140, and of membrane proteins, ARL13B and INPP5E. Similar also to IFT121/WDR35-depleted cells, *Thm1*-null MEF showed both reduced and delayed ciliogenesis. Reduced ciliary ARL13B in *Thm1*-null MEF may contribute to the reduced cilia assembly, since ARL13B is essential for ciliary membrane extension that is coupled to axoneme elongation [228].

Although ciliary presence of SMO was increased in *Thm1*-null and *Thm1*; *Thm2* dko MEF, *Gli1* expression was not induced by SAG treatment, suggesting THM1 is required for Hh pathway activation downstream of SMO ciliary localization. This result was unexpected since we previously observed increased *Gli1* and *Ptch1* expression in E10.5 *Thm1*-null ($Thm1^{aln/aln}$) whole-mount mouse embryos, and ventralization of the neural tube of E9.5 and E10.5 *Thm1*-null embryos indicating enhanced activation of the Hh pathway [50]. Two possibilities may explain this discrepancy. Additional signals or cell-cell interactions may be present *in vivo,* resulting in enhanced activation of the pathway during development. Alternatively, a study has demonstrated that *Thm1* can act as either a positive or negative regulator of Hh signaling in a cell-specific manner, since deletion of *Thm1* resulted in reduced Hh signaling in glial cells during cerebellum development [229]. Similarly, other *Ift* genes have been shown to positively or negatively regulate

the Hh pathway in a cell-type dependent manner [230]. We observed that SAG-treated triple allele mutant MEF had reduced pathway activation relative to control cells, indicating that in a *Thm1*-dose dependent manner, *Thm2* positively regulates Hh signaling downstream of SMO ciliary localization in MEF. In this light, absence of Hh activation in *Thm1*-null cells is consistent with *Thm1* acting as a positive modulator of Hh signaling in MEF. The factors that determine whether an *Ift* gene positively or negatively regulates the Hh pathway are yet to be defined.

Pathogenic mutations of *THM1* have been identified in approximately 5% of patients with ciliopathies [149]. Interestingly, one-third of patients with a homozygous mutation in another ciliary gene also harbored a heterozygote *Thm1* mutation, suggesting that *THM1* mutations can have causal or modifying effects in human ciliopathies. More recently, mutations in *THM2* were reported in male individuals with subfertility [156]. Our studies reveal that *Thm2* interacts with *Thm1*, and thus identifying mutations in *THM2* and *THM1* in the same individual may warrant investigation. Our findings that *Thm1*, alone and/or together with *Thm2*, regulates ciliary entry of membrane protein, ciliogenesis and cilia loss, Hh signaling, and development, provide insight into potential mechanisms underlying IFT-A related ciliopathies.

Chapter Five: Discussion, Future Directions and Significance

5.1 Discussion and novel contributions of my work

5.1.1 Establishing a novel role for *Thm1* in renal cystogenesis on a disease-gene background

ADPKD causes development of fluid-filled renal cysts and is the most common fatal monogenetic kidney disorder. A deficiency of the polycystins, which localize to primary cilia, causes ADPKD. Disruption of primary cilia also leads to cystic kidney disease. Recent studies revealed that deletion of certain primary cilia genes together with either *Pkd1* or *Pkd2* dramatically rescues PKD severity, through mechanisms that are unclear[115, 171, 201]. Additionally, the molecular mechanisms connecting cilia dysfunction to renal cystic disease are not understood. To help elucidate these mechanisms, I have ablated an *Ift-A* gene, *Thm1*, in juvenile and adult ADPKD mouse models.

Loss of *Thm1* results in ciliopathies that affect multiple tissues. Deletion of *Thm1* perinatally causes cystic kidney disease[143]. I have shown that relative to *Pkd2* cko mice, perinatal deletion of *Thm1* together with *Pkd2* results in a complex phenotype, with decreased KW/BW ratios, reduced cortical collecting duct-derived cysts, but increased proximal tubular dilations, and similar kidney function. In contrast, *Thm1* deletion in adult ADPKD mouse models markedly attenuates PKD renal cystogenesis, with reduced KW/BW ratios, reduced collecting duct- and loop of Henle-derived cysts, reduced proximal tubular dilations, and improved kidney function. Taken together, these data reveal a tubular- and maturation-dependent role for *Thm1* in the pathobiology of ADPKD.

Additionally, the role of *Thm1* loss in cilia length is also tubular- and maturation-specific. Relative to juvenile *Pkd2* cko mice, *Pkd2*;*Thm1* dko mice show similar cilia length in cortical collecting ducts, but elongated cilia in proximal tubules. In adult *Pkd1* and *Pkd2* mouse models, additional loss of *Thm1* normalizes cilia length. The differences in cilia length correlate with

differences in collecting duct-derived cystogenesis and proximal tubular dilation between juvenile and adult models, suggesting that the tubular microenvironment may play a role in regulating cilia length.

5.1.2 Establishing a novel role for *Thm1* in liver development and homeostasis

Primary cilia play essential roles in the pathogenesis of PLD, which is characterized by the growth of numerous hepatic cysts. In mice, loss of *Pkd1* or *Pkd2* also causes PLD, but interestingly, deletion of certain *Ift-B* genes together with *Pkd1* reduces PLD severity[201]. To examine the role of IFT-A in the pathogenesis of PLD, I deleted *Thm1* alone, or together with *Pkd2*, perinatally and during adulthood.

Interestingly, in contrast to the role of *Thm1* in the kidney, perinatal deletion of *Thm1* does not cause cysts in the liver, indicating that *Thm1*-mediated cystogenesis is tissue-specific. Instead, *Thm1* deletion causes a ductular reaction, which is characterized by aberrant proliferation of bile ducts. In *Thm1* cko mice at P21, we observed abnormal proliferation of cholangiocytes and hepatocytes, increased number of biliary ducts, and increased biliary fibrosis in the liver portal area. These data link primary cilia to biliary abnormalities and provide a new genetic model to study molecular mechanisms underlying biliary disease.

Additionally, perinatal deletion of *Thm1* together with *Pkd2* increases the severity of liver disease, causing increased LW/BW ratios, areas of necrosis, and enhanced activation of STAT3 signaling, suggesting an additive or synergistic effect. Unlike *Ift-B*, loss of *Ift-A* via *Thm1* in adult ADPKD mouse models does not ameliorate hepatic cystogenesis consistently at 6 months of age, indicating differences between IFT-A and IFT-B in adult onset hepatic cystogenesis. At most, we observed slightly decreased LW/BW ratios in adult-onset *Pkd2;Thm1* dko males at 6 months of

age. Histological analysis of *Pkd2*;*Thm1* dko male livers revealed variability in the severity of hepatic cystogenesis. Additionally, we observed that cystogenesis is reduced in *Pkd2*;*Thm1* dko livers at 4 months of age relative to *Pkd2* cko livers, indicating that adult loss of *Thm1* might slow liver cystic disease progression but does not alter the final outcome of PLD.

Previous studies revealed that primary cilia on cholangiocytes are found to be shortened with bulbous extensions in hypomorphic PKD animal models and ADPKD patients with liver symptoms[134-136]. Here we observed increased cilia length in *Pkd2* cko cholangiocytes relative to control. One possible explanation is that in our early onset *Pkd2* mouse model, we examined primary cilia on cholangiocytes at P21, when the liver is still undergoing growth and differentiation. However, in previous studies, primary cilia on cholangiocytes were examined in adult mice, ranging from 6 to 12 months of age, when mature livers are undergoing homeostasis. If the difference in cilia length is maturation-dependent, this would indicate that regulation of cilia length by *Pkd2* is influenced by a developmental window. Another possibility is that our *Pkd2* cko mice have greater PC2 deficiency than that of hypomorphic *Pkd2* mice, suggesting a role for PC2 dosage in regulating cilia length. In *Pkd2;Thm1* dko cholangiocytes, cilia length was the same as control, and shorter than those of *Pkd2* cko, suggesting that cilia length is normalized with additional loss of *Thm1* in *Pkd2* cko cholangiocytes. In contrast, primary cilia lengths relative to *Pkd2* cko juvenile kidneys are further increased in *Pkd2;Thm1* dko LTL+ tubules, but similar in *Pkd2;Thm1* dko DBA+ tubules. These differences reveal cell-specific effects of *Thm1* on cilia length.

5.1.3 Establishing genetic interactions between *Thm1* and *Thm2*

A BLAST homology search revealed that mouse THM2 is 49% identical to THM1 with a similar predicted protein structure[50], leading us to hypothesize that these paralogs share similar functions in primary cilia and ciliopathies. Recent studies show that mutations of *THM2* were associated with adult male subfertility[156]. Additionally, increased *THM2* expression correlates with a different proportion of immune cells in lung adenocarcinoma [157]. Our characterization of *Thm2* on a mixed FVB/C57BL6/J strain background revealed a lack of phenotype both in mice and in cultured cells. However, deletion of *Thm2* together with one allele of *Thm1* causes subfertility in males on a mixed FVB/C57BL6/J background, as well as skeletal defects on a more C57BL6/J background (5^{th} generation), suggesting that loss of *Thm2* is sensitive to *Thm1* dosage, and therefore, that the roles of THM1 and THM2 might be partially redundant. To expand our knowledge of *Thm1* and determine the function of the novel gene, *Thm2*, I generated control, *Thm1*-null, *Thm2*-null and *Thm2*-null;$Thm1^{+/-}$ (triple allele) and *Thm1*; *Thm2* dko MEF from embryonic day (E) 12.5 embryos.

Previous studies have shown that disruption of THM1 results in a shortened primary cilium with accumulation of ciliary proteins (such as IFT-A, IFT-B and GPCRs) at the distal tip forming a bulb-like structure, indicative of retrograde IFT defects[50, 146, 147]. I confirmed the role of THM1 in regulating retrograde IFT and established novel roles of THM1 in regulating ciliary entry of IFT-A and membrane-associated proteins. I also identified THM1 as a negative regulator of ciliogenesis upon serum re-stimulation of MEF. Importantly, this is the first demonstration of a role for IFT-A in cilia loss. Following serum re-stimulation, *Thm1*-null MEF show a decreased percentage of cilia with a bulbous distal tip, as well as evidence of shedding of accumulated IFT-B protein from the cilia tip, suggesting that cilia can get rid of accumulated proteins by decapitation

or ectocytosis when retrograde IFT is disrupted. Previous studies have shown that THM1 regulates Hh signaling negatively or positively in a cell-type dependent manner[50] [140] [148]. The factors that determine whether *Thm1* or other *Ift* genes will act as a positive or negative Hh regulator are unknown. My data reveal that in *Thm1*-null MEF, the Smoothened (SMO) signal transducer accumulates in cilia, but response to SMO agonist, SAG, is impaired, indicating that THM1 is required to activate Hh signaling downstream of SMO ciliary localization.

Timed matings of $Thm2^{+/-};Thm1^{+/-}$ intercrosses show that the number of live *Thm1;Thm2* dko embryos is reduced at E14.5 when compared with that of live *Thm1*-null embryos, indicating that additional loss of *Thm2* exacerbates the *Thm1*-null developmental phenotype causing mid-gestational lethality. In *Thm2*-null MEF, we confirmed that *Thm2* deletion does not cause any obvious phenotype in MEF. We also observed that triple allele mutant MEF with no defects in cilia structures had reduced pathway activation relative to control cells with SAG treatment, indicating that *Thm2* positively regulates Hh signaling downstream of SMO ciliary localization in a *Thm1*-dose dependent manner. Furthermore, in *Thm1*;*Thm2* dko MEF, cilia disappear more quickly after 2 hour-serum restimulation, and ciliary entry of membrane protein INPP5E is impaired, suggesting that *Thm2* regulates ciliary loss and cilia entry in a *Thm1*-dependent manner. Taken together, our studies establish unique and redundant roles for *Thm1* and *Thm2* in cilia loss, ciliary entry of membrane-associated protein, Hedgehog signaling, and embryogenesis, providing additional mechanisms underlying *Thm1*-, *Thm2*-, and IFT-A mediated ciliopathies.

5.2 Future directions

5.2.1 Expand knowledge of *Thm1* in cystic kidney disease

5.2.1.1 Determine effect of renal-tubule specific deletion of *Thm1* in juvenile ADPKD mouse models.

In Chapter Two, we deleted *Thm1* ubiquitously at P0 with a tamoxifen-inducible Rosa-*Cre* recombinase and observed a complex phenotype of renal cystogenesis that was tubular-specific. Interestingly, we also observed that primary cilia are present in myofibroblasts of *Pkd2* cko, and *Pkd2*;*Thm1* dko kidneys (Figure 5.1), and that glomerular dilations/cysts also exist in *Thm1* cko, *Pkd2* cko, and *Pkd2*;*Thm1* dko kidneys, suggesting that other cells in the kidney, in addition to renal tubular cells, may also contribute to the severity of cystic kidney disease. To specifically investigate the role of *Thm1* in renal tubules, a *Ksp*-Cre can be used to delete *Thm1* together with *Pkd1*. The *Ksp-Cre* is uniformly active in distal nephron segments including medullary thick ascending loop of Henle and collecting ducts[231]. We observed decreased cystogenesis of cortical collecting ducts yet similar BUN levels in *Pkd2;Thm1* dko mice relative to *Pkd2* cko mice using the *Rosa*-Cre, which results in global deletion. Thus, it would be interesting to determine whether specific deletion of *Thm1* together with *Pkd2* only in the loop of Henle and collecting ducts will improve kidney function.

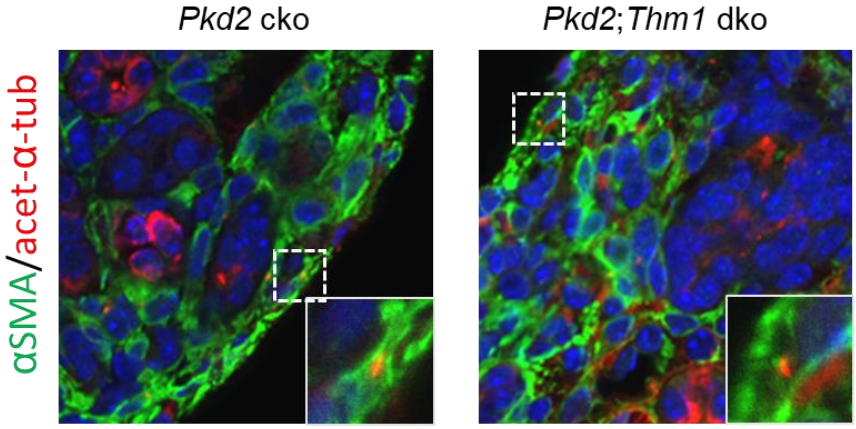

Figure 5.1 Myofibroblast cilia in *Pkd2* cko, and *Pkd2;Thm1* dko mice at P21
Representative immunostaining images of acetylated α-tubulin(red), αSMA (green) and DAPI (blue) in kidneys from 3-week-old *Pkd2* cko and *Pkd2;Thm1* dko mice.

5.2.1.2 Determine role of *Thm1* deletion in other PKD mouse models

Juvenile cystic kidney (*jck*) mice develop slowly progressing polycystic renal disease thought to recapitulate many aspects of human ADPKD[112]. The *jck* allele has a missense mutation in the gene *Nek8*, which encodes NIMA related kinase 8 that localizes to the proximal end of primary cilia[110]. An additional benefit of this mouse model is that instead of deleting *Thm1* simultaneously with a *Pkd* gene, deletion of *Thm1* can be performed during PKD progression, which will better illustrate the effect of disrupting primary cilia function in exploring potential pharmacologically or genetically therapeutic strategies against cystic kidney disease. Therefore, I also began to include *jck* mice in my studies to examine whether *Thm1* loss shows similar roles on a different genetic background.

To examine the effect of inducing IFT-A dysfunction during early PKD progression, we deleted *Thm1* at P0, and examined the renal phenotypes of control, *Thm1* cko, *jck* mutant and *jck*;*Thm1* double mutant mice at 6 weeks of age. At this stage on a pure C57BL/6J background, *Thm1* cko mice develop mild cystic kidney disease with small cysts of collecting duct and loop of Henle origin and dilations of proximal tubules (Figure 5.2A and 5.2.D). KW/BW ratios of *Thm1* cko mice are similar to those of control mice and BUN assays on sera of more *Thm1* cko mice will be required to determine if kidney function is impaired (Figure 5.2B and 5.2C). In *jck* mutant mice, renal cysts are derived from collecting ducts and the loop of Henle (Figure 5.2D), and KW/BW ratios (Figure 5.2B) and BUN levels (Figure 5.2C) are increased about 4X and 2X, respectively, relative to control. In *jck*;*Thm1* double mutant mice, cystic kidney disease is more severe, with cysts deriving from all renal tubules (Figure 5.2D), and KW/BW ratios (Figure 5.2B) and BUN levels (Figure 5.2C) are increased about 10X and 4X, respectively, relative to control.

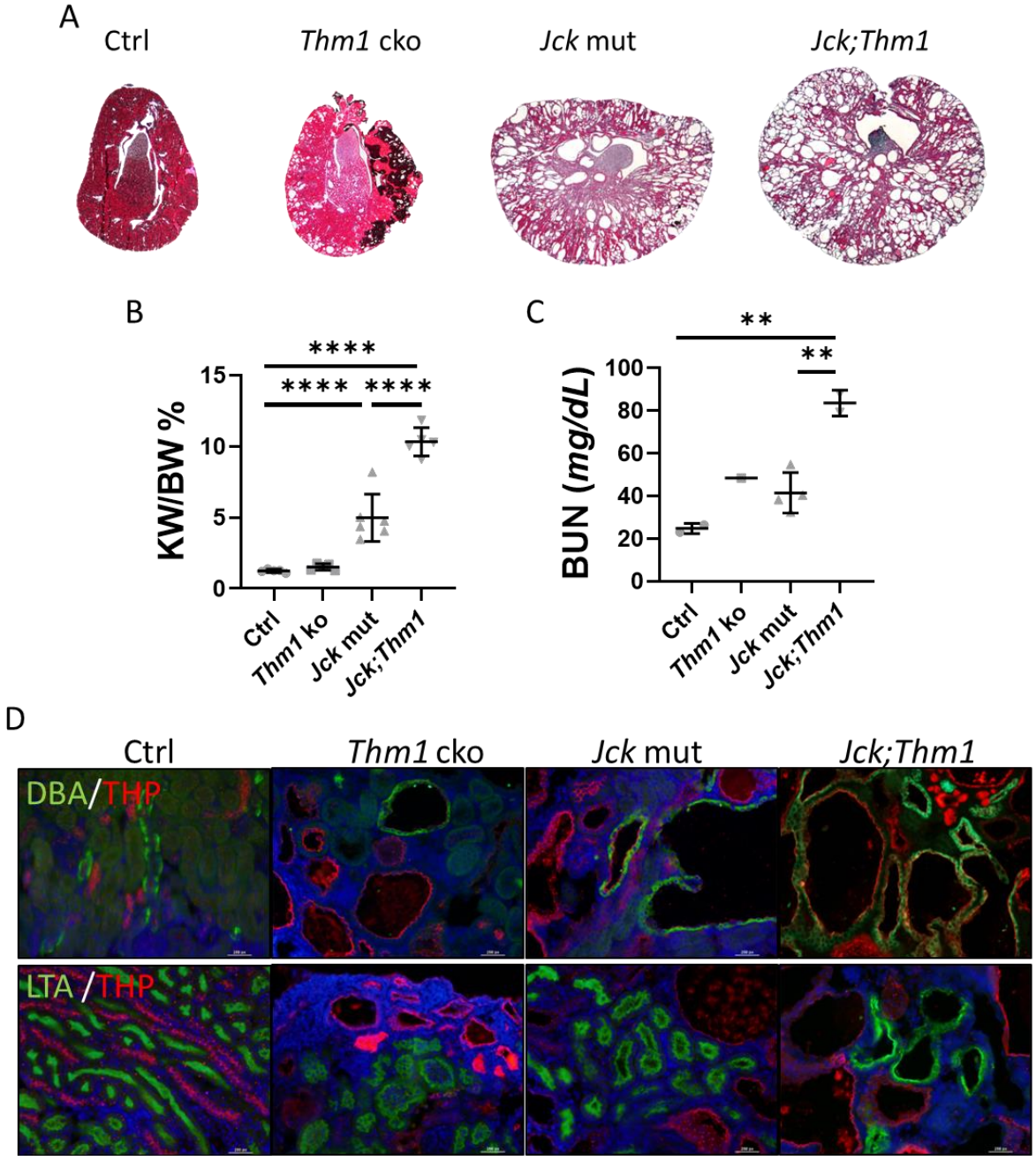

Figure 5.2 Cystic kidney disease in *Thm1* cko, *jck* mutant, and *jck;Thm1* double mutant mice at 6 weeks of age following perinatal *Thm1* deletion

(A) Representative images of H&E-stained whole kidney, (B) KW/BW ratios and (C) BUN levels, and (D) immune staining of renal tubule markers from 6-week-old control, *Thm1* cko, *jck* mutant and *jck;Thm1* double mutant mice. Statistical significance was determined by ANOVA. **P<0.01; ****P< 0.0001.

We next examined cell proliferation and renal fibrosis by immunostaining for PCNA and for αSMA, respectively. Both *Thm1* cko and *jck* mutant mice show increased proliferation of cyst-lining epithelia, normal tubule and interstitial cells (Figure 5.3). In *jck;Thm1* double mutant kidneys, there is relatively less proliferation than in *jck* mutant mice (Figure 5.3). PCNA staining with different tubule markers is necessary to compare proliferation levels in different renal tubules. αSMA staining revealed fibrosis around glomeruli and tubular dilations in *Thm1* cko kidneys, more fibrosis in *jck* mutant kidneys and the most fibrosis in *jck;Thm1* double mutant kidneys (Figure 5.3). Taken together, deletion of *Thm1* causes decreased proliferation yet increased fibrosis in *jck* mouse models.

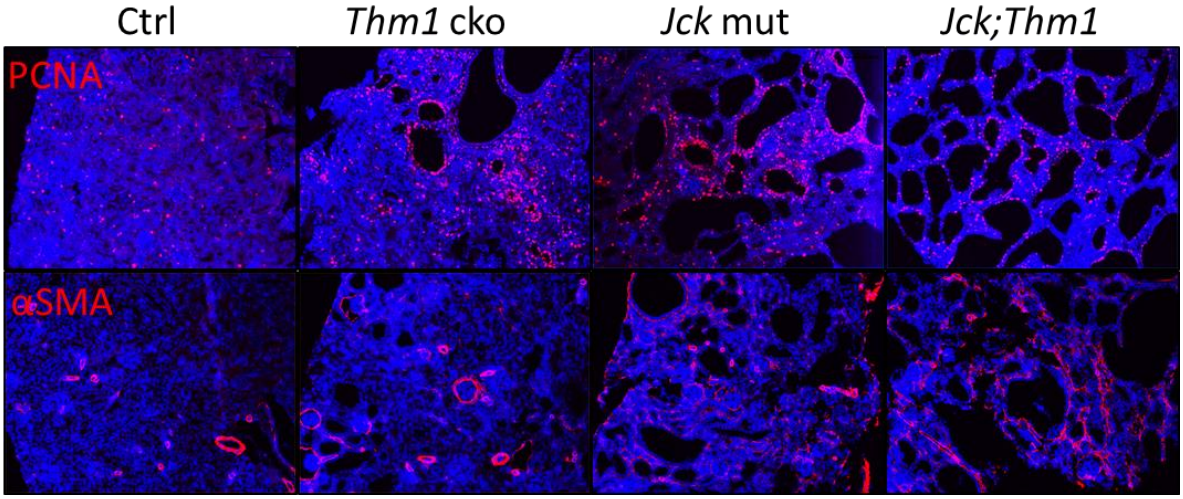

Figure 5.3 Proliferation and fibrosis in control, *Thm1* cko, *jck* mut and *jck;Thm1* double mutant kidneys
Representative images for PCNA (red, top), αSMA (red, bottom) and DAPI (blue) in kidneys from 6-week-old control, *Thm1* cko, *jck* mut and *jck;Thm1* double mutant mice.

We next examined the effect of inducing IFT-A deficiency during PKD progression in adult *jck* mice. We deleted *Thm1* at P28 and examined the renal phenotypes of control, *Thm1* cko, *jck* mutant and *jck*;*Thm1* double mutant mice at 9 weeks of age (P63). At this stage, *Thm1* cko mice show normal kidneys (Figure 5.4). *jck* mutant mice show renal cysts in collecting duct and loop of Henle (Figure 5.4D), increased KW/BW ratios (Figure 5.4B) and BUN levels (Figure 5.4C). *jck;Thm1* double mutant mice also show renal cysts derived from collecting duct and loop of Henle (Figure 5.4D); KW/BW ratios (Figure 5.4B) and BUN levels (Figure 5.4C) are similar to *jck* mice, in both males and females. Thus, additional loss of *Thm1* during adulthood does not affect the progression of cystic kidney disease in *jck* mouse models.

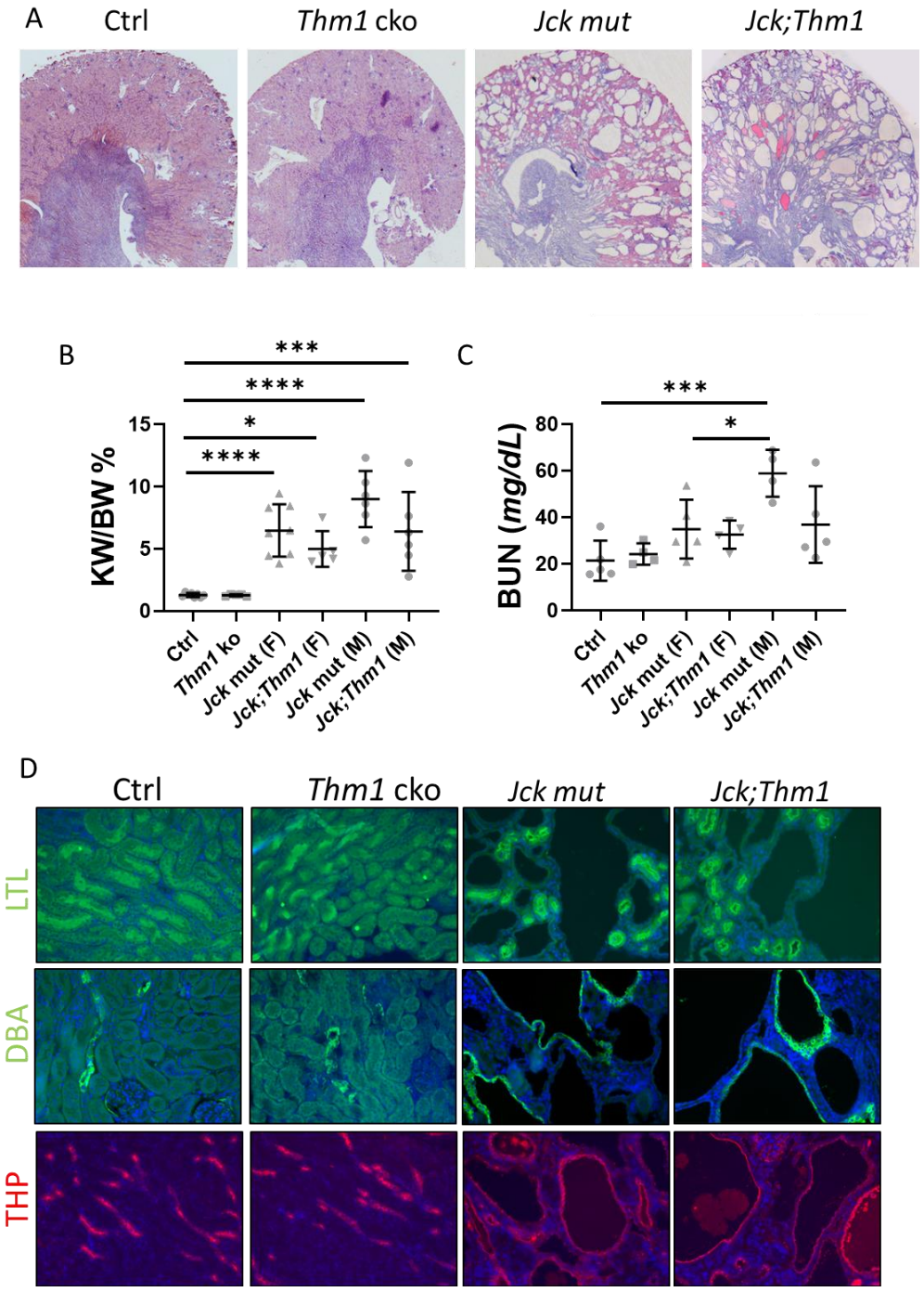

Figure 5.4 Cystic kidney disease in *Thm1* cko, *jck* mutant, and *jck;Thm1* double mutant mice at 9 weeks of age following *Thm1* deletion during early adulthood

(A) Representative images of H&E-stained whole kidney, (B) KW/BW ratios and (C) BUN levels, and (D) immune staining of renal tubule markers from 9-week-old control, *Thm1* cko, *jck* mutant and *jck;Thm1* double mutant mice. Statistical significance was determined by ANOVA. *P<0.05; ***P<0.001; ****P< 0.0001.

We examined cilia length and IFT by co-immunostaining for acetylated, α-tubulin together with IFT81 in kidneys with *Thm1* deletion at both P0 and P28. Loss of *Thm1* on a *jck* mutant background results in a combinatorial effect on cilia phenotype. *Thm1* cko mice have shortened cilia with accumulation of IFT81 in a bulbous distal tip, while *jck* mutants have elongated primary cilia. *Thm1*; *jck* double mutants have long primary cilia, a feature of *jck* mutant cilia, and a bulb-like structure at the distal tip, a feature of *Thm1* mutant cilia (Figure 5.5).

Taken together, these data reveal that perinatal loss of *Thm1* exacerbates cystic kidney disease in the *jck* mouse model, while loss of *Thm1* during adulthood does not affect the progression of cystic kidney disease. These seemingly additive effects of *Thm1* deletion in *jck* mice may reflect independent cyst-promoting roles for *Thm1* and *jck*. Further, the contrasting effects of *Thm1* deletion in *Pkd2* and *jck* mutants may suggest divergent mechanisms underlying *Pkd2* and *jck* renal cystogenesis.

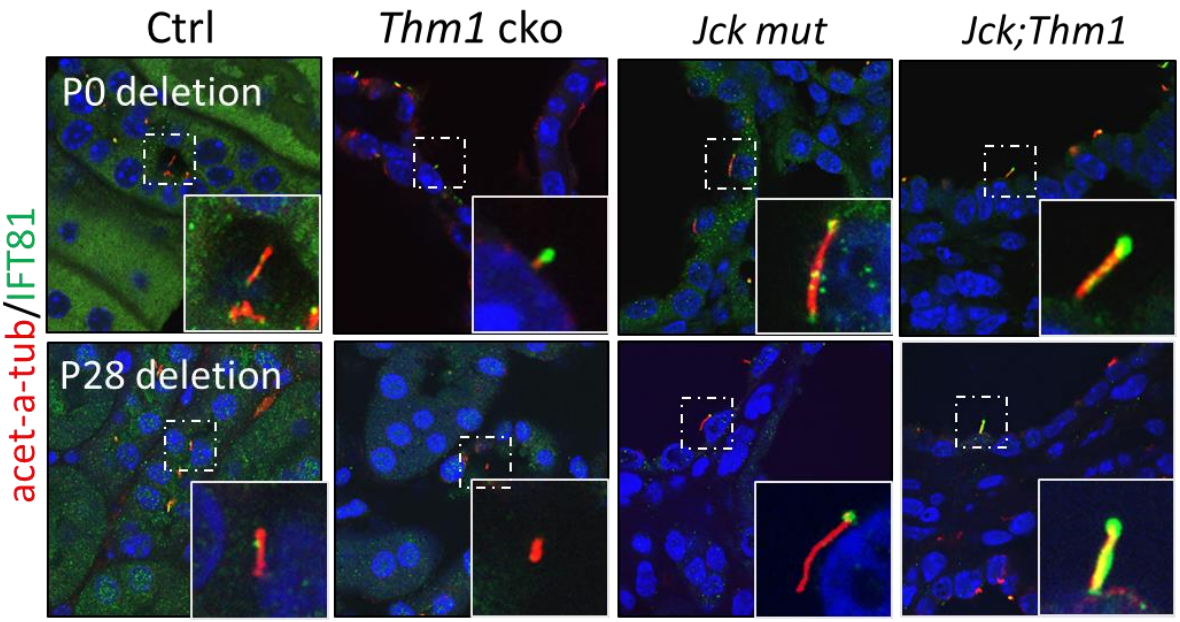

Figure 5.5 Primary cilia of control, *Thm1* cko, *jck* mutant, and *jck*;*Thm1* double mutant kidneys
Representative images of immunostaining for acetylated α-tubulin(red), IFT81 (green) and DAPI (blue) in renal tubules of 6-week-old (top) and 9-week-old (bottom) control, Thm1 cko, jck mutant and jck;Thm1 double mutant mice.

5.2.1.3 Expand knowledge of signaling pathways downstream of *Thm1* deficiency in ADPKD mouse models

Our data reveal that STAT3 activation is enhanced in early-onset *Pkd2;Thm1* dko whole kidney extracts but reduced in adult-onset *Pkd1;Thm1* dko whole kidney extracts, relative to those of *Pkd1*/*2* cko kidneys. Future directions could include co-staining kidney sections for P-STAT3 together with different renal tubule markers (DBA, LTL and THP) to identify which cells have the most expression of P-STAT3 and whether the expression correlates with renal cystogenesis. In many tumors, STAT3 has been reported to be consistently activated to induce transcription of cytokines, chemokines and growth factors, which are associated with macrophage activation and inflammatory responses[209]. Cancer cells and cyst-lining cells share similarities, such as enhanced proliferation. Thus, there is a possibility that STAT3 activation in kidneys may regulate the inflammatory microenvironment. We will co-stain pSTAT3 with immune cell markers or myofibroblast marker αSMA to determine if STAT3 activation is associated with immune cell infiltration and/or kidney fibrosis. Cell proliferation marker, PCNA, can also be used to determine whether STAT3 activation drives cell proliferation.

Signaling pathways that are known to be elevated in ADPKD, such as the ERK, AKT and mTOR signaling pathways, can also be examined by Western blot and immunofluorescence to determine how their levels are changed in mutant and double mutant kidneys.

5.2.1.4 Determine mechanisms by which IFT-A deficiency attenuates cystic kidney disease severity in adult ADPKD models.

Our data reveal that loss of *Thm1* attenuated cystic kidney disease in adult ADPKD models, but the underlying mechanisms remain unclear. One hypothesis is that the polycystins are negative

regulators of signaling pathways that promote renal cystogenesis in a primary cilia-dependent manner. Thus, when cilia function is disrupted, loss of polycystins cannot activate those signaling pathways to initiate cystogenesis. To test this hypothesis, kidney phenotypes can be examined longitudinally at different time points to determine the pre-cystic stage of cystic kidney disease. A global transcriptome approach, such as single cell RNA sequencing of pre-cystic kidneys can be used to identify potential cystogenic signaling pathways in a cell-type specific manner, particularly since our data consistently reveal differences between collecting duct and proximal tubule and between cortex and medulla. Quantitative PCR and Western blots of candidate molecules/pathways can also be used to identify possible downstream targets of *Thm1* deficiency. Further, cilia phenotypes in pre-cystic kidneys can be examined by immunofluorescence for IFT and membrane-associated proteins such as ARL13B, INPP5E. Membrane-associated proteins may play essential roles in regulating signaling pathways that are also regulated by both primary cilia and the polycystins.

5.2.1.5 Determine mechanisms by which IFT-A deficiency does not attenuate cystic kidney disease in juvenile ADPKD mouse models.

In contrast to deletion in adult models, deletion of either *Tulp3*, an IFT-A adaptor protein[115, 171], or of *Thm1*, an IFT-A component, in juvenile *Pkd1* or *Pkd2* mouse models did not rescue PKD severity. The mechanisms underlying the differences between juvenile and adult ADPKD mouse models are still unknown. We hypothesize that in juvenile ADPKD mouse models, in which kidneys are undergoing differentiation and maturation, IFT-A is required for proper development of the kidney (as shown by *Thm1* cko mice) and that IFT-A deficiency activates cystogenic signaling pathways (*e.g.* STAT3) promoting cystic kidney disease. Interestingly,

deletion of the *Ift-B* genes, which ablates primary cilia, has been shown to attenuate PKD severity in juvenile ADPKD mouse models[201], indicating that there may also be pathways that require primary cilia to be activated, as in adult kidneys.

Future experiments could include single-cell RNA sequencing of kidneys from juvenile control, *Thm1* cko, *Pkd2* cko, and *Pkd2;Thm2* dko mice. The results can be compared with those of adult kidneys to uncover specific cystogenic signaling pathways during kidney development.

In addition to *in vivo* experiments, we can generate primary renal tubular epithelial cells from juvenile and adult single and double knock-out mutants and analyze localization and expression of ciliary proteins that regulate signaling pathways such as STAT3, ERK and mTOR *in vitro*. Additionally, our late-onset adult ADPKD mouse models show that loss of *Thm1* together with *Pkd1* restores *Ccl2*, a cytokine that recruits immune cells, to normal levels. Thus, we can also examine the expression of *Ccl2* in *Pkd1* cko and *Pkd1*;*Thm1* dko primary cells. These analyses could reveal the direct effect of deficiency of IFT-A, of the polycystins and of both in renal tubule epithelial cells and can help us identify the underlying mechanisms that lead to enhanced or rescued renal cystogenesis.

5.2.2 Expand knowledge of *Thm1* in biliary and liver ciliopathies

5.2.2.1 Expand characterization of ductular reaction in *Thm1* cko mice

Our data show that loss of *Thm1* at P0 results in a ductular reaction, characterized by increased proliferation of cholangiocytes, and increased numbers of biliary ducts. Current experiments have been performed in livers of 3-week-old mice, when the liver is still maturing. Additional analyses of livers in adult mice, such as at 6 weeks and 12 weeks of age would establish a timeline of disease progression. The aspartate aminotransferase (AST) test and alanine

aminotransferase (ALT) test could be used to assess liver function. To examine underlying mechanisms, CK19, a marker of cholangiocytes, could be used to quantify the number of cholangiocytes in the biliary region. F4/80, a marker of macrophages, could be used to evaluate immune cell infiltration in periportal areas. We did not observe a difference in STAT3 and ERK signaling between control and *Thm1* cko whole liver extracts using Western blots. Since the liver extracts may contain a high content of hepatocytes, immunostaining for P-STAT3 and P-ERK on liver sections could determine whether P-STAT3 and P-ERK are increased in cholangiocytes.

Further, although primary cilia are present in cholangiocytes not in hepatocytes, PCNA staining indicates increased proliferation in hepatocytes in *Thm1* cko livers. It is not known whether loss of *Thm1* has a non-ciliary effect on hepatocytes. A hepatocyte-specific *Cre* and a cholangiocyte-specific *Cre* to delete *Thm1* specifically in hepatocytes and cholangiocytes, respectively, could help answer this question.

5.2.2.2 Expand upon the role of *Thm1* in polycystic liver disease

A previous study has shown that IFT-B deficiency induced at 4 weeks of age dramatically ameliorates hepatic cystogenesis at 4 months of age in a *Pkd1* cko mice using *UBC-Cre* recombinase [201]. Our data reveal that adult global deletion of *Thm1* and *Pkd2* using the *Rosa26-Cre* recombinase does not affect hepatic cystogenesis in females and slightly reduced LW/BW ratios in males at 6 months of age. Further, histological analysis revealed a lot of variability in hepatic cystic index. It is possible that 6 months of age represents a late stage of polycystic liver disease. Thus, more animals will be analyzed at 4 months of age, which will provide an earlier stage of cystic liver disease. LW/BW ratios and hepatic cystic index will be characterized to

determine if *Thm1* loss attenuates polycystic liver disease in adult-onset *Pkd2* cko mice at an earlier stage.

Perinatal deletion of *Thm1* exacerbates cystic liver disease with increased areas of necrosis in *Pkd2* cko mice at 3 weeks of age. Future experiments could include performing AST and ALT tests to determine whether loss of *Thm1* causes additional liver function impairment. To examine underlying mechanisms, immunostaining liver sections for CK19 can be used to quantify the number of cholangiocytes in cyst-lining epithelia, and for F4/80 to evaluate immune cell filtration. Additionally, the TUNEL assay can be used to stain for apoptotic cells. We observed increased STAT3 activation but no difference in ERK activation in *Pkd2;Thm1* dko livers using Western blots, relative to *Pkd2* cko livers. Immunostaining for P-STAT3 and P-ERK in liver sections will be performed to determine if P-STAT3 and P-ERK are increased in cyst-lining epithelial cholangiocytes.

5.2.3 Expand upon knowledge of *Thm1* and *Thm2* in ciliary structure and cilia-regulated signaling pathways

5.2.3.1 Expand knowledge of *Thm1* and IFT-A in cilia disassembly

We observed that upon serum restimulation in a cilia loss assay, primary cilia of *Thm1*-null MEF disappear faster than those of control MEF. One possible mechanism would be that THM1 loss promotes cilia disassembly. To further confirm the role of *Thm1* in cilia disassembly, immunofluorescence for phosphorylated Aurora A kinase (AurA), which localizes to the basal body during cilia disassembly[219], can be performed. Additionally, an AurA inhibitor can be used to examine whether the reduction of cilia length and of percentage of ciliated cells can be

rescued in *Thm1*-null MEF. Further, to prove that IFT-A is required to counter cilia disassembly, the role of other *Ift-A* genes, such as *Ift140* or *Ift122,* can be examined using similar assays.

5.2.3.2 Expand knowledge of *Thm1* and IFT-A in ectocytosis

Using immunofluorescence, we observed that *Thm1*-null MEF sheds off accumulated IFT-B from the cilia tip, suggesting that cilia can get rid of accumulated proteins by ectocytosis. To better illustrate the role of *Thm1* in promoting ectocytosis, future directions include live cell imaging of IFT-GFP labelled *Thm1*-mutant cells to reveal the process of ectocytosis and to determine if *Thm1*-null cells undergo increased ectocytosis. Additionally, immunostaining for components of IFT-A, BBSome, and ciliary membrane proteins, such as INPP5E and ARL13B, can be performed to determine if the proteins also exit cilia via ectocytosis. To prove more broadly that IFT-A is required to counter ectocytosis, the role of other *Ift-A* genes, such as *Ift140* or *Ift122*, can be examined in a similar fashion.

5.2.3.3 Expand knowledge of *Thm1* in regulating Hh signaling

Previous studies suggest that THM1 regulates Hh signaling negatively or positively in a cell-type dependent manner[50] [140] [148]. Our data reveal *Thm1*-null MEF have an impaired response to Hedgehog agonist, SAG. We can expand our analyses to other cell types such as M-1, RPE, and/or IMCD3 cells to determine which cells similarly demonstrate a lack of response to SAG or which show increased Hh signaling as observed in the ventral neural tube. Additionally, since SMO accumulates in cilia in *Thm1*-null MEF, we can examine ciliary localization of Hh modifiers that act downstream of SMO, such as the negative Hh regulator GPR161. The factors

that determine whether an IFT protein will positively or negatively regulate the Hh pathway are unknown.

5.2.3.4 Expand knowledge of the role of *Thm2* in other cell types

Since the expression of *Thm2* is low in MEF, the effect of *Thm2* loss we observed in cilia loss and ciliary entry is not obvious. *Thm1*$^{+/-}$*; Thm2*-null mice develop postnatal skeletal defects, indicating that the expression of *Thm2* may be higher in developing bone cells. To better characterize the role of *Thm1* and *Thm2*, we can generate *Thm1*$^{+/-}$*; Thm2*-null or *Thm1;Thm2* dko primary chondrocytes and osteocytes and then examine ciliogenesis, cilia loss, ciliary trafficking and Hh signaling in these cells.

5.3 Significance of these studies

ADPKD causes development of fluid-filled renal cysts and is the most common fatal monogenetic kidney disorder with limited therapies and no cure. PLD occurs in isolation or as an extrarenal manifestation in more than 90% of ADPKD patients[124]. Primary cilia play an essential role in the pathobiology of both PKD and PLD. However, the molecular mechanisms connecting cilia dysfunction to renal and hepatic cystic disease are not understood. We proposed to uncover the roles of IFT-A paralogs, *Thm1* and *Thm2*, in juvenile and adult ADPKD mouse models and in MEF, respectively. As a result, my work is the first to demonstrate that IFT-A deficiency affects renal and hepatic cystogenesis in a cell type- and maturation-dependent manner in ADPKD mouse models. My work is also the first to show novel interactive roles for THM1 and THM2 in cilia loss, ciliary entry of membrane protein, Hedgehog signaling, and embryogenesis. Taken together, my dissertation work provides greater mechanistic and physiological

understanding of IFT-A in ciliopathies, including in ADPKD, that will be essential to devising future therapeutic strategies.

References

1. Goetz, S.C. and K.V. Anderson, *The primary cilium: a signalling centre during vertebrate development.* Nat Rev Genet, 2010. **11**(5): p. 331-44.
2. Ishikawa, T., *Axoneme Structure from Motile Cilia.* Cold Spring Harb Perspect Biol, 2017. **9**(1).
3. Jain, R., et al., *Sensory functions of motile cilia and implication for bronchiectasis.* Frontiers in bioscience (Scholar edition), 2012. **4**: p. 1088-1098.
4. Satir, P., L.B. Pedersen, and S.T. Christensen, *The primary cilium at a glance.* Journal of Cell Science, 2010. **123**(4): p. 499-503.
5. Gonçalves, J. and L. Pelletier, *The Ciliary Transition Zone: Finding the Pieces and Assembling the Gate.* Molecules and cells, 2017. **40**(4): p. 243-253.
6. Silva, L.M., et al., *Analysis of primary cilia in renal tissue and cells.* Methods Cell Biol, 2019. **153**: p. 205-229.
7. Nigg, E.A. and T. Stearns, *The centrosome cycle: Centriole biogenesis, duplication and inherent asymmetries.* Nat Cell Biol, 2011. **13**(10): p. 1154-60.
8. Paridaen, J.T., M. Wilsch-Brauninger, and W.B. Huttner, *Asymmetric inheritance of centrosome-associated primary cilium membrane directs ciliogenesis after cell division.* Cell, 2013. **155**(2): p. 333-44.
9. Malicki, J.J. and C.A. Johnson, *The Cilium: Cellular Antenna and Central Processing Unit.* Trends Cell Biol, 2017. **27**(2): p. 126-140.
10. Anvarian, Z., K. Mykytyn, and S. Mukhopadhyay, *Cellular signalling by primary cilia in development, organ function and disease.* 2019. **15**(4): p. 199-219.
11. Mukhopadhyay, S., et al., *TULP3 bridges the IFT-A complex and membrane phosphoinositides to promote trafficking of G protein-coupled receptors into primary cilia.* Genes Dev, 2010. **24**(19): p. 2180-93.
12. Hirano, T., Y. Katoh, and K. Nakayama, *Intraflagellar transport-A complex mediates ciliary entry and retrograde trafficking of ciliary G protein-coupled receptors.* Molecular biology of the cell, 2017. **28**(3): p. 429-439.
13. Picariello, T., et al., *A global analysis of IFT-A function reveals specialization for transport of membrane-associated proteins into cilia.* Journal of Cell Science, 2019. **132**(3): p. jcs220749.
14. Nachury, M.V., *The molecular machines that traffic signaling receptors into and out of cilia.* Current opinion in cell biology, 2018. **51**: p. 124-131.
15. Nachury, M.V., *The molecular machines that traffic signaling receptors into and out of cilia.* Curr Opin Cell Biol, 2018. **51**: p. 124-131.
16. Spasic, M. and C.R. Jacobs, *Primary cilia: Cell and molecular mechanosensors directing whole tissue function.* Semin Cell Dev Biol, 2017. **71**: p. 42-52.
17. Pablo, J.L., P.G. DeCaen, and D.E. Clapham, *Progress in ciliary ion channel physiology.* 2017. **149**(1): p. 37-47.
18. Delling, M., et al., *Primary cilia are specialized calcium signalling organelles.* Nature, 2013. **504**(7479): p. 311-4.
19. Yuan, S., et al., *Intraciliary calcium oscillations initiate vertebrate left-right asymmetry.* Curr Biol, 2015. **25**(5): p. 556-67.

20. Praetorius, H.A. and K.R. Spring, *Bending the MDCK cell primary cilium increases intracellular calcium.* J Membr Biol, 2001. **184**(1): p. 71-9.
21. Praetorius, H.A. and K.R. Spring, *The renal cell primary cilium functions as a flow sensor.* Curr Opin Nephrol Hypertens, 2003. **12**(5): p. 517-20.
22. Masyuk, A.I., et al., *Cholangiocyte cilia detect changes in luminal fluid flow and transmit them into intracellular Ca2+ and cAMP signaling.* Gastroenterology, 2006. **131**(3): p. 911-20.
23. Tsiokas, L., et al., *Specific association of the gene product of PKD2 with the TRPC1 channel.* Proc Natl Acad Sci U S A, 1999. **96**(7): p. 3934-9.
24. Pazour, G.J., et al., *Polycystin-2 localizes to kidney cilia and the ciliary level is elevated in orpk mice with polycystic kidney disease.* Curr Biol, 2002. **12**(11): p. R378-80.
25. Yoder, B.K., X. Hou, and L.M. Guay-Woodford, *The polycystic kidney disease proteins, polycystin-1, polycystin-2, polaris, and cystin, are co-localized in renal cilia.* J Am Soc Nephrol, 2002. **13**(10): p. 2508-16.
26. Gradilone, S.A., et al., *Cholangiocyte cilia express TRPV4 and detect changes in luminal tonicity inducing bicarbonate secretion.* Proc Natl Acad Sci U S A, 2007. **104**(48): p. 19138-43.
27. Flannery, R.J., N.K. Kleene, and S.J. Kleene, *A TRPM4-dependent current in murine renal primary cilia.* 2015. **309**(8): p. F697-707.
28. Delling, M., et al., *Primary cilia are not calcium-responsive mechanosensors.* Nature, 2016. **531**(7596): p. 656-60.
29. Nüsslein-Volhard, C. and E. Wieschaus, *Mutations affecting segment number and polarity in Drosophila.* Nature, 1980. **287**(5785): p. 795-801.
30. Skoda, A.M., et al., *The role of the Hedgehog signaling pathway in cancer: A comprehensive review.* Bosn J Basic Med Sci, 2018. **18**(1): p. 8-20.
31. Aoto, K., et al., *Mouse Shh is required for prechordal plate maintenance during brain and craniofacial morphogenesis.* J Dev Biol, 2009. **327**(1): p. 106-20.
32. Fernandes-Silva, H. and J. Correia-Pinto, *Canonical Sonic Hedgehog Signaling in Early Lung Development.* 2017. **5**(1).
33. Litingtung, Y., et al., *Sonic hedgehog is essential to foregut development.* Nat Genet, 1998. **20**(1): p. 58-61.
34. Motoyama, J., et al., *Essential function of Gli2 and Gli3 in the formation of lung, trachea and oesophagus.* Nat Genet, 1998. **20**(1): p. 54-7.
35. Pepicelli, C.V., P.M. Lewis, and A.P. McMahon, *Sonic hedgehog regulates branching morphogenesis in the mammalian lung.* Curr Biol, 1998. **8**(19): p. 1083-6.
36. Mill, P., et al., *Sonic hedgehog-dependent activation of Gli2 is essential for embryonic hair follicle development.* Genes Dev, 2003. **17**(2): p. 282-94.
37. Seppala, M., et al., *Sonic Hedgehog Signaling and Development of the Dentition.* J Dev Biol, 2017. **5**(2).
38. Yang, J., et al., *The Hedgehog signalling pathway in bone formation.* Int J Oral Sci, 2015. **7**(2): p. 73-9.
39. Bitgood, M.J., L. Shen, and A.P. McMahon, *Sertoli cell signaling by Desert hedgehog regulates the male germline.* Curr Biol, 1996. **6**(3): p. 298-304.
40. Mastronardi, F.G., et al., *Co-localization of patched and activated sonic hedgehog to lysosomes in neurons.* Neuroreport, 2000. **11**(3): p. 581-5.

41. Christensen, S.T. and C.M. Ott, *Cell signaling. A ciliary signaling switch.* Science, 2007. **317**(5836): p. 330-1.
42. Sasaki, H., et al., *Regulation of Gli2 and Gli3 activities by an amino-terminal repression domain: implication of Gli2 and Gli3 as primary mediators of Shh signaling.* Development, 1999. **126**(17): p. 3915-24.
43. Aza-Blanc, P., et al., *Proteolysis that is inhibited by hedgehog targets Cubitus interruptus protein to the nucleus and converts it to a repressor.* Cell, 1997. **89**(7): p. 1043-53.
44. Bai, C.B., D. Stephen, and A.L. Joyner, *All mouse ventral spinal cord patterning by hedgehog is Gli dependent and involves an activator function of Gli3.* Dev Cell, 2004. **6**(1): p. 103-15.
45. Goetz, S.C., P.J. Ocbina, and K.V. Anderson, *The primary cilium as a Hedgehog signal transduction machine.* Methods Cell Biol, 2009. **94**: p. 199-222.
46. Briscoe, J. and P.P. Thérond, *The mechanisms of Hedgehog signalling and its roles in development and disease.* Nature Reviews Molecular Cell Biology, 2013. **14**(7): p. 416-429.
47. Huangfu, D., et al., *Hedgehog signalling in the mouse requires intraflagellar transport proteins.* Nature, 2003. **426**(6962): p. 83-7.
48. Liu, A., B. Wang, and L.A. Niswander, *Mouse intraflagellar transport proteins regulate both the activator and repressor functions of Gli transcription factors.* Development, 2005. **132**(13): p. 3103-11.
49. Houde, C., et al., *Hippi is essential for node cilia assembly and Sonic hedgehog signaling.* Dev Biol, 2006. **300**(2): p. 523-33.
50. Tran, P.V., et al., *THM1 negatively modulates mouse sonic hedgehog signal transduction and affects retrograde intraflagellar transport in cilia.* Nat Genet, 2008. **40**(4): p. 403-410.
51. Qin, J., et al., *Intraflagellar transport protein 122 antagonizes Sonic Hedgehog signaling and controls ciliary localization of pathway components.* Proc Natl Acad Sci U S A, 2011. **108**(4): p. 1456-61.
52. Bangs, F. and K.V. Anderson, *Primary Cilia and Mammalian Hedgehog Signaling.* Cold Spring Harb Perspect Biol, 2017. **9**(5).
53. Liem, K.F., Jr., et al., *The IFT-A complex regulates Shh signaling through cilia structure and membrane protein trafficking.* The Journal of Cell Biology, 2012. **197**(6): p. 789-800.
54. Caspary, T., C.E. Larkins, and K.V. Anderson, *The graded response to Sonic Hedgehog depends on cilia architecture.* Dev Cell, 2007. **12**(5): p. 767-78.
55. Chavez, M., et al., *Modulation of Ciliary Phosphoinositide Content Regulates Trafficking and Sonic Hedgehog Signaling Output.* Dev Cell, 2015. **34**(3): p. 338-50.
56. Garcia-Gonzalo, F.R., et al., *Phosphoinositides Regulate Ciliary Protein Trafficking to Modulate Hedgehog Signaling.* Dev Cell, 2015. **34**(4): p. 400-409.
57. Gerdes, J.M., et al., *Disruption of the basal body compromises proteasomal function and perturbs intracellular Wnt response.* Nat Genet, 2007. **39**(11): p. 1350-60.
58. Ezratty, E.J., et al., *A role for the primary cilium in Notch signaling and epidermal differentiation during skin development.* Cell, 2011. **145**(7): p. 1129-41.
59. Clement, C.A., et al., *TGF-beta signaling is associated with endocytosis at the pocket region of the primary cilium.* Cell Rep, 2013. **3**(6): p. 1806-14.

60. Kim, W., M. Kim, and E.H. Jho, *Wnt/beta-catenin signalling: from plasma membrane to nucleus.* Biochem J, 2013. **450**(1): p. 9-21.
61. Corbit, K.C., et al., *Kif3a constrains beta-catenin-dependent Wnt signalling through dual ciliary and non-ciliary mechanisms.* Nat Cell Biol, 2008. **10**(1): p. 70-6.
62. Ocbina, P.J., M. Tuson, and K.V. Anderson, *Primary cilia are not required for normal canonical Wnt signaling in the mouse embryo.* PLoS One, 2009. **4**(8): p. e6839.
63. Reiter, J.F. and M.R. Leroux, *Genes and molecular pathways underpinning ciliopathies.* Nature Reviews Molecular Cell Biology, 2017. **18**(9): p. 533-547.
64. Tobin, J.L. and P.L. Beales, *The nonmotile ciliopathies.* Genet Med, 2009. **11**(6): p. 386-402.
65. Kumar, N. and A.K. Singh, *Trends of male factor infertility, an important cause of infertility: A review of literature.* J Hum Reprod Sci, 2015. **8**(4): p. 191-6.
66. Kagan, K.O., A. Dufke, and U. Gembruch, *Renal cystic disease and associated ciliopathies.* Curr Opin Obstet Gynecol, 2017. **29**(2): p. 85-94.
67. Pan, J., T. Seeger-Nukpezah, and E.A. Golemis, *The role of the cilium in normal and abnormal cell cycles: emphasis on renal cystic pathologies.* Cell Mol Life Sci, 2013. **70**(11): p. 1849-74.
68. Lanktree, M.B., et al., *Prevalence Estimates of Polycystic Kidney and Liver Disease by Population Sequencing.* Journal of the American Society of Nephrology, 2018. **29**(10): p. 2593-2600.
69. Willey, C.J., et al., *Prevalence of autosomal dominant polycystic kidney disease in the European Union.* Nephrology Dialysis Transplantation, 2016. **32**(8): p. 1356-1363.
70. Quinlan, R.J., J.L. Tobin, and P.L. Beales, *Modeling ciliopathies: Primary cilia in development and disease.* Curr Top Dev Biol, 2008. **84**: p. 249-310.
71. Ekser, B. and P. Rigotti, *Images in clinical medicine. Autosomal dominant polycystic kidney disease.* N Engl J Med, 2010. **363**(1): p. 71.
72. Hindryckx, A. and L. De Catte, *Prenatal diagnosis of congenital renal and urinary tract malformations.* Facts, views & vision in ObGyn, 2011. **3**(3): p. 165-174.
73. Malekshahabi, T., et al., *Autosomal dominant polycystic kidney disease: Disrupted pathways and potential therapeutic interventions.* Journal of Cellular Physiology, 2019. **234**(8): p. 12451-12470.
74. Cornec-Le Gall, E., A. Alam, and R.D. Perrone, *Autosomal dominant polycystic kidney disease.* The Lancet, 2019. **393**(10174): p. 919-935.
75. Gevers, T.J.G. and J.P.H. Drenth, *Diagnosis and management of polycystic liver disease.* Nature Reviews Gastroenterology & Hepatology, 2013. **10**(2): p. 101-108.
76. Cornec-Le Gall, E., V.E. Torres, and P.C. Harris, *Genetic Complexity of Autosomal Dominant Polycystic Kidney and Liver Diseases.* J Am Soc Nephrol, 2018. **29**(1): p. 13-23.
77. Porath, B., et al., *Mutations in GANAB, Encoding the Glucosidase IIalpha Subunit, Cause Autosomal-Dominant Polycystic Kidney and Liver Disease.* Am J Hum Genet, 2016. **98**(6): p. 1193-1207.
78. Cornec-Le Gall, E., et al., *Monoallelic Mutations to DNAJB11 Cause Atypical Autosomal-Dominant Polycystic Kidney Disease.* Am J Hum Genet, 2018. **102**(5): p. 832-844.

79. Bastos, A.P. and L.F. Onuchic, *Molecular and cellular pathogenesis of autosomal dominant polycystic kidney disease.* Braz J Med Biol Res, 2011. **44**(7): p. 606-17.
80. Bergmann, C., et al., *Polycystic kidney disease.* Nature reviews. Disease primers, 2018. **4**(1): p. 50-50.
81. Parnell, S.C., et al., *Polycystin-1 activation of c-Jun N-terminal kinase and AP-1 is mediated by heterotrimeric G proteins.* J Biol Chem, 2002. **277**(22): p. 19566-72.
82. Qian, F., et al., *Cleavage of polycystin-1 requires the receptor for egg jelly domain and is disrupted by human autosomal-dominant polycystic kidney disease 1-associated mutations.* Proc Natl Acad Sci U S A, 2002. **99**(26): p. 16981-6.
83. Kurbegovic, A., et al., *Novel functional complexity of polycystin-1 by GPS cleavage in vivo: role in polycystic kidney disease.* Mol Cell Biol, 2014. **34**(17): p. 3341-53.
84. Paul, B.M. and G.B. Vanden Heuvel, *Kidney: polycystic kidney disease.* Wiley Interdiscip Rev Dev Biol, 2014. **3**(6): p. 465-87.
85. Ibraghimov-Beskrovnaya, O. and N. Bukanov, *Polycystic kidney diseases: from molecular discoveries to targeted therapeutic strategies.* Cell Mol Life Sci, 2008. **65**(4): p. 605-19.
86. Merrick, D., et al., *Polycystin-1 cleavage and the regulation of transcriptional pathways.* Pediatr Nephrol, 2014. **29**(4): p. 505-11.
87. Torres, V.E. and P.C. Harris, *Mechanisms of Disease: autosomal dominant and recessive polycystic kidney diseases.* Nat Clin Pract Nephrol, 2006. **2**(1): p. 40-55; quiz 55.
88. Hogan, M.C., et al., *Characterization of PKD protein-positive exosome-like vesicles.* J Am Soc Nephrol, 2009. **20**(2): p. 278-88.
89. Shen, P.S., et al., *The Structure of the Polycystic Kidney Disease Channel PKD2 in Lipid Nanodiscs.* Cell, 2016. **167**(3): p. 763-773.e11.
90. Brill, A.L. and B.E. Ehrlich, *Polycystin 2: A calcium channel, channel partner, and regulator of calcium homeostasis in ADPKD.* Cell Signal, 2020. **66**: p. 109490.
91. Douguet, D. and A. Patel, *Structure and function of polycystins: insights into polycystic kidney disease.* 2019. **15**(7): p. 412-422.
92. Zhou, J., *Polycystins and primary cilia: primers for cell cycle progression.* Annu Rev Physiol, 2009. **71**: p. 83-113.
93. Semmo, M., M. Kottgen, and A. Hofherr, *The TRPP subfamily and polycystin-1 proteins.* Handb Exp Pharmacol, 2014. **222**: p. 675-711.
94. Su, Q., et al., *Structure of the human PKD1-PKD2 complex.* Science, 2018. **361**(6406): p. eaat9819.
95. Watnick, T., et al., *Mutations of PKD1 in ADPKD2 cysts suggest a pathogenic effect of trans-heterozygous mutations.* Nat Genet, 2000. **25**(2): p. 143-4.
96. Pei, Y., et al., *Somatic PKD2 mutations in individual kidney and liver cysts support a "two-hit" model of cystogenesis in type 2 autosomal dominant polycystic kidney disease.* J Am Soc Nephrol, 1999. **10**(7): p. 1524-9.
97. Lantinga-van Leeuwen, I.S., et al., *Lowering of Pkd1 expression is sufficient to cause polycystic kidney disease.* Hum Mol Genet, 2004. **13**(24): p. 3069-77.
98. Hopp, K., et al., *Functional polycystin-1 dosage governs autosomal dominant polycystic kidney disease severity.* The Journal of clinical investigation, 2012. **122**(11): p. 4257-4273.

99. Wallace, D.P., *Cyclic AMP-mediated cyst expansion.* Biochim Biophys Acta, 2011. **1812**(10): p. 1291-300.
100. Calvet, J.P., *The Role of Calcium and Cyclic AMP in PKD*, in *Polycystic Kidney Disease*, X. Li, Editor. 2015, Codon Publications. Copyright: The Author.: Brisbane (AU).
101. Torres, V.E. and P.C. Harris, *Strategies targeting cAMP signaling in the treatment of polycystic kidney disease.* J Am Soc Nephrol, 2014. **25**(1): p. 18-32.
102. Yamaguchi, T., et al., *Calcium restriction allows cAMP activation of the B-Raf/ERK pathway, switching cells to a cAMP-dependent growth-stimulated phenotype.* J Biol Chem, 2004. **279**(39): p. 40419-30.
103. Magenheimer, B.S., et al., *Early embryonic renal tubules of wild-type and polycystic kidney disease kidneys respond to cAMP stimulation with cystic fibrosis transmembrane conductance regulator/Na(+),K(+),2Cl(-) Co-transporter-dependent cystic dilation.* J Am Soc Nephrol, 2006. **17**(12): p. 3424-37.
104. Chebib, F.T., et al., *A Practical Guide for Treatment of Rapidly Progressive ADPKD with Tolvaptan.* 2018. **29**(10): p. 2458-2470.
105. Parfrey, P.S., *Autosomal-recessive polycystic kidney disease.* Kidney Int, 2005. **67**(4): p. 1638-48.
106. Bergmann, C., *Genetics of Autosomal Recessive Polycystic Kidney Disease and Its Differential Diagnoses.* Frontiers in Pediatrics, 2018. **5**(221).
107. Lu, H., et al., *Mutations in DZIP1L, which encodes a ciliary-transition-zone protein, cause autosomal recessive polycystic kidney disease.* 2017. **49**(7): p. 1025-1034.
108. Nagao, S., et al., *Animal models for human polycystic kidney disease.* Exp Anim, 2012. **61**(5): p. 477-88.
109. Leuenroth, S.J., et al., *Triptolide reduces cystogenesis in a model of ADPKD.* J Am Soc Nephrol, 2008. **19**(9): p. 1659-62.
110. Atala, A., et al., *Juvenile cystic kidneys (jck): a new mouse mutation which causes polycystic kidneys.* Kidney Int, 1993. **43**(5): p. 1081-5.
111. Pazour, G.J., et al., *Chlamydomonas IFT88 and its mouse homologue, polycystic kidney disease gene tg737, are required for assembly of cilia and flagella.* J Cell Biol, 2000. **151**(3): p. 709-18.
112. Smith, L.A., et al., *Development of Polycystic Kidney Disease in Juvenile Cystic Kidney Mice: Insights into Pathogenesis, Ciliary Abnormalities, and Common Features with Human Disease.* Journal of the American Society of Nephrology, 2006. **17**(10): p. 2821-2831.
113. Freedman, B.S., et al., *Reduced ciliary polycystin-2 in induced pluripotent stem cells from polycystic kidney disease patients with PKD1 mutations.* J Am Soc Nephrol, 2013. **24**(10): p. 1571-86.
114. Cai, Y., et al., *Altered trafficking and stability of polycystins underlie polycystic kidney disease.* J Clin Invest, 2014. **124**(12): p. 5129-44.
115. Hwang, S.-H., et al., *Tulp3 Regulates Renal Cystogenesis by Trafficking of Cystoproteins to Cilia.* Current Biology, 2019. **29**(5): p. 790-802.e5.
116. Ma, M., et al., *Loss of cilia suppresses cyst growth in genetic models of autosomal dominant polycystic kidney disease.* Nat Genet, 2013. **45**(9): p. 1004-12.

117. Husson, H., et al., *Reduction of ciliary length through pharmacologic or genetic inhibition of CDK5 attenuates polycystic kidney disease in a model of nephronophthisis.* Hum Mol Genet, 2016.
118. Lantinga, M.A., T.J. Gevers, and J.P. Drenth, *Evaluation of hepatic cystic lesions.* World J Gastroenterol, 2013. **19**(23): p. 3543-54.
119. van Aerts, R.M.M., et al., *Clinical management of polycystic liver disease.* Journal of Hepatology, 2018. **68**(4): p. 827-837.
120. Morgan, D.E., et al., *Polycystic liver disease: multimodality imaging for complications and transplant evaluation.* Radiographics, 2006. **26**(6): p. 1655-68; quiz 1655.
121. Aussilhou, B., et al., *Treatment of polycystic liver disease. Update on the management.* Journal of Visceral Surgery, 2018. **155**(6): p. 471-481.
122. Starzl, T.E., et al., *Liver Transplantation for Polycystic Liver Disease.* Archives of Surgery, 1990. **125**(5): p. 575-577.
123. Russell, R.T. and C.W. Pinson, *Surgical management of polycystic liver disease.* World J Gastroenterol, 2007. **13**(38): p. 5052-9.
124. Hogan, M.C., et al., *Liver involvement in early autosomal-dominant polycystic kidney disease.* Clin Gastroenterol Hepatol, 2015. **13**(1): p. 155-64.e6.
125. Temmerman, F., et al., *Systematic review: the pathophysiology and management of polycystic liver disease.* Alimentary Pharmacology & Therapeutics, 2011. **34**(7): p. 702-713.
126. Patel, A., A.B. Chapman, and A.E. Mikolajczyk, *A Practical Approach to Polycystic Liver Disease.* Clinical liver disease, 2019. **14**(5): p. 176-179.
127. Santos-Laso, A., et al., *New Advances in Polycystic Liver Diseases.* Semin Liver Dis, 2017. **37**(1): p. 45-55.
128. Lee-Law, P.Y., et al., *Genetics of polycystic liver diseases.* Curr Opin Gastroenterol, 2019. **35**(2): p. 65-72.
129. Besse, W., et al., *Isolated polycystic liver disease genes define effectors of polycystin-1 function.* The Journal of clinical investigation, 2017. **127**(5): p. 1772-1785.
130. van de Laarschot, L.F.M. and J.P.H. Drenth, *Genetics and mechanisms of hepatic cystogenesis.* Biochimica et Biophysica Acta (BBA) - Molecular Basis of Disease, 2018. **1864**(4, Part B): p. 1491-1497.
131. Wills, E.S., R. Roepman, and J.P. Drenth, *Polycystic liver disease: ductal plate malformation and the primary cilium.* Trends Mol Med, 2014. **20**(5): p. 261-70.
132. Perugorria, M.J., et al., *Polycystic liver diseases: advanced insights into the molecular mechanisms.* Nat Rev Gastroenterol Hepatol, 2014. **11**(12): p. 750-61.
133. Carpentier, R., et al., *Embryonic Ductal Plate Cells Give Rise to Cholangiocytes, Periportal Hepatocytes, and Adult Liver Progenitor Cells.* Gastroenterology, 2011. **141**(4): p. 1432-1438.e4.
134. Masyuk, T.V., et al., *Biliary dysgenesis in the PCK rat, an orthologous model of autosomal recessive polycystic kidney disease.* Am J Pathol, 2004. **165**(5): p. 1719-30.
135. Stroope, A., et al., *Hepato-renal pathology in pkd2ws25/- mice, an animal model of autosomal dominant polycystic kidney disease.* Am J Pathol, 2010. **176**(3): p. 1282-91.
136. Alvaro, D. and M.G. Mancino, *New insights on the molecular and cell biology of human cholangiopathies.* Mol Aspects Med, 2008. **29**(1-2): p. 50-7.

137. Spirli, C., et al., *Cyclic AMP/PKA-dependent paradoxical activation of Raf/MEK/ERK signaling in polycystin-2 defective mice treated with sorafenib.* Hepatology, 2012. **56**(6): p. 2363-2374.
138. Banales, J.M., et al., *Hepatic cystogenesis is associated with abnormal expression and location of ion transporters and water channels in an animal model of autosomal recessive polycystic kidney disease.* Am J Pathol, 2008. **173**(6): p. 1637-46.
139. Herron, B.J., et al., *Efficient generation and mapping of recessive developmental mutations using ENU mutagenesis.* Nat Genet, 2002. **30**(2): p. 185-9.
140. Stottmann, R.W., et al., *Ttc21b is required to restrict sonic hedgehog activity in the developing mouse forebrain.* Developmental Biology, 2009. **335**(1): p. 166-178.
141. Schock, E.N., et al., *A tissue-specific role for intraflagellar transport genes during craniofacial development.* 2017. **12**(3): p. e0174206.
142. Snedeker, J. and E.N. Schock, *Unique spatiotemporal requirements for intraflagellar transport genes during forebrain development.* 2017. **12**(3): p. e0173258.
143. Tran, P.V., et al., *Downregulating hedgehog signaling reduces renal cystogenic potential of mouse models.* J Am Soc Nephrol, 2014. **25**(10): p. 2201-12.
144. Jacobs, D.T., et al., *Intraflagellar-transport A dysfunction causes hyperphagia-induced systemic insulin resistance in a pre-obese state.* Faseb j, 2020. **34**(1): p. 148-160.
145. Jacobs, D.T., et al., *Dysfunction of intraflagellar transport-A causes hyperphagia-induced obesity and metabolic syndrome.* 2016. **9**(7): p. 789-98.
146. Hirano, T., Y. Katoh, and K. Nakayama, *Intraflagellar transport-A complex mediates ciliary entry and retrograde trafficking of ciliary G protein-coupled receptors.* Mol Biol Cell, 2017. **28**(3): p. 429-439.
147. Niwa, S., *The nephronophthisis-related gene ift-139 is required for ciliogenesis in Caenorhabditis elegans.* Sci Rep, 2016. **6**: p. 31544.
148. Driver, A.M., C. Shumrick, and R.W. Stottmann, *Ttc21b Is Required in Bergmann Glia for Proper Granule Cell Radial Migration.* 2017. **5**(4).
149. Davis, E.E., et al., *TTC21B contributes both causal and modifying alleles across the ciliopathy spectrum.* Nat Genet, 2011. **43**(3): p. 189-96.
150. Otto, E.A., et al., *Mutation analysis of 18 nephronophthisis associated ciliopathy disease genes using a DNA pooling and next generation sequencing strategy.* J Med Genet, 2011. **48**(2): p. 105-16.
151. McInerney-Leo, A.M., et al., *Whole exome sequencing is an efficient, sensitive and specific method for determining the genetic cause of short-rib thoracic dystrophies.* Clin Genet, 2015. **88**(6): p. 550-7.
152. Bullich, G., et al., *Contribution of the TTC21B gene to glomerular and cystic kidney diseases.* Nephrol Dial Transplant, 2017. **32**(1): p. 151-156.
153. Cong, E.H., et al., *A Homozygous Missense Mutation in the Ciliary Gene TTC21B Causes Familial FSGS.* Journal of the American Society of Nephrology, 2014. **25**(11): p. 2435-2443.
154. Zhang, H., et al., *Mutations in TTC21B cause different phenotypes in two childhood cases in China.* Nephrology (Carlton), 2018. **23**(4): p. 371-376.
155. Chen, L., et al., *Potential Mutations in Chinese Pathologic Myopic Patients and Contributions to Phenotype.* Curr Mol Med, 2018. **18**(10): p. 689-697.

156. Liu, W., et al., *Bi-allelic Mutations in TTC21A Induce Asthenoteratospermia in Humans and Mice.* Am J Hum Genet, 2019. **104**(4): p. 738-748.
157. Wang, W., et al., *Increased expression of TTC21A in lung adenocarcinoma infers favorable prognosis and high immune infiltrating level.* International Immunopharmacology, 2020. **78**: p. 106077.
158. Torres, V.E., et al., *Tolvaptan in patients with autosomal dominant polycystic kidney disease.* N Engl J Med, 2012. **367**(25): p. 2407-18.
159. Blair, H.A., *Tolvaptan: A Review in Autosomal Dominant Polycystic Kidney Disease.* Drugs, 2019.
160. Porath, B., et al., *Mutations in GANAB, Encoding the Glucosidase IIalpha Subunit, Cause Autosomal-Dominant Polycystic Kidney and Liver Disease.* Am J Hum Genet, 2016. **98**(6): p. 1193-207.
161. Walker, R.V., et al., *Ciliary exclusion of Polycystin-2 promotes kidney cystogenesis in an autosomal dominant polycystic kidney disease model.* Nat Commun, 2019. **10**(1): p. 4072.
162. Fu, W., et al., *Role for the IFT-A Complex in Selective Transport to the Primary Cilium.* Cell Rep, 2016. **17**(6): p. 1505-1517.
163. Liem, K.F., Jr., et al., *The IFT-A complex regulates Shh signaling through cilia structure and membrane protein trafficking.* J Cell Biol, 2012. **197**(6): p. 789-800.
164. Yoder, B.K., et al., *Polaris, a protein disrupted in orpk mutant mice, is required for assembly of renal cilium.* Am J Physiol Renal Physiol, 2002. **282**(3): p. F541-52.
165. Jonassen, J.A., et al., *Disruption of IFT complex A causes cystic kidneys without mitotic spindle misorientation.* J Am Soc Nephrol, 2012. **23**(4): p. 641-51.
166. Lin, F., et al., *Kidney-specific inactivation of the KIF3A subunit of kinesin-II inhibits renal ciliogenesis and produces polycystic kidney disease.* Proc Natl Acad Sci U S A, 2003. **100**(9): p. 5286-91.
167. Davis, E.E., et al., *TTC21B contributes both causal and modifying alleles across the ciliopathy spectrum.* Nat Genet, 2011. **43**(3): p. 189-96.
168. Srivastava, S., et al., *Many Genes-One Disease? Genetics of Nephronophthisis (NPHP) and NPHP-Associated Disorders.* Front Pediatr, 2017. **5**: p. 287.
169. Eggenschwiler, J.T. and K.V. Anderson, *Cilia and developmental signaling.* Annu Rev Cell Dev Biol, 2007. **23**: p. 345-73.
170. Viau, A., et al., *Cilia-localized LKB1 regulates chemokine signaling, macrophage recruitment, and tissue homeostasis in the kidney.* EMBO J, 2018. **37**(15).
171. Legue, E. and K.F. Liem, Jr., *Tulp3 Is a Ciliary Trafficking Gene that Regulates Polycystic Kidney Disease.* Curr Biol, 2019. **29**(5): p. 803-812.e5.
172. Wang, W., et al., *Genetic interaction of mammalian IFT-A paralogs regulates cilia disassembly, ciliary entry of membrane protein, Hedgehog signaling, and embryogenesis.* FASEB J, 2020.
173. Jacobs, D.T., et al., *Dysfunction of intraflagellar transport-A causes hyperphagia-induced obesity and metabolic syndrome.* Dis Model Mech, 2016. **9**(7): p. 789-98.
174. Piontek, K., et al., *A critical developmental switch defines the kinetics of kidney cyst formation after loss of Pkd1.* Nat Med, 2007. **13**(12): p. 1490-5.
175. Takakura, A., et al., *Pyrimethamine inhibits adult polycystic kidney disease by modulating STAT signaling pathways.* Hum Mol Genet, 2011. **20**(21): p. 4143-54.

176. Yamaguchi, T., et al., *cAMP stimulates the in vitro proliferation of renal cyst epithelial cells by activating the extracellular signal-regulated kinase pathway.* Kidney Int, 2000. **57**(4): p. 1460-71.
177. Yamaguchi, T., et al., *Cyclic AMP activates B-Raf and ERK in cyst epithelial cells from autosomal-dominant polycystic kidneys.* Kidney Int, 2003. **63**(6): p. 1983-94.
178. Bhunia, A.K., et al., *PKD1 induces p21(waf1) and regulation of the cell cycle via direct activation of the JAK-STAT signaling pathway in a process requiring PKD2.* Cell, 2002. **109**(2): p. 157-68.
179. Shibazaki, S., et al., *Cyst formation and activation of the extracellular regulated kinase pathway after kidney specific inactivation of Pkd1.* Hum Mol Genet, 2008. **17**(11): p. 1505-16.
180. Zheng, D., et al., *Urinary excretion of monocyte chemoattractant protein-1 in autosomal dominant polycystic kidney disease.* J Am Soc Nephrol, 2003. **14**(10): p. 2588-95.
181. Viau, A., et al., *Tubular STAT3 Limits Renal Inflammation in Autosomal Dominant Polycystic Kidney Disease.* J Am Soc Nephrol, 2020.
182. Hopp, K., et al., *Functional polycystin-1 dosage governs autosomal dominant polycystic kidney disease severity.* J Clin Invest, 2012. **122**(11): p. 4257-73.
183. Smith, L.A., et al., *Development of polycystic kidney disease in juvenile cystic kidney mice: insights into pathogenesis, ciliary abnormalities, and common features with human disease.* J Am Soc Nephrol, 2006. **17**(10): p. 2821-31.
184. Besschetnova, T.Y., et al., *Identification of signaling pathways regulating primary cilium length and flow-mediated adaptation.* Curr Biol, 2010. **20**(2): p. 182-7.
185. Kim, J.I., et al., *Reduction of oxidative stress during recovery accelerates normalization of primary cilia length that is altered after ischemic injury in murine kidneys.* Am J Physiol Renal Physiol, 2013. **304**(10): p. F1283-94.
186. Upadhyay, V.S., et al., *Roles of dopamine receptor on chemosensory and mechanosensory primary cilia in renal epithelial cells.* Front Physiol, 2014. **5**: p. 72.
187. Nikonova, A.S., et al., *Nedd9 restrains renal cystogenesis in Pkd1-/- mice.* Proc Natl Acad Sci U S A, 2014. **111**(35): p. 12859-64.
188. Husson, H., et al., *Reduction of ciliary length through pharmacologic or genetic inhibition of CDK5 attenuates polycystic kidney disease in a model of nephronophthisis.* Hum Mol Genet, 2016. **25**(11): p. 2245-2255.
189. Verghese, E., et al., *Renal cilia display length alterations following tubular injury and are present early in epithelial repair.* Nephrol Dial Transplant, 2008. **23**(3): p. 834-41.
190. Verghese, E., et al., *Renal primary cilia lengthen after acute tubular necrosis.* J Am Soc Nephrol, 2009. **20**(10): p. 2147-53.
191. Han, S.J., et al., *Hepatic ischemia/reperfusion injury disrupts the homeostasis of kidney primary cilia via oxidative stress.* Biochim Biophys Acta Mol Basis Dis, 2017. **1863**(7): p. 1817-1828.
192. Park, K.M., *Can Tissue Cilia Lengths and Urine Cilia Proteins Be Markers of Kidney Diseases?* Chonnam Med J, 2018. **54**(2): p. 83-89.
193. Hwang, S.H., et al., *Tulp3 Regulates Renal Cystogenesis by Trafficking of Cystoproteins to Cilia.* Curr Biol, 2019. **29**(5): p. 790-802 e5.
194. Patel, V., et al., *Acute kidney injury and aberrant planar cell polarity induce cyst formation in mice lacking renal cilia.* Hum Mol Genet, 2008. **17**(11): p. 1578-90.

195. Cruz, N.M., et al., *Organoid cystogenesis reveals a critical role of microenvironment in human polycystic kidney disease.* Nat Mater, 2017. **16**(11): p. 1112-1119.
196. Nigro, E.A., et al., *Polycystin-1 Regulates Actomyosin Contraction and the Cellular Response to Extracellular Stiffness.* Sci Rep, 2019. **9**(1): p. 16640.
197. Kiseleva, A.A., et al., *Unexpected Activities in Regulating Ciliation Contribute to Off-target Effects of Targeted Drugs.* Clin Cancer Res, 2019. **25**(13): p. 4179-4193.
198. Shaheen, R., et al., *Biallelic Mutations in Tetratricopeptide Repeat Domain 26 (Intraflagellar Transport 56) Cause Severe Biliary Ciliopathy in Humans.* Hepatology. **n/a**(n/a).
199. Zimmerman, K.A., et al., *Primary cilia disruption differentially affects the infiltrating and resident macrophage compartment in the liver.* Am J Physiol Gastrointest Liver Physiol, 2018. **314**(6): p. G677-g689.
200. Spirli, C., et al., *ERK1/2-dependent vascular endothelial growth factor signaling sustains cyst growth in polycystin-2 defective mice.* Gastroenterology, 2010. **138**(1): p. 360-371.e7.
201. Ma, M., et al., *Loss of cilia suppresses cyst growth in genetic models of autosomal dominant polycystic kidney disease.* Nature genetics, 2013. **45**(9): p. 1004-1012.
202. Jiang, L., et al., *Inhibition of Mast Cell Degranulation With Cromolyn Sodium Exhibits Organ-Specific Effects in Polycystic Kidney (PCK) Rats.* Int J Toxicol, 2018. **37**(4): p. 308-326.
203. Sato, K., et al., *Ductular Reaction in Liver Diseases: Pathological Mechanisms and Translational Significances.* Hepatology, 2019. **69**(1): p. 420-430.
204. Fabris, L., et al., *Pathobiology of inherited biliary diseases: a roadmap to understand acquired liver diseases.* 2019. **16**(8): p. 497-511.
205. Huang, B.Q., et al., *Isolation and characterization of cholangiocyte primary cilia.* American Journal of Physiology-Gastrointestinal and Liver Physiology, 2006. **291**(3): p. G500-G509.
206. Mariotti, V., et al., *Animal models of biliary injury and altered bile acid metabolism.* Biochimica et Biophysica Acta (BBA) - Molecular Basis of Disease, 2018. **1864**(4, Part B): p. 1254-1261.
207. Septer, S., et al., *Yes-associated protein is involved in proliferation and differentiation during postnatal liver development.* American journal of physiology. Gastrointestinal and liver physiology, 2012. **302**(5): p. G493-G503.
208. Gadd, V.L., et al., *The portal inflammatory infiltrate and ductular reaction in human nonalcoholic fatty liver disease.* Hepatology, 2014. **59**(4): p. 1393-405.
209. Tang, X., et al., *Anti-tumour strategies aiming to target tumour-associated macrophages.* Immunology, 2013. **138**(2): p. 93-104.
210. Plotnikova, O.V., E.N. Pugacheva, and E.A. Golemis, *Primary cilia and the cell cycle.* Methods Cell Biol, 2009. **94**: p. 137-60.
211. Brown, J.M. and G.B. Witman, *Cilia and Diseases.* Bioscience, 2014. **64**(12): p. 1126-1137.
212. Keeling, J., L. Tsiokas, and D. Maskey, *Cellular Mechanisms of Ciliary Length Control.* Cells, 2016. **5**(1).
213. Picariello, T., et al., *A global analysis of IFT-A function reveals specialization for transport of membrane-associated proteins into cilia.* J Cell Sci, 2019. **132**(3).

214. Jin, H., et al., *The conserved Bardet-Biedl syndrome proteins assemble a coat that traffics membrane proteins to cilia.* Cell, 2010. **141**(7): p. 1208-19.
215. Zhang, Q., et al., *Bardet-Biedl syndrome 3 (Bbs3) knockout mouse model reveals common BBS-associated phenotypes and Bbs3 unique phenotypes.* Proc Natl Acad Sci U S A, 2011. **108**(51): p. 20678-83.
216. Iomini, C., et al., *Retrograde intraflagellar transport mutants identify complex A proteins with multiple genetic interactions in Chlamydomonas reinhardtii.* Genetics, 2009. **183**(3): p. 885-96.
217. Stottmann, R.W., et al., *Ttc21b is required to restrict sonic hedgehog activity in the developing mouse forebrain.* Dev Biol, 2009. **335**(1): p. 166-78.
218. Zhu, B., et al., *Functional exploration of the IFT-A complex in intraflagellar transport and ciliogenesis.* PLoS Genet, 2017. **13**(2): p. e1006627.
219. Pugacheva, E.N., et al., *HEF1-dependent Aurora A activation induces disassembly of the primary cilium.* Cell, 2007. **129**(7): p. 1351-63.
220. Mirvis, M., T. Stearns, and W. James Nelson, *Cilium structure, assembly, and disassembly regulated by the cytoskeleton.* Biochem J, 2018. **475**(14): p. 2329-2353.
221. Spalluto, C., D.I. Wilson, and T. Hearn, *Evidence for reciliation of RPE1 cells in late G1 phase, and ciliary localisation of cyclin B1.* FEBS Open Bio, 2013. **3**: p. 334-40.
222. Phua, S.C., et al., *Dynamic Remodeling of Membrane Composition Drives Cell Cycle through Primary Cilia Excision.* Cell, 2017. **168**(1-2): p. 264-279 e15.
223. Eguether, T., et al., *IFT27 links the BBSome to IFT for maintenance of the ciliary signaling compartment.* Dev Cell, 2014. **31**(3): p. 279-290.
224. Liew, G.M., et al., *The intraflagellar transport protein IFT27 promotes BBSome exit from cilia through the GTPase ARL6/BBS3.* Dev Cell, 2014. **31**(3): p. 265-78.
225. Corbit, K.C., et al., *Vertebrate Smoothened functions at the primary cilium.* Nature, 2005. **437**(7061): p. 1018-21.
226. Bai, C.B., et al., *Gli2, but not Gli1, is required for initial Shh signaling and ectopic activation of the Shh pathway.* Development, 2002. **129**(20): p. 4753-61.
227. Mirvis, M., et al., *Primary cilium loss in mammalian cells occurs predominantly by whole-cilium shedding.* PLoS Biol, 2019. **17**(7): p. e3000381.
228. Lu, H., et al., *A function for the Joubert syndrome protein Arl13b in ciliary membrane extension and ciliary length regulation.* Dev Biol, 2015. **397**(2): p. 225-36.
229. Driver, A.M., C. Shumrick, and R.W. Stottmann, *Ttc21b Is Required in Bergmann Glia for Proper Granule Cell Radial Migration.* J Dev Biol, 2017. **5**(4).
230. Chang, C.F., et al., *Craniofacial Ciliopathies Reveal Specific Requirements for GLI Proteins during Development of the Facial Midline.* PLoS Genet, 2016. **12**(11): p. e1006351.
231. Shao, X., S. Somlo, and P. Igarashi, *Epithelial-specific Cre/lox recombination in the developing kidney and genitourinary tract.* J Am Soc Nephrol, 2002. **13**(7): p. 1837-46.